

---

# Unitized Bidirectional Vanadium-Air Redox Flow Battery

---

## Kombinierte bidirektionale Vanadium-Luft-Redox-Fluss-Batterie

von der Fakultät für Mathematik und Naturwissenschaften der Carl von Ossietzky  
Universität Oldenburg zur Erlangung des Grades und Titels eines Doktors der  
Naturwissenschaften (Dr. rer. nat.) angenommene Dissertation

von

Jan Bernhard grosse Austing

geboren am 12.06.1983 in Lohne (Oldb.)

angefertigt am

NEXT ENERGY EWE-Forschungszentrum für Energietechnologie e.V. in Oldenburg

**Erstgutachter**

Prof. Dr. Gunther Wittstock (Universität Oldenburg)

**Zweitgutachter**

Prof. Dr. Carsten Agert (Universität Oldenburg)

**Tag der Disputation**

05.04.2016

“...provides multi-megawatt energy storage solutions using –  
and I have no idea what this is – vanadium redox fuel cells.

That’s one of the coolest things I’ve ever said out loud!”

(Barack Obama)



# Abstract

The all-vanadium redox flow battery (VRFB) is a promising battery technology for the compensation of the intermittent electricity production of renewable energy generators due to its high cycle life, reasonable round-trip efficiency and fast response time. However, the VRFB suffers from low energy density which can be a hindrance in decentralized, residential storage installations. In contrast, the vanadium-air redox flow battery (VARFB) promises a significant higher energy density (roughly doubled) due to virtually eliminating one electrolyte tank.

In this thesis a new concept for a unitized (i.e. combined) bidirectional VARFB was developed, investigated and optimized. The proposed setup comprised a two-layered positive electrode to support both the oxygen evolution reaction (OER) as the charging reaction as well as the oxygen reduction reaction (ORR) as the discharging reaction of the positive half-cell. Side reactions were suspected to reduce the efficiency. Thus, transfer processes through the membrane were investigated by means of UV/Vis spectroscopy and inductively coupled plasma mass spectroscopy (ICP-MS) of the electrolytes. The major part of the coulombic efficiency losses was attributed to oxygen permeation through the membrane. However, a considerable amount of the vanadium ions of the negative electrolyte underwent crossover during cycling. As the vanadium amount in the negative electrolyte determines the capacity of the VARFB, the vanadium crossover is crucial for its life-time. Thus, a layer-by-layer (LbL) modification routine of the Nafion 117 (N117) membrane with multilayers of polyethylenimine (PEI) and Nafion ionomer was developed to significantly reduce vanadium crossover and oxygen permeation. As a result, the energy and coulombic efficiency were increased substantially as well as the indicated life-time of the VARFB.



# Zusammenfassung

Die Vanadium-Redox-Fluss-Batterie (VRFB) ist aufgrund der hohen Zyklenlebensdauer, der Energieeffizienz und der schnellen Ansprechzeiten ein vielversprechendes System zur Kompensation der Fluktuation bei der Stromerzeugung durch erneuerbare Energien. Die geringe Energiedichte von VRFB ist jedoch ein Hemmnis für die Anwendung als dezentrales Speichersystem. Die Vanadium-Luft-Redox-Fluss-Batterie (VARFB) hingegen, bei der nur ein Elektrolyttank benötigt wird, verspricht eine nahezu verdoppelte Energiedichte.

In dieser Dissertation wurde eine neuartige kombinierte bidirektionale VARFB konstruiert, untersucht und optimiert. Um sowohl den Anforderungen an die Sauerstoffentwicklung beim Laden als auch an die Sauerstoffreduktion beim Entladen in der positiven Halbzelle gerecht zu werden, wurde eine aus zwei Lagen bestehende positive Elektrode entwickelt und eingesetzt. Als Ursache für verringerte Effizienzen im Betrieb der VARFB wurden Nebenreaktionen vermutet. Daher wurden Transferprozesse durch die Membran mithilfe von UV/Vis-Spektroskopie sowie Massenspektrometrie mit induktiv gekoppeltem Plasma der Elektrolytlösungen intensiv untersucht. Ein Großteil der Ladungseffizienz-Verluste wurde durch Sauerstoff-Permeation verursacht. Der ebenfalls stattfindende Durchgang von Vanadium-Ionen durch die Membran verringerte hingegen die Lebensdauer der VARFB, da die Kapazität der Batterie von der Menge an Vanadium-Ionen im negativen Elektrolyten abhängt. Aus diesem Grund wurde ein Verfahren zur Beschichtung der Membran mit Polyethylenimin und Nafion-Ionomer entwickelt, wodurch sich eine deutliche Reduktion des Vanadium-Ionen-Durchgangs durch die Membran erreichen ließ. Als Folge zeigte sich eine Verbesserung der Energieeffizienz und Ladungseffizienz der VARFB sowie eine verbesserte Prognose bzgl. der Lebensdauer der VARFB.



# Contents

<b>Abstract</b>	<b>v</b>
<b>Zusammenfassung</b>	<b>vii</b>
<b>1 Introduction and Motivation</b>	<b>1</b>
1.1 Global Warming, Renewable Energies and Energy Storage Technologies	1
1.2 Outline of this Thesis . . . . .	4
<b>2 Redox Flow Batteries</b>	<b>7</b>
2.1 Setup . . . . .	8
2.2 General Properties of Redox Flow Batteries . . . . .	9
2.3 Types of Redox Flow Batteries . . . . .	16
2.4 Concepts for Increased Energy Density . . . . .	20
<b>3 Vanadium-Air Redox Flow Batteries</b>	<b>23</b>
3.1 Introduction and State of the Art . . . . .	23
3.2 Contributions within this Thesis . . . . .	25
3.3 Author Contributions to PUBLICATIONS I-III . . . . .	29
<b>4 Conclusion and Outlook</b>	<b>31</b>
<b>References</b>	<b>35</b>
<b>List of Abbreviations and Symbols</b>	<b>41</b>
<b>Publications</b>	<b>45</b>
Publication I . . . . .	47
Publication II . . . . .	59
Publication III . . . . .	73
<b>Erklärung I</b>	<b>89</b>

<b>Erklärung II</b>	<b>91</b>
<b>List of Publications</b>	<b>93</b>
<b>CV</b>	<b>97</b>
<b>Danksagung</b>	<b>99</b>

# 1 Introduction and Motivation

## 1.1 Global Warming, Renewable Energies and Energy Storage Technologies

The influence of anthropogenic greenhouse gas emissions such as CO<sub>2</sub> on terrestrial global warming is widely consensus in scientific publications [1, 2]. In December 2015, 196 countries agreed in the United Nations conference on climate change in Paris that the global temperature rise should be well below 2 °C in comparison to pre-industrial levels to avoid dangerous climate change [3]. A recent report of the United Kingdom's national weather service indicates that the average surface temperature of the year 2015 will be presumably 1.02 °C above the temperature average of the pre-industrial era from 1850-1900 [4] (Fig. 1). That is, half of the maximum acceptable temperature increase has already been reached in 2015.

Additionally, the global energy use will continue to rise: a growth of +33 % (based on 2015) till the year 2040 is expected according to the World Energy Outlook 2015 of the International Energy Agency (IEA) [7]. The rising energy demand is linked to increasing CO<sub>2</sub> emissions due to combustion of fossil fuels. In 2040, the energy-related global CO<sub>2</sub> emissions will be 16 % higher compared to 2013 as predicted by the IEA [7].

A promising approach to mitigate CO<sub>2</sub> emissions related to electricity production is to increase the share of renewable energies in electricity generation. However, the production of renewable electricity generators such as photovoltaics (PV) and wind turbines is fluctuating depending on the presence of insolation or wind. The matching of electricity supply and demand within a grid can be increased via communication between electricity appliances and sources (the so-called “smart grids”). Another important element for the harmonization of electricity generation and consumption are batteries. They are suitable to shift an excess of produced electricity to periods with an intermittent shortage of electricity generation within storage time spans of up to a few days. The battery is charged in periods with a surplus of electricity production (Fig. 2). In turn, it is discharged in times when power generation of

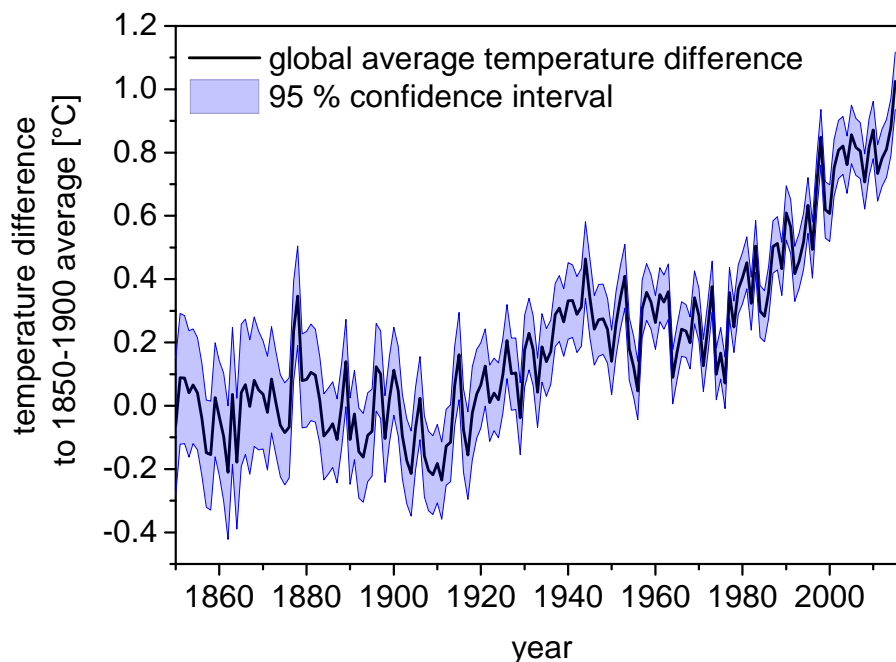


**Figure 1:** Global mean temperature difference from the 1850-1900 average [°C] (data from [5], data set described in [6]).

photovoltaic devices and wind turbines does not meet the demand. Therefore, electricity storage devices such as batteries are regarded as an essential element for an increased renewable electricity production without risking the reliability of the electricity supply [8–12].

Amongst the existing battery technologies, redox flow batteries (RFB) have a high potential for balancing electricity generation and consumption in grids with a high share of renewable energies. RFB properties are the scalability of power and energy independent from each other, a high cycle life [14], fast response times and a good round-trip efficiency [15]. The most developed redox flow battery is the all-vanadium redox flow battery (VRFB). However, like all redox flow battery technologies the VRFB suffers from low specific energy and low energy density (Fig. 3), i.e. the amount of energy stored in the battery per unit volume and/or mass of the battery is low. In most redox flow systems this is caused by limited solubility of active species and therefore a high ratio of inactive materials (e.g. water,  $\text{H}_2\text{SO}_4$ ) to the active materials (e.g. vanadium ions). For instance, the concentration of the electroactive vanadium ions in common electrolytes employed in VRFB does not exceed  $2 \text{ mol}\cdot\text{L}^{-1}$ .

While a low energy density and low specific energy is generally not a major concern in stationary storage applications, especially the volumetric energy density can be an obstacle for residential installations with limited space. Various approaches to

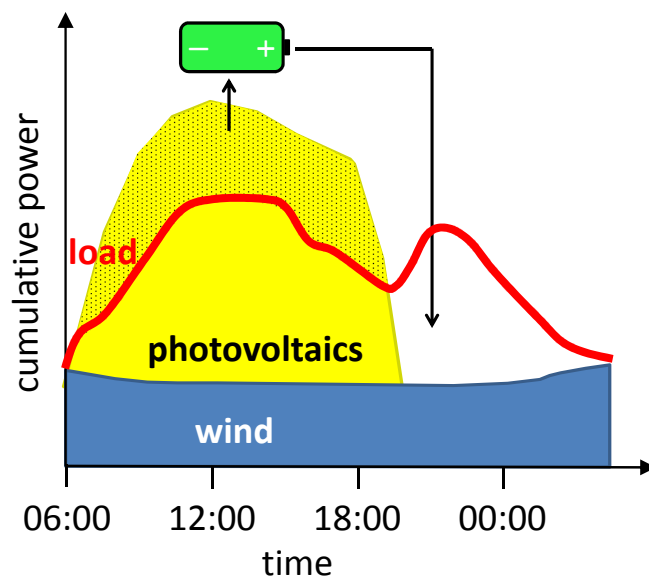


**Figure 2:** PV and wind power vs. load on a typical summer day in Germany (based on data from [13]).

increase the energy density of redox flow batteries were proposed in literature; e.g. utilization of additives to increase the solubility of active species [16–20], application of organic solvents or ionic liquids (IL) to increase the available potential window [21] and concepts involving solid species such as metals [14].

Another promising approach to increase the energy density is the vanadium-air redox flow battery (VARFB). The positive<sup>1</sup> redox couple ( $\text{VO}_2^+/\text{VO}^{2+}$ ) is replaced by the couple  $\text{O}_2/\text{H}_2\text{O}$  which leads to an increased thermodynamic cell potential. The oxygen is provided from the ambient air and the size of the  $\text{H}_2\text{O}$  container is negligible small [22]. Therefore, the theoretical energy density and specific energy of the VARFB are more than doubled compared to the VRFB.

At the beginning of the research for this thesis, there were only publications in which a VARFB consisting of *two* different reaction units had been demonstrated [23, 24]. Although this setup allows the individual tailoring of the reaction unit

<sup>1</sup> In this thesis the half-cells of electrochemical cells (such as batteries) are denoted with the terms “positive” and “negative” according to the potential of the electrodes versus each other. This convention is independent of whether the half-cell is being charged or discharged. Likewise, the liquid electrolyte in the positive half-cell is denoted as “positive electrolyte” and the term “negative electrolyte” is used for the electrolyte in the negative half-cell compartment. Another common naming in the field of batteries are the terms “anode” and “cathode” which are assigned according to the discharging process and this naming is maintained for the charging process as well. Despite of the fact that the terms “anode” and “cathode” are commonly used when dealing with batteries, this nomenclature can lead to confusion. Thus, these terms are not used in this thesis despite of PUBLICATION I after which the potential ambiguousness was realized.

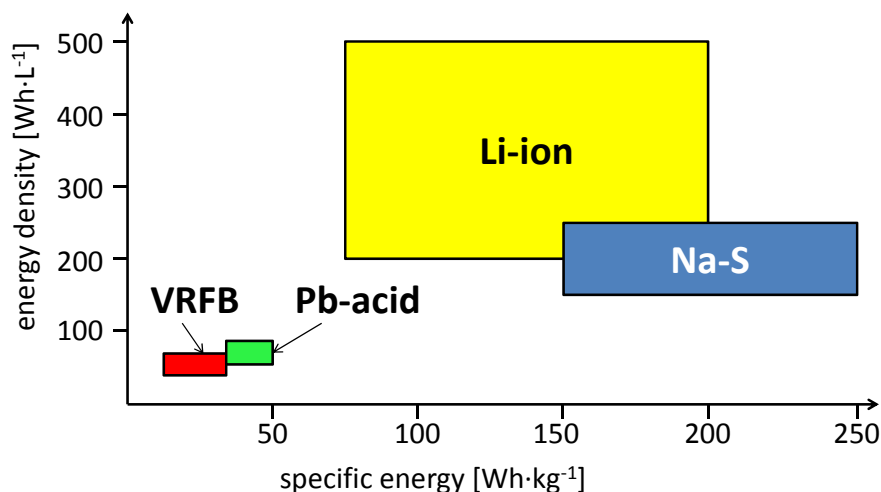


**Figure 3:** Energy density [ $\text{Wh}\cdot\text{L}^{-1}$ ] and mass-specific energy [ $\text{Wh}\cdot\text{kg}^{-1}$ ] of different battery technologies (based on data from [12]). Pb-acid = lead acid batteries; Na-S = sodium sulfur batteries, Li-ion = lithium ion batteries.

concerning the opposite requirements of the reactions, the utilization of two reaction units is at the expense of the weight, volume and costs of the system. Other reports [25, 26] present and discuss only the discharge process of the VARFB which can also be regarded as a vanadium-air *fuel* cell (VOFC). However, these systems represent only an incomplete battery as the vanadium electrolyte has to be regenerated externally.

## 1.2 Outline of this Thesis

The scope of this work was to develop a new VARFB cell with a *combined* reaction unit (i.e. a single reaction unit in which both charging and discharging can be conducted). Furthermore, the performance of this system was investigated in order to identify possible loss mechanisms. This analysis served as a starting point for the rational optimization of the system. The results of this cumulative thesis are presented in three articles (denoted as PUBLICATIONS I-III) published in peer-reviewed journals.

The structure of the thesis is described briefly in the following. First, RFB are introduced and discussed in general to provide an overview about the properties and state of the art of this energy storage technology. Thereupon, the VARFB is reviewed in detail and its properties are discussed. The own publications are described in this context and their synopsis and interconnection are given. Additionally, the contributions of the author to each publication are itemized. The thesis closes with a Conclusion and Outlook chapter which summarizes and evaluates the outcome of

this work and discusses outstanding questions related to the VARFB and those that came up during the course of the thesis. The own PUBLICATIONS I-III are attached at the end of this thesis.

In PUBLICATION I (“Study of an unitised bidirectional vanadium-air redox flow battery comprising a two-layered cathode”) a novel VARFB utilizing a combined reaction unit with a two-layered positive electrode is described. The performance of this system is investigated at different operation conditions. Transfer processes through the membrane were hypothesized to cause a performance decay during operation and were thus investigated in PUBLICATION II (“Investigation of crossover processes in a unitized bidirectional vanadium/air redox flow battery”). A combination of UV/Vis spectroscopic and inductively coupled plasma mass spectroscopy (ICP-MS) analysis of the electrolytes was applied to identify and quantify the crossover of vanadium species through the membrane as well as the oxygen permeation. An approach to improve the performance of the VARFB by the modification of the membrane is presented in PUBLICATION III (“Layer-by-layer modification of Nafion membranes for increased life-time and efficiency of vanadium/air redox flow batteries”). Via layer-by-layer (LbL) deposition of polyelectrolytes on the membrane, the transfer of vanadium and oxygen through the membrane was reduced significantly which lead to an improved efficiency of the VARFB and an indicated enhancement of the life-time.



## 2 Redox Flow Batteries

The history of RFB goes back to the 1950s. A patent was issued to Kangro in 1949 in which the storage of electrical energy is claimed in liquids with dissolved reducible and oxidable species [27]. However, substantial analysis on RFB was not undertaken before the 1970s. During that time, extensive research such as screening of suitable redox couples was conducted at the National Aeronautic and Space Administration (NASA) [15, 28].

In 1983, the polysulfide/bromine redox technology was invented. It was developed and commercialized owing to the promising costs and abundance of the redox species [15]. Another relevant hybrid RFB available on the market is the zinc/bromine RFB which was developed in the 1980s [15].

A promising approach to mitigate capacity fading problems induced by ion crossover is the employment of two redox couples which are based on the same element. The most prominent example is the VRFB comprising the redox couples  $V^{2+}/V^{3+}$  and  $VO_2^+/VO^{2+}$ . The VRFB was invented and developed in the 1980s by Skyllas-Kazacos et al. at the University of New South Wales [21]. This RFB system received most attention in scientific research [19, 21, 29] and is the most successfully commercialized RFB (commercialized from 1993 on) [14, 30]. However, the major drawback of RFB in general is the low energy density which is also inherent in VRFB. Thus, limited available space can obstruct their application.

Beyond that, numerous different redox flow concepts have been proposed and studied [8, 14, 15, 19, 21, 28, 30, 31]. New RFB approaches include the utilization of water-soluble organic redox active species such as anthraquinones [32, 33], redox-active polymers [34] or other organic redox active species [35] and systems with new metal-based redox couples such as all-iron [36] or all-copper RFB [37]. However, in the following the focus will be laid on those types of redox flow batteries which have overcome the status of laboratory research and have been tested in demonstration projects.

## 2.1 Setup

In conventional battery systems the storage of electroactive material and its conversion is in the identical place. In contrast, this is spatially separated in RFB. The conversion between chemical and electrical energy occurs in the reaction unit while the (dissolved) electroactive species are stored in external electrolyte tanks (Fig. 4). For operation of the battery, the electrolytes are circulated through the reaction unit using pumps. The setup of RFB is similar to that of fuel cells (FC), however, the latter are open electrochemical systems (exchange of matter with the ambient surrounding) and they are generally not electrochemically reversible [19, 31].

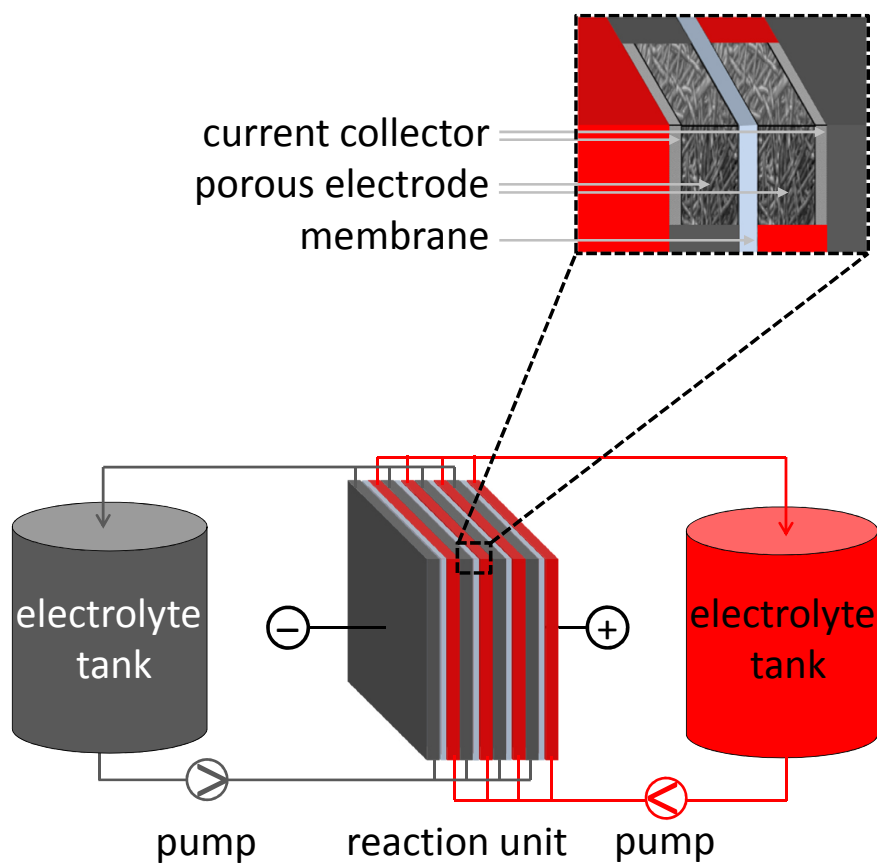


**Figure 4:** Schematic of a RFB and the components of one cell of the reaction unit (magnification).

The reaction unit (also referred to as “stack”) consists of several single cells connected in series to obtain a higher output voltage. The basic parts of a single cell are the current collectors or bipolar plates (BPP), the (porous) electrodes and the electrically insulating ion exchange membrane which separates the two half-cells

from each other (Fig. 4). In case of RFB operation, the two electrolytes are pumped through the porous electrodes, electrons can be exchanged between the active species and the electrode surface and are conducted via the BPP to the outer circuit. Ions such as  $H^+$  or  $SO_4^{2-}$  are transferred through the membrane (cation or anion exchange membrane) to close the circuit.

## 2.2 General Properties of Redox Flow Batteries

### 2.2.1 Independence of Power and Capacity

One unique property of RFB is entailed by the modular setup: the decoupling of power and capacity from each other. The numbers of cells in the stack and their active area determine the power of the RFB whereas the volume of electrolyte and the concentration of active species therein influence its capacity. Therefore, by scaling the reaction unit and the electrolyte volumes in an appropriate manner, the RFB can be designed to meet exactly the individual power and capacity demands. This is especially of interest for those storage installations where power and capacity need to be tailorable independent from each other to fulfill efficiently any given requirements.

### 2.2.2 Efficiency and Loss Mechanisms

#### 2.2.2.1 Energy Efficiency

A common measure for the performance of an electrochemical storage device is the energy efficiency  $\eta_E$ . It describes the ratio of the electrical energy that can be extracted from the battery during discharging  $W_{\text{discharge}}$  relative to the energy brought into the system during charging  $W_{\text{charge}}$  (Eq. 1). The electrical energy can be obtained by integration of the product of the current  $I(t)$  and the voltage  $U(t)$  over the time of the discharging or charging process.

$$\eta_E = \frac{W_{\text{discharge}}}{W_{\text{charge}}} = \frac{\int_{\text{discharge}} I(t) U(t) dt}{\int_{\text{charge}} I(t) U(t) dt} \quad (1)$$

The energy efficiency of common RFB systems is in the range of approx. 75-85 % [38]. Additionally to the general internal losses caused by crossover, side reactions or overpotentials of the reactions, the energy efficiency of RFB is lowered due to energy consumption of external devices such as temperature control units and pumps which are necessary for electrolyte circulation. In comparison to other common storage

techniques, the energy efficiency of RFB is competitive (Fig. 5).

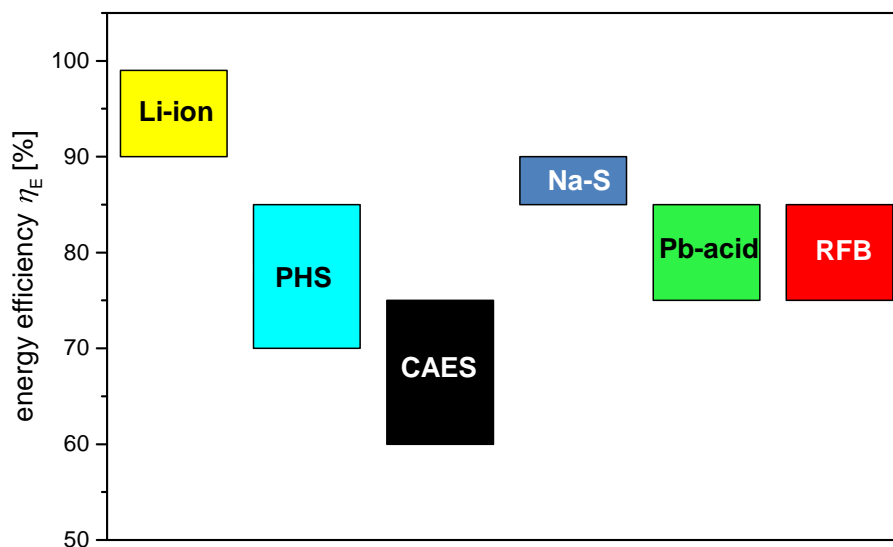


**Figure 5:** Energy efficiencies of electricity storage technologies suitable for stationary applications (data from [38, 39]).

### 2.2.2.2 Coulombic Efficiency

The coulombic efficiency  $\eta_C$  is the ratio of the charge during discharging  $Q_{\text{discharge}}$  relative to the charge during charging  $Q_{\text{charge}}$  (Eq. 2).

$$\eta_C = \frac{Q_{\text{discharge}}}{Q_{\text{charge}}} = \frac{\int_{\text{discharge}} I(t) dt}{\int_{\text{charge}} I(t) dt} \quad (2)$$

A low value indicates that electrical energy consuming side reactions occur. For instance, these can be gassing reactions such as hydrogen evolution (HER) at the negative electrode or oxygen evolution reaction (OER) at the positive electrode. Another well known loss mechanism is the crossover of active species through the membrane which leads to self-discharging of the battery. Ions of the active species pass the ion-conduction membrane and react with the active species of the other half-cell. This leads to lowered coulombic efficiency. Additionally, this leads to a loss of capacity in those RFB in which the two redox couples are not based on the same element/molecule. The species that underwent crossover are in the “wrong” half-cell of the battery and therefore not accessible for further charging/discharging.

Another parasitic phenomenon observed in RFB are the so-called shunt currents. The intended electric and ionic current path can be described as follows. Ions are

exchanged between two half-cells of a cell which are ionically connected through the membrane. Electric current is transmitted between the cells which are connected electrically via BPP (Fig. 6). However, two half-cells with the same polarity are also connected by the highly conductive electrolyte which is in the manifolds and channels (Fig. 6). Thus, parallel to the intended current path, parasitic currents can flow between two half-cells of the same polarity. Indeed, these shunt currents can severely reduce the coulombic and therefore the energy efficiency [40–42]. For example, Yin et al. [42] reported for a non-optimized 5-cell stack a decrease in coulombic efficiency of 22.1 % compared to a single cell due to shunt currents ( $\eta_{C, \text{single cell}} = 95.3\%$ ;  $\eta_{C, 5 \text{ cells}} = 73.1\%$ ). Nevertheless, with an optimized electrolyte flow channel design with high electrical resistance (i.e. low cross section area) these currents can be limited to make up only 2-5 % of the overall energy efficiency losses [38, 42]. In this thesis, single cell setups were used. Therefore, it was not necessary to consider shunt currents in the PUBLICATIONS I-III.

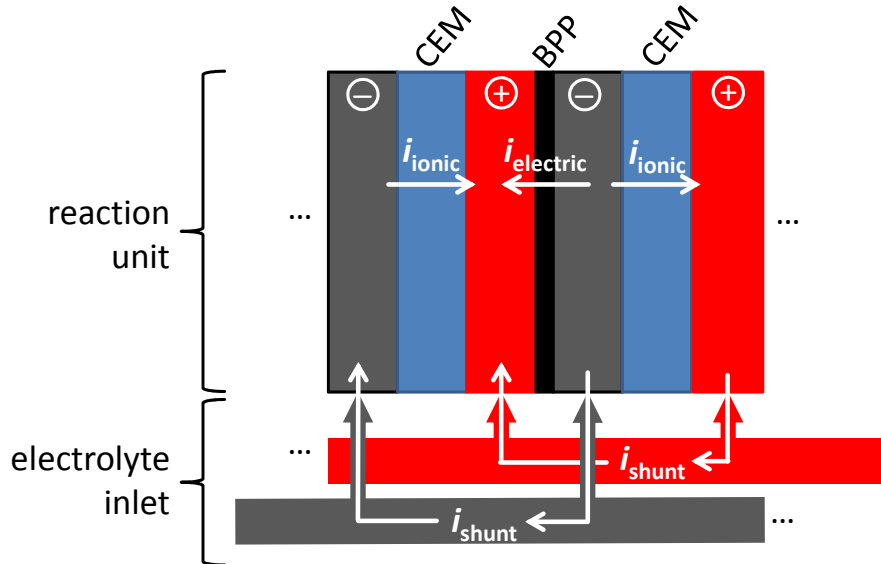


**Figure 6:** Schematic of the intended ionic current path  $i_{\text{ionic}}$  and electric current path  $i_{\text{electric}}$  and the undesired path for the shunt currents  $i_{\text{shunt}}$  via the electrolyte inlet system. The example depicts a RFB with a cation exchange membrane (CEM). Shunt currents can be transmitted analogously through the electrolyte outlet (not shown).

An advantage of RFB is that no self-discharge of the entire electrolyte should occur when the electrolyte remains in the tanks and the valves to the tanks are closed [8]. Conventional batteries are subject to self-discharge and therefore not suitable for storing energy for a long time period.

### 2.2.2.3 Voltaic Efficiency

The voltaic efficiency  $\eta_V$  obtained as the ratio of  $\eta_E$  to  $\eta_C$  (Eq. 3) describes the average discharge voltage in relation to the average charge voltage. It reflects resistances of the whole battery process such as ohmic cell resistances, charge transfer resistances of the reactions or concentration polarization resistances. Thus, it is strongly dependent on operational parameters such as temperature, current density as well as pumping rates.

$$\eta_V = \frac{\eta_E}{\eta_C} \quad (3)$$

### 2.2.3 Energy Density and Specific Energy

The energy density is the electrical energy stored in the battery per unit volume. It depends on the concentration of the active species, the number of transferred electrons and the cell voltage [31]. Similarly, the (mass) specific energy is the energy per unit mass of the system. For mobile applications, both the energy density and specific energy need to be high to achieve lightweight devices (high specific energy) whose interior is not completely possessed by battery cells (high energy density). For stationary applications, in many cases the (mass) specific energy is not relevant. However, the energy density is of importance especially in applications with limited space.

The low energy density being inherent to most RFB types is an important field of research activities. In most “true” (i.e. only dissolved redox species) RFB systems it is less than  $25 \text{ Wh}\cdot\text{L}^{-1}$  [21]. The low energy density and specific energy are caused by two limitations in an aqueous electrolyte. First, the solubility limitations of the redox species lead to a high mass and volume of inactive material in a RFB. For instance, a positive electrolyte typically employed in a VRFB with the concentration of  $2 \text{ mol}\cdot\text{L}^{-1}$   $\text{VO}_2^+$  in  $2 \text{ mol}\cdot\text{L}^{-1}$   $\text{H}_2\text{SO}_4$  has a density of  $1.283 \text{ kg}\cdot\text{L}^{-1}$  [43]. This means that 2 mol or 101.8 g vanadium (as metal) are dissolved in 1.283 kg electrolyte, i.e. the active metal accounts for only 7.9 mass-% of the overall electrolyte mass. Second, the water splitting reaction limits the usable potential window. The thermodynamic half-cell potential under standard conditions is  $E^0 = 0 \text{ V}$  vs. standard hydrogen electrode (SHE) for the HER and  $E^0 = 1.23 \text{ V}$  vs. SHE for the OER. Due to the overpotentials of HER and OER on several electrode materials, the practical potential window can be expanded to a certain extent. For example, the HER is negligible on graphite

felt electrodes which are commonly used in VRFB up to approx.  $-0.5$  V vs. SHE [44]. The feasible potential window of aqueous electrolytes using graphite electrodes (green area) and standard potentials of redox couples relevant for RFB are depicted in Fig. 7.

Nevertheless, the maximal voltage achievable in aqueous solutions is approx.  $2.0$  V [45], the highest discharge voltage in aqueous electrolytes was reported for a zinc-cerium RFB as  $2.1$  V [46]. Substantial increase of the potential window is only possible when using alternative solvents (Sec. 2.4). The low energy density of VRFB is the major motivation for investigating the concept of a VARFB which is the topic of this thesis.

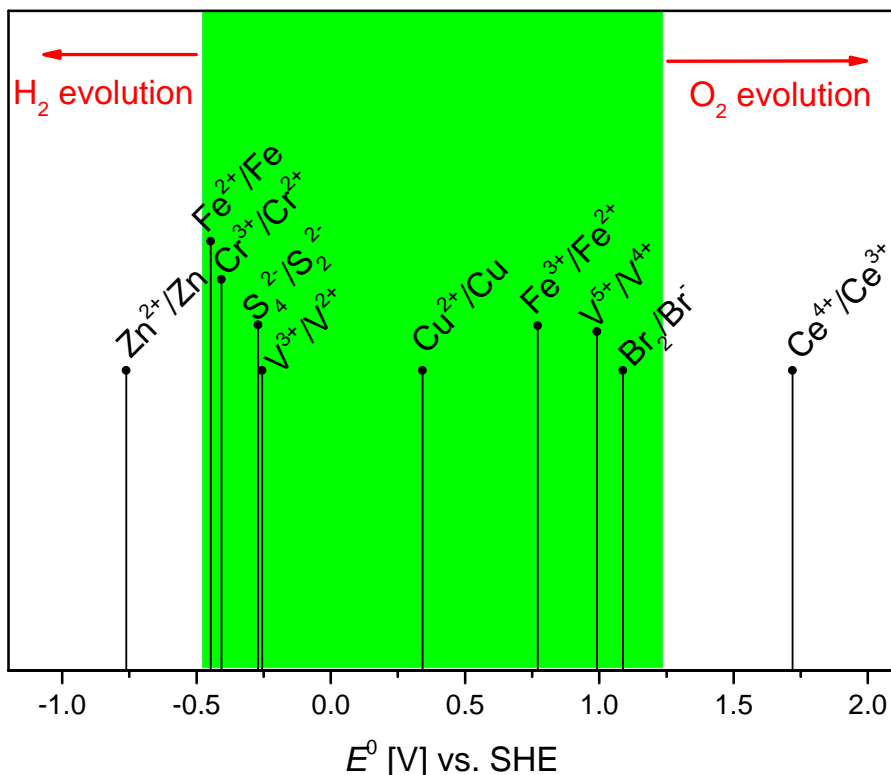


**Figure 7:** Standard potentials of redox couples in aqueous solutions as well as HER and OER on graphite electrodes (data from [47]; except  $S_4^{2-}/S_2^{2-}$ : [29]). The green area represents the viable potential window on graphite electrodes under consideration of overpotentials.

### 2.2.4 Cycle Life

The cycle life of a battery is the number of charge-discharge cycles that can be conducted until the battery reaches a defined minimum performance. This end-of-life

criterion is in most battery applications a minimal capacity that is retained (e.g. 60 % [39]). The cycle life depends on the cycling conditions, e.g. the charge/discharge current densities, the depth of discharge and the operation temperature [10]. In contrast to other types of batteries, most RFB exhibit a very high cycle life. Li-ion batteries have a rated cycle life of 4000-8000 cycles, Pb-acid batteries can be operated up to 3000 cycles and RFB are reported to perform for more than 13000 cycles [39]. In conventional batteries morphological changes occur during battery operation. This can cause the loss of electrical contact between active material and current collector which in turn results in a reduction of capacity. The origin is mechanical stress that occurs in the electrode during charging and discharging. In a “true” (i.e. only dissolved redox species) RFB the active species are present in dissolved state and hence are not prone to capacity loss due to morphological changes of the active material [38]. For the same reason, deep discharging of a RFB is unproblematic whereas in most other battery types this causes instantly a capacity decay [8].

### 2.2.5 Operation Temperature

The RFB should not exceed certain temperature limits as the solubility of active species in the electrolyte is temperature dependent. Therefore, some RFB require an active temperature management system which negatively influences the energy efficiency [21]. The operation temperature of a VRFB should not be lower than 10 °C (precipitation of  $V^{2+}$  and/or  $V^{3+}$  as oxides) and should not exceed 40 °C (precipitation of  $VO_2^+$  as  $V_2O_5$ ) [30]. An advantage of RFB is that the operation does not require high temperatures as this is the case with Na-S batteries [15].

### 2.2.6 Safety

An important criterion for storage technologies is its safety. High-temperature batteries such as Na-S batteries suffer from the ability to catch fire due to the presence of highly reactive molten sodium and molten sulfur. In 2011, a Na-S battery installed in Japan caught fire [48]. Similarly, several incidents with Li-ion batteries have been reported [49] and highlighted the need of safety considerations. High energy densities, thin separators and volatile, flammable solvents bear potential risks. A single defective cell can create excessive heat (e.g. due to a short-circuit) and provoke a so-called “thermal runaway” (self-accelerating process due to excessive heat released by exothermic reactions) of surrounding cells which can lead to fire or explosion of the battery pack [49].

RFB are intrinsically safe energy storage devices concerning fire or explosion events which is originated from their setup and components. Aqueous solutions and the high heat capacity thereof can act as cooling agent in case of heat release due to unwanted reactions. The external storage of the active material makes a dangerous side-reaction involving the total active material unlikely to happen [21].

However, many RFB employ acidic heavy metal containing electrolytes (e.g. vanadium ion containing electrolytes in VRFB) and thus leaking of the battery or spilling of the electrolyte could occur [38]. Due to environmental and health concerns, heavy metals should not escape from the systems. Likewise, in RFB employing the  $\text{Br}^-/\text{Br}_3^-$  redox couple it needs to be ensured that no toxic  $\text{Br}_2$  is released. These safety hazards can be tackled by sophisticated sealing strategies to avoid leakages and an extra surrounding dike to prevent electrolyte from leaving the battery.

### 2.2.7 Costs

Besides technological features, the costs of a storage technology for stationary application is generally the main criterion for market penetration. Common types of cost are the investment costs per power [ $\text{k}\$ \cdot \text{kW}^{-1}$ ], investment costs per capacity [ $\$ \cdot \text{kWh}^{-1}$ ] and the costs per capacity and per cycle number [ $\$ \cdot (\text{MWh} \cdot (\text{total number of cycles}))^{-1}$ ]. The latter number also takes into account the cycle life of the specific system, therefore it represents the costs per capacity over the lifetime of the battery. Tab. 1 compares the costs of several energy storage devices.

**Table 1:** Costs of different electricity storage devices [39]. URFC = unitized regenerative fuel cell; PHS = pumped hydro storage; CAES = compressed air energy storage.

system	power costs [ $\text{k}\$ \cdot \text{kW}^{-1}$ ]	capacity costs [ $\$ \cdot \text{kWh}^{-1}$ ]	cycle costs [ $\$ \cdot (\text{MWh} \cdot \text{cycle})^{-1}$ ]
PHS	0.4-5.6	10-350	0.5-3
CAES	1.7-2.2	130-550	4-18
VRFB	3.2	900	$\ll 70$
Li-ion	3-4	600	150-200
Na-S	3.5	550	90-130
Pb-acid	4.6	130	150
URFC	17	>10000	200

The modular setup of RFB allows easy assembling especially in comparison to other battery types. A cell-making process like in Li-ion batteries which can account

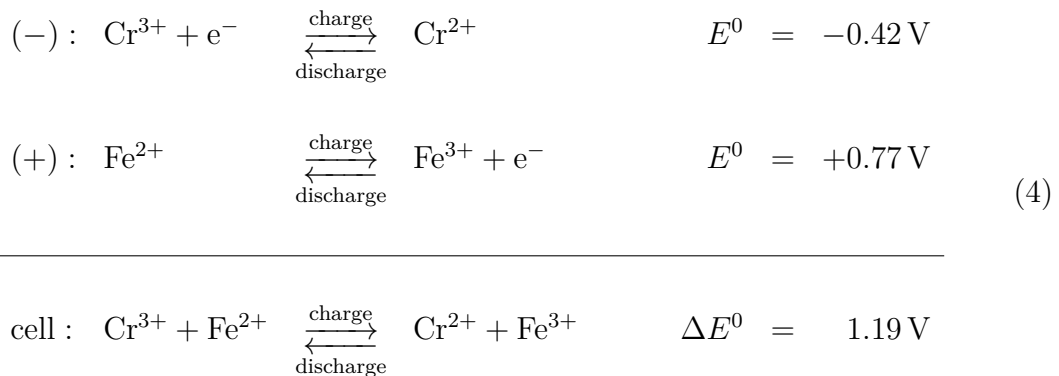
for a substantial amount of the final battery cell costs (e.g. the active material makes up less than 50 % of the cell costs in Li-ion batteries [21]) is not necessary.

RFB are interesting especially for large capacities but moderate power because costs per kWh do not increase linearly unlike in other battery technologies. The comparison in Tab. 1 reveals that in terms of power costs and cycle costs RFB are more expensive than PHS and CAES but cheaper than other storage technologies such as Li-ion or Pb-acid batteries. However, PHS and CAES are subject to geological and geographical restrictions. Thus, RFB can compete with existing storage technologies, especially when distinguishing between initial investment costs and “life-time” costs. Additionally, recent costs analysis of VRFB predict even lower investment costs as the values given in Tab. 1. Crawford et al. [50] estimate the costs for a VRFB with a capacity of 4 times the rated power to be less than 350 \$·kWh<sup>-1</sup> and predict that optimization and economies of scale can reduce the investment costs down to 160 \$·kWh<sup>-1</sup>.

## 2.3 Types of Redox Flow Batteries

### 2.3.1 Iron-Chromium

The iron-chromium RFB was one of the first intensively investigated RFB. Judging by cost and availability of the redox species as criteria, the Fe<sup>2+</sup>/Fe<sup>3+</sup>//Cr<sup>2+</sup>/Cr<sup>3+</sup> system was identified by researchers of the NASA as the most promising one [15].



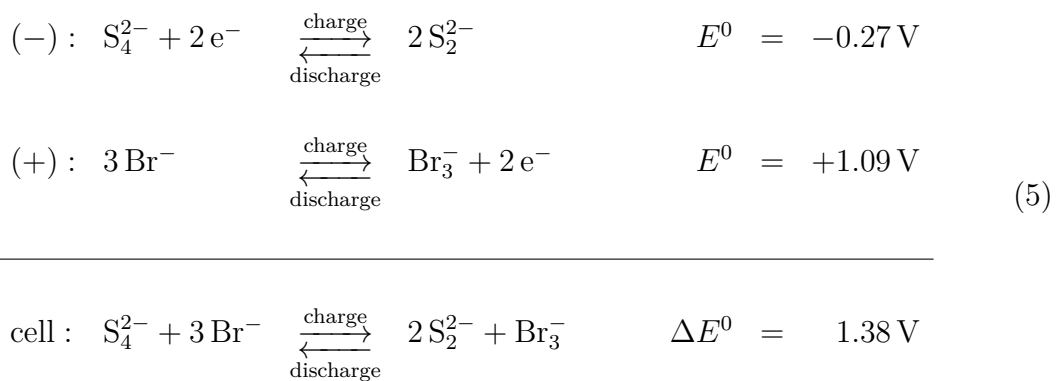
The iron-chromium RFB suffers from ion crossover through the membrane and thereby induced capacity decay [21] as well as poor electrochemical reversibility of the chromium reaction [30]. Additionally, the very negative standard potential of

$\text{Cr}^{2+}/\text{Cr}^{3+}$  leads to a high rate of HER as a parasitic side reaction [21].

The problem of capacity decay due to crossover can be tackled by intentionally premixing the chromium and iron containing electrolytes, however, this approach is accompanied by the need of additional amounts of iron and chromium not usable for energy storage [30]. For practical applications, the electrochemical reaction kinetics of the chromium redox couple need to be enhanced by application of catalysts. Lead and alloys of lead with noble metals are well suited for this purpose and these materials additionally increase the overpotential for hydrogen evolution, thus leading to reduced side reactions [19]. Remaining challenges are the really low specific energy of the iron-chromium RFB of less than  $10 \text{ Wh}\cdot\text{kg}^{-1}$  and the need of noble metals for the catalyst alloys [30]. Nevertheless, the US company EnerVault recently installed a 250 kW/1 MWh iron-chromium RFB in the USA [31].

### 2.3.2 Polysulfide-Bromine

The polysulfide-bromine RFB does not utilize any metals as redox active species but abundant sulfur and bromine are the basis for the redox couples. This latter fact and the high solubility of the redox couples make this RFB promising concerning the capacity-related costs [29]. However, the reversibility of the reactions on cheap carbon electrodes is quite low. Therefore, cobalt or nickel electrodes are used as the negative electrode for enhancing the reaction rates of the redox couple  $\text{S}_4^{2-}/\text{S}_2^{2-}$  [19]. The polysulfide-bromine RFB also suffers from capacity fading induced by crossmixing of the electrolytes through the membrane [30]. Beyond that, formation of poisonous  $\text{Br}_2$  and  $\text{H}_2\text{S}$  needs to be prevented [15].

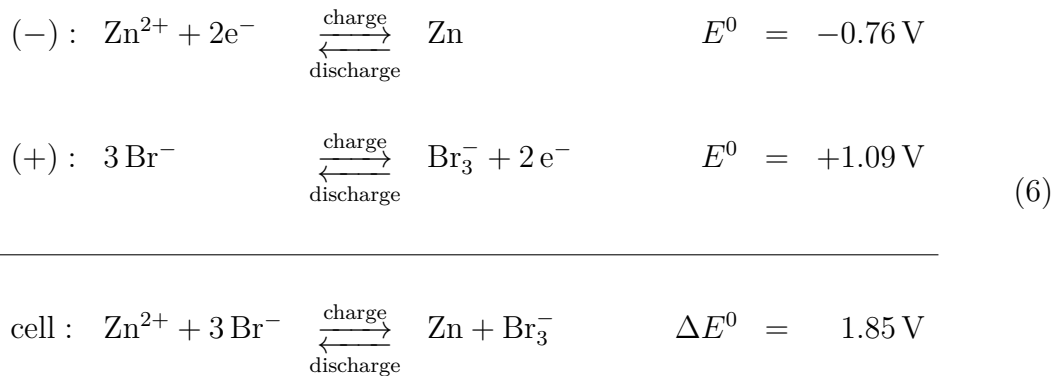


The polysulfide-bromine RFB was developed for commercialization by the company Regenesys Technologies Ltd. between 1991 and 2004 and a 1 MW test facility was

operated [30, 51]. The reported energy density for the system was 20-30 Wh·L<sup>-1</sup> [30]. However, Regenesys stopped its activities in 2003 [31]. In a technological-economic analysis of a polysulfide-bromide RFB the authors concluded that a significant enhancement of the electrochemical rate constants is necessary to be able to operate this storage technology economically [52]. Up to date, polysulfide-bromide RFB are not commercially available.

### 2.3.3 Zinc-Bromine

The zinc-bromine RFB is a so-called *hybrid* redox flow system, i.e. not all species of the redox couples are present in dissolved state [15]. During charging, the zinc cation is reduced to elemental zinc metal in the negative electrode compartment. Due to the involvement of a solid species, there is no limitation concerning solubility and higher energy densities are possible compared to conventional redox flow batteries. The theoretical specific energy is 440 Wh·kg<sup>-1</sup> while in practical applications 65-75 Wh·kg<sup>-1</sup> have been demonstrated [30].



Similar to the polysulfide-bromine RFB, precautions are required against the release of toxic Br<sub>2</sub>. In technical application, this issue is tackled by using complexing agents and/or an additional organic solvent which stabilizes the bromide complexes [31]. Another obstacle is the self-discharging due to bromine crossover and its subsequent reaction with the zinc [30]. Nevertheless, an energy efficiency of 80 % was reported for a zinc-bromine RFB [14]. The most important issue is the dendrite growth of zinc during deposition which can lead to internal electrical shorting [21]. Despite of these challenges, the zinc-bromine RFB represents a relatively mature technology and is produced and sold by companies, e.g. RedFlow Ltd. in Australia and Primus Power in the USA [31].

### 2.3.4 All-Vanadium

Inter-crossover of species between the half-cells is a common issue in RFB because it leads generally to a capacity decay and hence limited lifetime of the battery. Employing redox couples based on the same element in different oxidation states, ion crossover only leads to lowered cycle efficiency but not to capacity fading. As such, the VRFB in which all active species are based on the element vanadium is a very promising technology (Fig. 8).

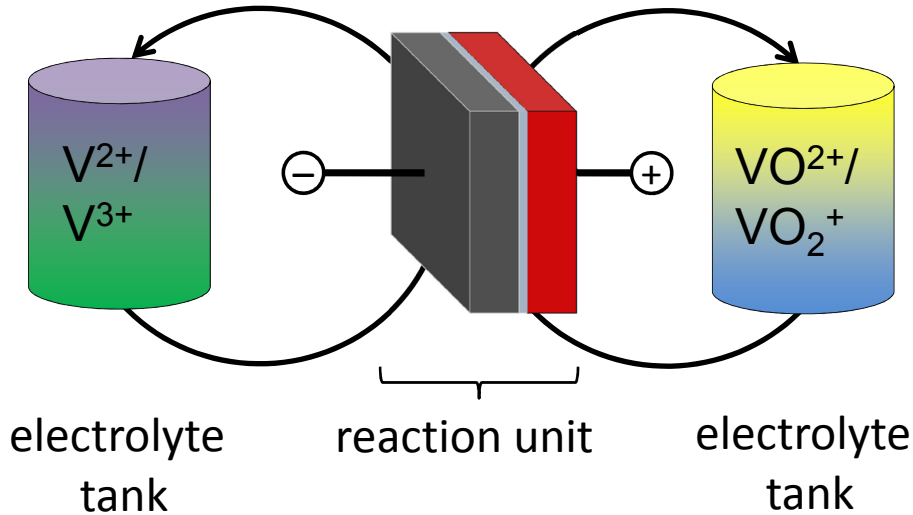
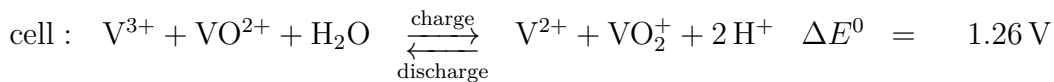
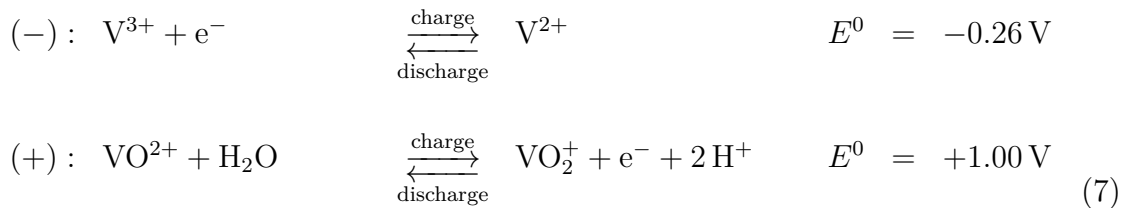


**Figure 8:** Schematic of the VRFB.



Unlike other RFB, the VRFB does not need any catalysts or special electrode materials as both half-cell reactions proceed with acceptable rates on activated carbon felts [30]. The absence of catalysts reduces costs and therefore enhances the commercial viability of the system. Another advantage, particular in comparison to

zinc-bromine RFB, is the low gas evolution rate [30]. Gas evolution in one electrode compartment leads to inequality of the capacities of the two electrolytes. As the electrolyte with the lowest capacity is limiting the overall battery capacity, gas evolution induces a capacity decay due to imbalance of electrolytes.

A disadvantage of the VRFB is the presence of vanadium in the oxidation state +5. This vanadium species is corrosive which needs to be considered for the material selection for VRFB [30]. The solubility of the vanadium species in the sulfuric acid containing electrolyte is limited and temperature-dependent. As already described above, the upper temperature limit is caused by precipitation of  $\text{VO}_2^+$  as  $\text{V}_2\text{O}_5$ . One of the main drawbacks of the VRFB is the low specific energy of  $25\text{-}30 \text{ Wh}\cdot\text{kg}^{-1}$  [30] and energy density of  $25\text{-}30 \text{ Wh}\cdot\text{L}^{-1}$  [8]. The VARFB which is the focus of this thesis (PUBLICATIONS I-III) aims to overcome the two main disadvantages of the VRFB: The temperature window will be enlarged due to elimination of the  $\text{VO}^{2+}/\text{VO}_2^+$  couple and the theoretical energy density and specific energy is increased substantially.

## 2.4 Concepts for Increased Energy Density

### 2.4.1 Non-Aqueous Electrolytes

Recent research trends in the field of RFB are the utilization of non-aqueous electrolytes for enhancing the possible potential window [14, 21]. Ionic liquids (IL) for example have the potential for electrolytes with increased energy density. However, up to date the reported solubilities of redox couples in non-aqueous electrolytes are quite low ( $<1.0 \text{ mol}\cdot\text{L}^{-1}$ ) [14, 53]. Additionally, non-aqueous RFB systems have low coulombic efficiencies ( $< 90 \%$ ) and high electrolyte and membrane resistances [31]. Therefore, non-aqueous RFB systems do not yet compete with conventional, aqueous systems in terms of energy density [21, 53]. In addition to the described limitations, the use of non-aqueous solvents would substantially increase the costs of RFB [31] and involve new safety issues (e.g. flammability of the solvents).

### 2.4.2 Additives

Common additives in many aqueous RFB electrolytes are acids to improve the (ionic) conductivity and in some cases to prevent the dissolved active species from precipitation. For instance, in VRFB sulfuric acid or mixed sulfuric acid and hydrochloric acid electrolytes are employed [16–20] and in iron-chromium RFB

electrolytes hydrochloric acid is used [30]. However, concentrations of solutes in aqueous electrolytes investigated for relevant RFB systems generally do not exceed  $2.0 \text{ mol}\cdot\text{L}^{-1}$  [54]. Various additives were investigated for enhancing the solubility of different redox couples with a focus on the  $\text{VO}^{2+}/\text{VO}_2^+$  redox couples employed in the VRFB [20, 55–59]. The stability of highly concentrated vanadium electrolytes can be enhanced by additives such as methyl orange or polyvinyl alcohol [17, 19]. However, the solubility of vanadium salts is limited to  $2.5\text{--}3.0 \text{ mol}\cdot\text{L}^{-1}$  even with additives [19, 31] Thus, the possible energy density using additives is not substantially high. Additionally, additives can lead to new problems, e.g. possible evolution of poisonous chlorine when using chloride additives or new side reactions when using organic additives which can be oxidized by vanadium(V) [19].

### 2.4.3 Hybrid Redox Flow Batteries

Hybrid redox flow batteries are distinguished from conventional flow batteries in the way that at least one of the involved redox active species is not present in dissolved or liquid form but is a gas or a metal [21, 31, 38].

Hybrid RFB involving metal deposition such as the zinc-bromine RFB promise higher energy densities compared to conventional RFB due to the occurrence of a solid metal (high density) as active species. The most developed and commercially available hybrid RFB is the zinc-bromine RFB [29]. However, the metal deposition and dissolution which occurs in most hybrid RFB is challenging because of dendrite growth [21] which can lead to failure due to short-circuiting. Additionally, the zinc-bromine RFB suffers from high self-discharge and low energy efficiency as already mentioned above [14]. Other examples for hybrid RFB involving metal deposition are the flowing lead acid RFB [38], the all-copper RFB [31] or the all-iron RFB [19]. Alternative concepts for hybrid redox flow batteries are proposed with lithium as an active species [19, 21]. Energy densities of up to  $100 \text{ Wh}\cdot\text{L}^{-1}$  and specific energies of up to  $100 \text{ Wh}\cdot\text{kg}^{-1}$  are predicted for RFB containing solid/semi solid slurries [14]. However, these systems are all in the state of early fundamental research and far away from commercial viability.

An example for a hybrid flow battery involving a gaseous redox active species is the hydrogen-bromine RFB which has a cell voltage of  $\Delta E^0 = 1.09 \text{ V}$  [19] and a high theoretical specific energy ( $353 \text{ Wh}\cdot\text{kg}^{-1}$  [31]). However, the energy density (in  $\text{Wh}\cdot\text{L}^{-1}$ ) of the system strongly depends on the way of hydrogen storage (e.g. in pressurized form). Other issues occurring in hydrogen-bromine RFB are the crossover of bromine species [60], the oxidation of carbon electrodes and the dissolution of the

platinum catalyst [61].

In terms of energy density and specific energy, the VARFB represents the most promising hybrid RFB using gaseous compounds. It is described and discussed in detail in chapter 3 and is the subject of PUBLICATIONS I-III.

# 3 Vanadium-Air Redox Flow Batteries

## 3.1 Introduction and State of the Art

The VARFB can be regarded as a combination of the negative half-cell of a VRFB (redox couple:  $V^{2+}/V^{3+}$ ) and the positive half-cell of a URFC (redox couple:  $O_2/H_2O$ ). It can also be considered as a URFC with vanadium species as “fuel”. From the latter perspective, the VARFB has the advantage that no storage of hydrogen is necessary as it is the case in a conventional (i.e.  $H_2/O_2$ ) URFC. Such a URFC has a very low energy density if the hydrogen is stored at ambient pressure, whereas compression of the hydrogen leads to energy losses. In the VARFB there is no need for storing gas as oxygen is provided by ambient air. The reactions occurring in the VARFB and their standard potentials are given in Eq. 8. The general setup of the VARFB is depicted in Fig. 9.

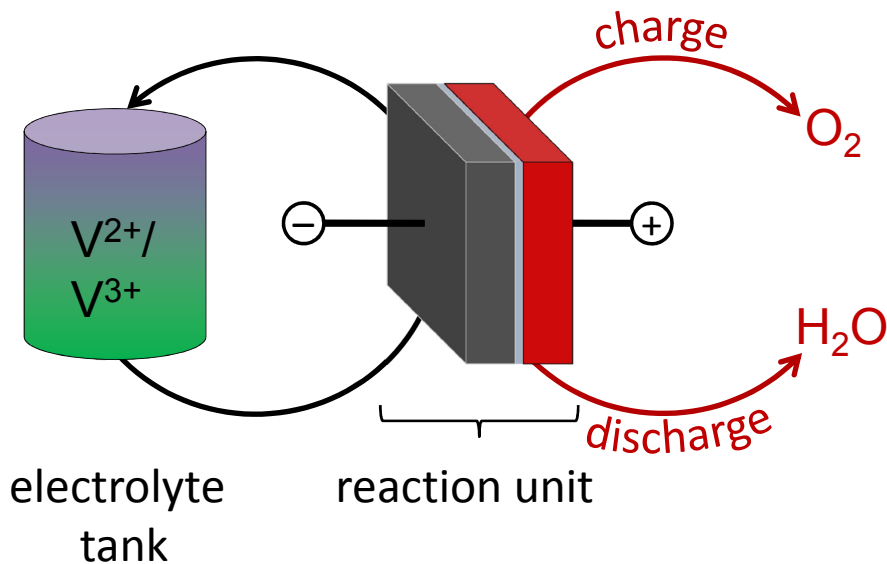
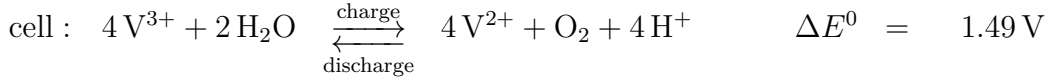
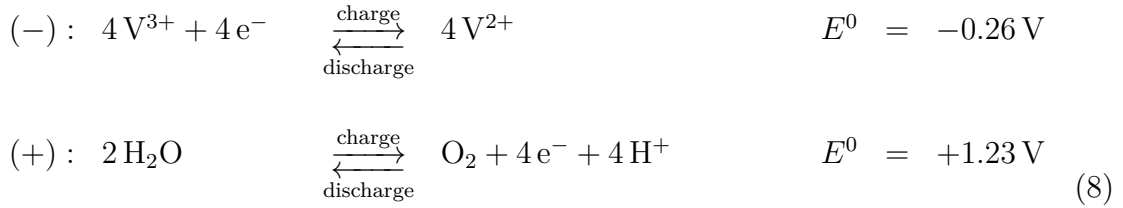


Figure 9: Schematic of the VARFB.



The VARFB system has a significantly increased theoretical (i.e. thermodynamic) energy density and specific energy in comparison to VRFB. The standard cell potential of the VARFB is 18 % higher than that of the VRFB ( $\Delta E_{\text{VRFB}}^0 = 1.26 \text{ V}$  vs.  $\Delta E_{\text{VARFB}}^0 = 1.49 \text{ V}$ ). Thus, the theoretical energy density and specific energy are increased by 18 % assuming that mass and volume of the two systems are equal. Furthermore, in the VARFB one electrolyte tank is virtually eliminated. The oxygen consumed at the positive electrode during discharging is provided by the ambient air and thus no storage is needed. The water split during charging occupies a negligible volume. In relation to the volume of the negative electrolyte with a vanadium concentration of  $c_{\text{V}} = 1.5 \text{ mol}\cdot\text{L}^{-1}$ , the volume of water needed for OER is only approx. 1.3 %<sup>1</sup>. Assuming a VARFB with high capacity and low power and hence small and light reaction unit in comparison to the volume and mass of the electrolytes, the saving of one electrolyte tank yields almost a doubling of energy density and specific energy. Hence, the overall theoretical energy density and specific energy of a VARFB is about 2.39 times the one of a VRFB ( $\Delta E_{\text{VARFB}}^0 = 1.18 \cdot \Delta E_{\text{VRFB}}^0$ ; factor two due to elimination of one electrolyte tank).

However, it should be mentioned that the *practical* energy density and specific energy is lower than the theoretical values discussed above. The major reasons are the high overpotentials of OER and oxygen reduction reaction (ORR). Therefore, the practical cell potential will deviate from the thermodynamic value of 1.49 V. Nevertheless, the practical energy density and specific energy will increase significantly due to the massive reduction of electrolyte.

---

1

$$\begin{aligned}
 \text{reaction ratio:} & \quad n_{\text{V}^{3+}} : n_{\text{H}_2\text{O}} & = & \quad 2 \text{ mol} : 1 \text{ mol} & & \text{(see Eq. 8)} \\
 \text{concentration ratio:} & \quad c_{\text{V}^{3+}} : c_{\text{H}_2\text{O}} & = & \quad 1.5 \text{ mol}\cdot\text{L}^{-1} : 55.6 \text{ mol}\cdot\text{L}^{-1} \\
 \Rightarrow \text{volume ratio:} & \quad V_{\text{V}^{3+}} : V_{\text{H}_2\text{O}} & = & \quad 1 \text{ L} : 0.0134 \text{ L}
 \end{aligned}$$

The increase of energy density and specific energy is the main motivation for the development of a VARFB. Additionally, the VARFB bears further benefits in comparison to VRFB. In the positive electrolyte of a VRFB vanadium occurs as  $\text{VO}_2^+$  (oxidation state +5). The avoidance of this vanadium species in the VARFB is advantageous as on the one hand vanadium(V) is suspected to be carcinogenic [62, 63] and on the other hand the precipitation of  $\text{VO}_2^+$  as  $\text{V}_2\text{O}_5$  is the reason for the upper temperature limit of the VRFB [38]. Thus, the VARFB has no upper temperature limit due to the absence of  $\text{VO}_2^+$ .

There are not many publications that deal with the VARFB. It was first described in a patent by Kaneko et al. in 1992 [24]. Operation tests were performed using two different reaction units for charging and discharging. An experimental study of a VARFB employing two different hot-pressed membrane electrode assemblies (MEA) with titanium electrodes was published by Hosseiny et al. [23]. Menictas et al. [26] and Noack et al. [25] reported the performance data of a VOFC.

In this monodirectional device only the discharge process of a VARFB is conducted. Furthermore, the VOFC was modeled by Wandschneider et al. [64]. Other publication only mentioned the VARFB but did not provide any results or data on the system [65–67]. Until today, there is only a scarce number of publications about VARFB and the results are insufficient. For instance, Hosseiny et al. [23] achieved an energy efficiency of 26.67 % at 40 °C operation temperature and at the low current density of  $0.24 \text{ mA}\cdot\text{cm}^{-2}$ . Likewise, Kaneko et al. [24] reported an energy efficiency of only  $\eta_E = 27.4 \%$  ( $50 \text{ mA}\cdot\text{cm}^{-2}$  charging current density;  $10 \text{ mA}\cdot\text{cm}^{-2}$  discharge current density; 25 °C). Thus, the aim of this thesis is to contribute to the investigation and improvement of the VARFB performance and to develop a more compact VARFB employing a unitized reaction unit.

## 3.2 Contributions within this Thesis

### 3.2.1 Unitized Vanadium-Air Redox Flow Battery Setup

In the aforementioned publications, only monodirectional (i.e. only charging or discharging) systems such as the VOFC [25, 26, 64] or bidirectional systems utilizing separated charge-discharge units [23, 24] were presented. These systems have the disadvantage that either a fully reversible battery operation is not possible (monodirectional systems) or two different reaction units are necessary which increases the costs, volume and mass of the system. Due to these reasons, a combined or uni-

tized bidirectional VARFB is desirable. In PUBLICATION I (“Study of an unitised bidirectional vanadium-air redox flow battery comprising a two-layered cathode”) a novel VARFB with a combined reaction unit is described and the performance is investigated at different operation conditions. An arrangement of the positive electrode was presented in which both OER and ORR can be conducted. The challenge for this setup are the opposite requirements for ORR and OER: While the ORR is catalyzed by Pt and the electrode should be hydrophobic to repel produced water and avoid clogging of the electrode, the OER is catalyzed best by IrO<sub>2</sub> and the electrode material should be hydrophilic. These contradictory demands were overcome by using a two-layered electrode setup. One layer consisted of a hydrophilic, IrO<sub>2</sub>-modified graphite felt for the OER, the other layer was a hydrophobic gas diffusion layer decorated with platinum supported on carbon black (Pt/C) and Nafion ionomer similar as it is used in proton exchange membrane fuel cells (PEMFC).

These two electrode layers were assembled in the test cell and compressed between membrane and current collector, i.e. no hot-pressing was necessary. This is advantageous as both Hosseiny et al. [23] and Menictas et al. [26] used MEAs obtained via hot-pressing of the gas diffusion electrodes (GDE) with the membrane and Menictas et al. [26] reported about serious issues with the detachment of the GDE due to swelling of the membrane. A detachment of the catalyst layer of a catalyst-coated membrane during VOFC operation was also reported by Noack et al. [25]. The hot-pressing technique of MEAs is well-known and established in the area of PEMFC. However, in contrast to PEMFC, the MEA used in a VARFB is in contact with liquid aqueous solutions and thus swelling of the membrane is more pronounced. Generally, membranes become dry during hot-pressing and therefore the swelling due to water uptake from the aqueous electrolyte can be significant. An additional concern is that a MEA for a VARFB does not contain a GDE on both sides but only on one side. The other electrode is in general a porous, compressible graphite felt. Thus, equally distributed and sufficient pressure on both sides of the MEA is more difficult to achieve in a VARFB than in PEMFC. This promotes delamination of the catalyst layer and/or GDL in VARFB. Due to the problems arising from utilizing hot-pressed MEAs, a new approach was sought in this thesis that avoids the use of an unsymmetrical hot-pressed MEA. A two-layered positive electrode obtained without the need of hot-pressing was presented in PUBLICATION I. Moreover, the straightforward preparation of the IrO<sub>2</sub>-modified graphite felt and its characterization was shown in PUBLICATION I followed by the performance analysis of the VARFB. Half-cell potentials were recorded during operation with an integrated

dynamic hydrogen electrode and the behaviour at different current densities and over several cycles was evaluated. With the presented setup a maximum energy efficiency of 42 % was achieved ( $j = 20 \text{ mA cm}^{-2}$ , room temperature) which is the highest value reported for a VARFB operated at room temperature. A performance decrease in terms of coulombic and voltaic efficiency was observed during cycling and it was hypothesized that crossover of vanadium species and corrosion of carbon materials are the reasons for performance decay.

### 3.2.2 Investigation of Membrane Transfer Processes

The identification and quantification of unwanted membrane transfer processes as possible reasons for the losses in coulombic efficiency and capacity during VARFB cycling are presented in PUBLICATION II (“Investigation of crossover processes in a unitized bidirectional vanadium/air redox flow battery”). These investigations are the basis for optimization strategies of the VARFB system. Up to date, there were only suppositions and hypotheses about possible loss mechanisms in a VARFB but no experimental investigation and quantification. For instance, Hosseiny et al. [23] suspected permeation of dissolved oxygen which was produced during charging to be the major cause of efficiency losses. Therefore, MEAs with different morphology of the titanium electrode (mesh and sintered material, respectively) were used to avoid trapping of oxygenated water in the electrode and its subsequent permeation through the membrane. Menictas et al. [26] concluded that oxygen permeation would only play a minor role in a VOFC as they observed a high utilization of active material (i.e.  $\text{V}^{2+}$  electrolyte). This is not in contradiction to the observation of Hosseiny et al. [23] as they presumed the oxygen produced during *charging* to undergo permeation while Menictas et al. [26] conducted only the *discharging* reaction of a VARFB in the investigated VOFC. Permeation of  $\text{O}_2$  was not mentioned in other publications (e.g. Noack et al. [25], Wandschneider et al. [64] and Kaneko et al. [24]). However, due to initial experiments conducted in the course of this thesis, oxygen permeation was suspected to be a relevant phenomenon and this hypothesis was investigated in PUBLICATION II.

Besides oxygen permeation, other processes and side reactions such as hydrogen evolution, crossover of  $\text{V}^{2+}$  and/or  $\text{V}^{3+}$  from the negative to the positive electrode can be imagined to occur. Therefore, a combination of analysing methods was employed in PUBLICATION II. An experimental setup was designed in order to monitor the concentrations of  $\text{V}^{2+}$  and  $\text{V}^{3+}$  in the negative electrolyte *in situ* during the VARFB operation using UV/Vis spectroscopy with a flow-through cuvette.

Additionally, the vanadium concentration of the initially vanadium-free positive electrolyte was determined after charging and discharging with ICP-MS to quantify the vanadium crossover from the negative to the positive electrode. These data combined with *ex situ* determinations of diffusion coefficients of  $V^{2+}$  and  $V^{3+}$  through Nafion 117 (N117) membranes revealed the relation of the different loss mechanisms to each other and the differentiation between diffusional vanadium crossover and migrational/electroosmotic crossover. It was found that oxygen permeation rather than vanadium ion crossover is the major cause for lowered coulombic efficiency. During operation with  $j = 20 \text{ mA}\cdot\text{cm}^{-2}$  the vanadium crossover causes at most 20 % of the coulombic efficiency losses. The share of 58 % of the vanadium crossover is due to diffusion and consequently 42 % is related to migration/electroosmosis.

However, the most severe challenge of VARFB is the crossover of vanadium. It is described as an issue or possible issue in several of the publications that deal with VARFB or related systems [26, 64–69]. The considerable amount of 6 % of the vanadium species initially present in the negative anolyte underwent crossover during a cycle as presented in PUBLICATION II. In contrast to VRFB where vanadium crossover induces only a lowered coulombic efficiency, this process leads to a capacity fade and therefore limited lifetime of the VARFB. Hence, it is crucial to minimize the crossover of vanadium species for the long-term operability of the VARFB.

### 3.2.3 Membrane Modification for Enhanced VARFB Performance

In PUBLICATION III (“Layer-by-layer modification of Nafion membranes for increased life-time and efficiency of vanadium/air redox flow batteries”) a conventional proton exchange membrane (N117) is modified for improving the membrane performance concerning vanadium crossover and oxygen permeation and hence enabling a performance enhancement of the VARFB. This modification was carried out with a LbL deposition of polyelectrolytes. The LbL technique allows the convenient application of very thin multiple layers of oppositely charged polyelectrolytes on a substrate. Several properties of a substrate such as gas permeability and multivalent ion transfer rate can be tuned with the deposition of polyelectrolyte multilayer films. A modification of Nafion membranes with polyelectrolyte multilayers for reduced transfer rates of both multivalent ions and gases but maintained sufficient proton conductivity has not been reported before. The thin multilayers investigated in PUBLICATION III consisted of polyethylenimine (PEI) and Nafion ionomer. PEI

was chosen because it was used in LbL films to successfully reduce multivalent ion crossover and increase the selectivity towards  $H^+$  [70–72]. Nafion ionomer was employed as polyanion due to its advantageous properties such as chemical stability and high proton conductivity and because it was also used as substrate material. However, properties of this pair of polyelectrolytes have not been described yet in literature. The modification lead to reduced vanadium crossover and oxygen permeation but also to a decreased proton conductivity. The influence of the number of bilayers on the aforementioned properties was studied and the optimum was identified. The application of a N117 membrane modified with 10 bilayers of PEI/Nafion (denoted as “N117-(PEI/Nafion)<sub>10</sub>”) in a VARFB resulted in 13 % less oxygen permeation in comparison to unmodified membranes. Even more important, the vanadium crossover was reduced by 70 % during a cycle in comparison to an unmodified N117 membrane. This reduction is important for increased life-time of the VARFB as described above. Additionally, the coulombic efficiency during VARFB operation was increased by 12 % (N117:  $\eta_C = 81\%$ , N117-(PEI/Nafion)<sub>10</sub>:  $\eta_C = 93\%$ ) and the energy efficiency by 3.7 % (N117:  $\eta_E = 41.5\%$ , N117-(PEI/Nafion)<sub>10</sub>:  $\eta_E = 45.2\%$ ) while the voltaic efficiency was reduced by 2.5 % due to lowered proton conductivity. Thus, the modified membranes are promising concerning prolonged lifetime of the battery and improved energy and coulombic efficiency.

## 3.3 Author Contributions to Publications I-III

Publications in peer-reviewed journals are typically collaborative efforts. This applies to the PUBLICATIONS I-III of this thesis as well. The individual contributions of the author of this thesis are described below.

### 3.3.1 Publication I

The **idea** for the investigation of the presented system was a collaborative work of Eva-Maria Hammer, Lidiya Komsiyaska and the first author (author of this thesis). Most of the **conception/design of the experiments** was done by the first author while the co-authors gave input and advice for specific experimental questions. The two-layered cathode setup was the idea of the first author. The **conduction of the experiments** was mainly done by the first author. Exceptions are the construction of the test cell (in cooperation with Hayo Seeba and Dietmar Piehler), the preparation of some of the  $IrO_2$ -modified graphite felts used in the study (Andrea Ballarin), protonation of some of the membranes (Benedikt Berger), design and construction

of the dynamic hydrogen electrode (Frank Bättermann), X-ray diffraction (XRD) measurements (Martin Knipper) and ICP-MS sample preparation and analysis (Dana Schonvogel). All **data analysis** was done by the first author. The initial **composition of the manuscript** was performed together with Lidiya Komsiyyska and Carolina Nunes Kirchner. The **manuscript writing** was done by the first author with revisions, suggestions and corrections from all co-authors.

### 3.3.2 Publication II

The **idea** for this publication was from Carolina Nunes Kirchner, Lidiya Komsiyyska and the first author. The **conception/design of the experiments** was done by the author, except for the suggestion to incorporate the determination of diffusion coefficients (Gunther Wittstock). The **experiments** were conducted by the first author apart from a pre-study on the calibration of UV/Vis spectroscopy (Timo di Nardo) and ICP-MS analysis of prepared samples (Dana Schonvogel). All **data analysis** was performed by the first author. The initial **composition of the manuscript** was done by the first author. The **manuscript** was **written** by the first author with revisions, suggestions and corrections incorporated from all co-authors.

### 3.3.3 Publication III

The **idea** for this publication was from the first author. The **conception/design of the experiments** was planned by the first author apart from the suggestion to include TGA measurements in the study (Lidiya Komsiyyska). **Experiments** were performed by the first author, exceptions are initial experiments related to the polyelectrolyte deposition routine (Khrystyna Yezerska), the thermogravimetric analysis (TGA) measurements (Pratik Das), parts of the scanning electron microscopy (SEM) measurements and parts of the determinations of the diffusion coefficients (Benedikt Berger) and ICP-MS analysis of prepared samples (Dana Schonvogel). All **data analysis**, the initial **composition of the manuscript** and the **manuscript writing** were done by the first author. All co-authors contributed with suggestions and corrections to the (internal) revision of the manuscript.

## 4 Conclusion and Outlook

The aim of this thesis was to construct, characterize and optimize a unitized VARFB employing a single reaction unit for charging and discharging which had not been described in literature before. For this purpose, a new VARFB test cell was engineered comprising a two-layered cathode. The performance was assessed at different current densities (PUBLICATION I). With the presented setup an energy efficiency of 42 % was achieved at a current density of  $20 \text{ mA}\cdot\text{cm}^{-2}$  and at room temperature which is higher than the efficiency reported for non-unitized VARFB by Hosseiny et al. [23] and Kaneko et al. [24]. Consecutive charging-discharging cycles were conducted which revealed a performance decay due to capacity losses. Transfer processes through the membrane were suspected to diminish the efficiency and lifetime of the battery. The transfer reactions were studied in PUBLICATION II applying *in situ* UV/Vis spectroscopy of the negative electrolyte to monitor the concentrations of  $\text{V}^{2+}$  and  $\text{V}^{3+}$  during VARFB operation. To allow the identification and quantification of side reactions, these results were combined with the determination of the total vanadium crossover by ICP-MS analysis of the positive electrolyte. Oxygen permeation and vanadium crossover were ascertained as the major reason for the coulombic efficiency losses. Moreover, vanadium crossover leads to a limited life-time of the VARFB due to a continuous loss of capacity. During the studied cycle, a considerable amount of 6 % of the vanadium in the negative electrolyte underwent crossover. To achieve a reduction of the vanadium crossover, a novel modification routine of the membrane with thin layers of polyelectrolytes was studied in PUBLICATION III. The modification of N117 consisted of a layer-by-layer film of 10 bilayers of PEI and Nafion ionomer. It resulted in significantly reduced vanadium crossover (-70 %) and oxygen permeation (-13 %) in comparison to unmodified N117 which is advantageous for enhanced efficiency and life-time of the VARFB. In summary, a new unitized bidirectional VARFB system was established and analyzed in the course of this thesis. Based on this analysis, significant improvements of the performance could be demonstrated in comparison to the state of the art.

The obtained results might also be relevant for and applicable to other electro-

chemical systems. For instance, the issue of crossover is also known for VRFB, microbial fuel cells and direct methanol fuel cells. The membrane modification routine presented in this thesis can be applied to improve the performance of the aforementioned systems. Due to the identical reactions in the positive half-cell of a VARFB and unitized regenerative fuel cell (URFC), the positive electrode setup presented in this thesis might also be interesting for a URFC setup. However, the compatibility of the used polyelectrolytes with the aforementioned systems would need to be evaluated.

Not all open research questions were addressed in this thesis and some of them are described below.

The investigation of the corrosion stability of components employed in the reaction unit needs to be further evaluated. Half-cell potentials of more than 1.5 V vs. SHE are present at the positive electrode during charging, thus corrosion of carbon materials or of the Pt/C catalyst might occur. These degradation processes are suspected to have an impact on the long-term stability of the performance of the VARFB. Thus, further investigations in this direction are needed for the evaluation of the system.

As mentioned in this thesis, the costs of electrical storage system for stationary purposes are crucial. As such, expensive materials need to be avoided. In the presented VARFB setup precious metal catalysts such as IrO<sub>2</sub> and Pt were employed. For the viability of the VARFB as a stationary storage device, these catalysts need to be replaced by cheaper, non-noble metal catalysts. There are reports in literature about bidirectional oxygen catalysts that enhance both oxygen reduction reaction as well as oxygen evolution reaction (e.g. N-doped graphene [73]). A VARFB employing alternative catalysts which are not based on noble metals would be desirable.

Another influence that affects especially the voltaic efficiency of the VARFB requires further investigation. Both OER and ORR are subject to slow kinetics which is reflected in the overpotentials that are present during charging and discharging. The operation of the VARFB at higher temperatures enhances the kinetics of ORR and OER and thus lowers overpotentials. This would result in higher voltaic efficiencies and hence higher energy efficiency. However, a contrary effect might be an increased rate of vanadium crossover and/or oxygen permeation at elevated temperatures which would negatively influence the coulombic efficiency and subsequently lower the energy efficiency. The optimum temperature for the VARFB operation need to be evaluated in the future to achieve the best compromise between improved ORR and OER kinetics and minimized transfer processes through the membrane.

The remarkable achievement in optimizing the membrane properties presented in PUBLICATION III should not hide that the capacity fading is still too high for commercial applications. The crossover of vanadium species through the membrane which is responsible for the capacity loss needs to be close to zero or the capacity loss needs to be recoverable. In hydrogen-bromine RFB the crossover of bromine-species is tackled by simply returning back the bromine/bromide containing solutions that were transferred to the hydrogen electrode [60]. This is easily possible because in the gaseous half-cell (hydrogen electrode) there is no liquid phase present. This type of capacity recovery could also be pursued in VARFB. However, the procedure would need to be modified as in VARFB a liquid phase is intentionally present during charging. Another approach to face the capacity decay in a VARFB could be followed by merging a VRFB and a VARFB system. The charging reaction in such a system would be identical to VRFB until all  $\text{VO}^{2+}$  is converted to  $\text{VO}_2^+$ , subsequently OER would occur at the positive electrode as it is the case in VARFB. During discharging the situation is vice versa, i.e. reduction of  $\text{VO}_2^+$  to  $\text{VO}^{2+}$  followed by ORR. This system would have two charging steps and two discharging steps. The main advantage would be that vanadium species are intentionally present in the positive electrolyte and crossover of vanadium species merely results in lowered coulombic efficiency (as it is the case in VRFB) but not in capacity loss. However, the drawbacks of a VRFB (e.g. a temperature limit due to  $\text{V}_2\text{O}_5$  precipitation) will also be inherent in such a system and therefore it has to be evaluated whether such a combination is reasonable.

In conclusion, with the present thesis a copious basis is laid in the understanding of the novel unitized VARFB system and the relevant processes that occur in this battery. However, it is desirable to carry on the investigation of this VARFB system by further studies related to the unanswered questions that are described above.



# References

- [1] S. R. L. Stephen J. Farnsworth, S. R. L. Stephen J. Farnsworth, *Int. J. Public Opin. Res.* 24 (2012) 93–103.
- [2] J. Cook, D. Nuccitelli, S. A. Green, M. Richardson, B. Winkler, R. Painting, R. Way, P. Jacobs, A. Skuce, *Environ. Res. Lett.* 8 (2013) 024024.
- [3] UN Framework on Climate Change, Paris Agreement, 2015. <http://www.cop21.gouv.fr/en/more-details-about-the-agreement/> (Accessed: 28/12/2015).
- [4] Met Office, "Global temperatures set to reach 1 °C marker for first time", 2015. <http://www.metoffice.gov.uk/news/release/archive/2015/one-degree> (Accessed: 28/11/2015).
- [5] Met Office, HadCRUT4 data set, 2015. [http://hadobs.metoffice.com/hadcrut4/data/current/time\\_series/HadCRUT.4.4.0.0.annual\\_ns\\_avg.txt](http://hadobs.metoffice.com/hadcrut4/data/current/time_series/HadCRUT.4.4.0.0.annual_ns_avg.txt) (Accessed: 28/11/2015).
- [6] C. P. Morice, J. J. Kennedy, N. A. Rayner, P. D. Jones, *J. Geophys. Res. Atmos.* 117 (2012) 1–22.
- [7] International Energy Agency, World Energy Outlook 2015, 2015. <http://www.worldenergyoutlook.org/> (Accessed: 28/11/2015).
- [8] P. Alotto, M. Guarnieri, F. Moro, *Renew. Sustain. Energy Rev.* 29 (2014) 325–335.
- [9] M. Beaudin, H. Zareipour, A. Schellenberglabe, W. Rosehart, *Energy Sustain. Dev.* 14 (2010) 302–314.
- [10] K. Divya, J. Østergaard, *Electr. Power Syst. Res.* 79 (2009) 511–520.
- [11] B. Dunn, H. Kamath, J.-M. Tarascon, *Science* 334 (2011) 928–935.
- [12] J. Leadbetter, L. G. Swan, *J. Power Sources* 216 (2012) 376–386.

- 
- [13] J. Weniger, J. Bergner, T. Tjaden, V. Quaschnig, *Dezentrale Solarstromspeicher für die Energiewende*, Berliner Wissenschafts-Verlag, ISBN: 978-3-8305-3548-5, 2015.
- [14] Q. Huang, Q. Wang, *ChemPlusChem* 80 (2015) 312–322.
- [15] M. Skyllas-Kazacos, M. H. Chakrabarti, S. A. Hajimolana, F. S. Mjalli, M. Saleem, *J. Electrochem. Soc.* 158 (2011) R55.
- [16] M. Vijayakumar, W. Wang, Z. Nie, V. Sprenkle, J. Hu, *J. Power Sources* 241 (2013) 173–177.
- [17] G. Wang, J. Chen, X. Wang, J. Tian, H. Kang, X. Zhu, Y. Zhang, X. Liu, R. Wang, *J. Energy Chem.* 23 (2014) 73–81.
- [18] S. Roe, C. Menictas, M. Skyllas-Kazacos, *J. Electrochem. Soc.* 163 (2016) A5023–A5028.
- [19] J. Noack, N. Roznyatovskaya, T. Herr, P. Fischer, *Angew. Chemie* 127 (2015) 9912–9947.
- [20] L. Li, S. Kim, W. Wang, M. Vijayakumar, Z. Nie, B. Chen, J. Zhang, G. Xia, J. Hu, G. Graff, J. Liu, Z. Yang, *Adv. Energy Mater.* 1 (2011) 394–400.
- [21] W. Wang, Q. Luo, B. Li, X. Wei, L. Li, Z. Yang, *Adv. Funct. Mater.* 23 (2013) 970–986.
- [22] J. grosse Austing, C. Nunes Kirchner, E.-M. Hammer, L. Komsijska, G. Wittstock, *J. Power Sources* 273 (2015) 1163–1170.
- [23] S. Hosseiny, M. Saakes, M. Wessling, *Electrochem. Comm.* 13 (2011) 751–754.
- [24] H. Kaneko, A. Negishi, K. Nozaki, K. Sato, M. Nakajima, EU Patent 0517217A1, 1992.
- [25] J. Noack, C. Cremers, D. Bayer, J. Tübke, K. Pinkwart, *J. Power Sources* 253 (2014) 397–403.
- [26] C. Menictas, M. Skyllas-Kazacos, *J. Appl. Electrochem.* 41 (2011) 1223–1232.
- [27] W. Kangro, DE Patent 914264C, 1954.
- [28] M. Bartolozzi, *J. Power Sources* 27 (1989) 219–234.

- [29] A. Z. Weber, M. M. Mench, J. P. Meyers, P. N. Ross, J. T. Gostick, Q. Liu, J. Appl. Electrochem. 41 (2011) 1137–1164.
- [30] P. Leung, X. Li, C. Ponce de León, L. Berlouis, C. T. J. Low, F. C. Walsh, RSC Adv. 2 (2012) 10125.
- [31] G. L. Soloveichik, Chem. Rev. 115 (2015) 11533–11558.
- [32] K. Lin, Q. Chen, M. R. Gerhardt, L. Tong, S. B. Kim, L. Eisenach, A. W. Valle, D. Hardee, R. G. Gordon, M. J. Aziz, M. P. Marshak, Science 349 (2015) 1529–1532.
- [33] B. Huskinson, M. P. Marshak, C. Suh, S. Er, M. R. Gerhardt, C. J. Galvin, X. Chen, A. Aspuru-Guzik, R. G. Gordon, M. J. Aziz, Nature 505 (2014) 195–198.
- [34] T. Janoschka, N. Martin, U. Martin, C. Friebe, S. Morgenstern, H. Hiller, M. D. Hager, U. S. Schubert, Nature 527 (2015) 78–81.
- [35] T. Liu, X. Wei, Z. Nie, V. Sprenkle, W. Wang, Adv. Energy Mater. (2015).
- [36] M. C. Tucker, A. Phillips, A. Z. Weber, ChemSusChem 8 (2015) 3996–4004.
- [37] D. Lloyd, E. Magdalena, L. Sanz, L. Murtoimäki, K. Kontturi, J. Power Sources 292 (2015) 87–94.
- [38] M. Skyllas-Kazacos, M. H. Chakrabarti, S. A. Hajimolana, F. S. Mjalli, M. Saleem, J. Electrochem. Soc. 158 (2011) R55.
- [39] P. Alotto, M. Guarnieri, F. Moro, Renew. Sustain. Energy Rev. 29 (2014) 325–335.
- [40] F. T. Wandschneider, S. Röhm, P. Fischer, K. Pinkwart, J. Tübke, H. Nirschl, J. Power Sources 261 (2014) 64–74.
- [41] A. Tang, J. McCann, J. Bao, M. Skyllas-Kazacos, J. Power Sources 242 (2013) 349–356.
- [42] C. Yin, S. Guo, H. Fang, J. Liu, Y. Li, H. Tang, Appl. Energy 151 (2015) 237–248.
- [43] J. S. Lawton, a. Jones, T. Zawodzinski, J. Electrochem. Soc. 160 (2013) A697–A702.

- [44] Z. Yang, J. Zhang, M. C. W. Kintner-Meyer, X. Lu, D. Choi, J. P. Lemmon, J. Liu, *Chem. Rev.* 111 (2011) 3577–3613.
- [45] M. H. Chakrabarti, F. S. Mjalli, I. M. AlNashef, M. A. Hashim, M. A. Hussain, L. Bahadori, C. T. J. Low, *Renew. Sustain. Energy Rev.* 30 (2014) 254–270.
- [46] Z. Xie, Q. Liu, Z. Chang, X. Zhang, *Electrochim. Acta* 90 (2013) 695–704.
- [47] D. R. Lide (Ed.), *CRC Handbook of Chemistry and Physics, Internet Version*, CRC Press, Boca Raton, FL, 2005.
- [48] B. L. Ellis, L. F. Nazar, *Curr. Opin. Solid State Mater. Sci.* 16 (2012) 168–177.
- [49] N. S. Choi, Z. Chen, S. a. Freunberger, X. Ji, Y. K. Sun, K. Amine, G. Yushin, L. F. Nazar, J. Cho, P. G. Bruce, *Angew. Chemie - Int. Ed.* 51 (2012) 9994–10024.
- [50] A. Crawford, V. Viswanathan, D. Stephenson, W. Wang, E. Thomsen, D. Reed, B. Li, P. Balducci, M. Kintner-Meyer, V. Sprenkle, *J. Power Sources* 293 (2015) 388–399.
- [51] C. Ponce de León, a. Frías-Ferrer, J. González-García, D. Szánto, F. Walsh, *J. Power Sources* 160 (2006) 716–732.
- [52] D. P. Scamman, G. W. Reade, E. P. Roberts, *J. Power Sources* 189 (2009) 1231–1239.
- [53] S.-H. Shin, S.-H. Yun, S.-H. Moon, *RSC Adv.* 069 (2012) 12686–12689.
- [54] F. Pan, Q. Wang, *Molecules* 20 (2015) 20499–20517.
- [55] J. Zhang, L. Li, Z. Nie, B. Chen, M. Vijayakumar, S. Kim, W. Wang, B. Schwenzer, J. Liu, Z. Yang, *J. Appl. Electrochem.* 41 (2011) 1215–1221.
- [56] X. Wu, S. Liu, N. Wang, S. Peng, Z. He, *Electrochim. Acta* 78 (2012) 475–482.
- [57] F. Chang, C. Hu, X. Liu, L. Liu, J. Zhang, *Electrochim. Acta* 60 (2012) 334–338.
- [58] Y. Chen, K. Santhanam, A. Bard, *J. Electrochem. Soc.* 128 (1981) 1460–1467.
- [59] Y. Wen, H. Zhang, P. Qian, H. Zhou, P. Zhao, B. Yi, Y. Yang, *Electrochim. Acta* 51 (2006) 3769–3775.

- [60] G. Lin, P. Chong, V. Yarlagadda, T. Nguyen, R. J. Wycisk, P. N. Pintauro, M. Bates, S. Mukerjee, M. C. Tucker, a. Z. Weber, *J. Electrochem. Soc.* 163 (2016) A5049–A5056.
- [61] K. T. Cho, M. C. Tucker, M. Ding, P. Ridgway, V. S. Battaglia, V. Srinivasan, A. Z. Weber, *ChemPlusChem* 80 (2015) 402–411.
- [62] A. Léonard, R. Lauwerys, *Mutat. Res.* 239 (1990) 17–27.
- [63] L. Passantino, A. B. Muñoz, M. Costa, *Metallomics* 5 (2013) 1357–67.
- [64] F. Wandschneider, M. Küttinger, J. Noack, P. Fischer, K. Pinkwart, J. Tübke, H. Nirschl, *J. Power Sources* 259 (2014) 125–137.
- [65] O. David, K. Percin, T. Luo, Y. Gendel, M. Wessling, *J. Energy Storage* 1 (2015) 65–71.
- [66] C. Gutsche, C. J. Moeller, M. Knipper, H. Borchert, J. Parisi, T. Plaggenborg, *Electrocatalysis* 6 (2015) 455–464.
- [67] G. Merle, F. C. Ioana, D. E. Demco, M. Saakes, S. S. Hosseiny, *Membranes (Basel)*. 4 (2013) 1–19.
- [68] Y. Wen, J. Cheng, P. Ma, Y. Yang, Y. Xun, *Electrochim. Acta* 53 (2008) 6018–6023.
- [69] Y. H. Wen, J. Cheng, Y. Xun, P. H. Ma, Y. S. Yang, *Electrochim. Acta* 53 (2008) 6018–6023.
- [70] S. Abdu, M. C. Martí-Calatayud, J. E. Wong, M. García-Gabaldón, M. Wessling, *ACS Appl. Mater. Interfaces* 6 (2014) 1843–1854.
- [71] F. Guesmi, C. Hannachi, B. Hamrouni, *Ionics (Kiel)*. 18 (2012) 711–717.
- [72] T. Sata, T. Sata, W. Yang, *J. Memb. Sci.* 206 (2002) 31–60.
- [73] M. Li, L. Zhang, Q. Xu, J. Niu, Z. Xia, *J. Catal.* 314 (2014) 66–72.



# List of Abbreviations and Symbols

## Abbreviations

BPP	Bipolar plate
CAES	Compressed air energy storage
CEM	Cation exchange membrane
FC	Fuel cell
GDE	Gas diffusion electrode
HER	Hydrogen evolution reaction
ICP-MS	Inductively coupled plasma mass spectroscopy
IEA	International Energy Agency
IL	Ionic liquids
LbL	Layer-by-layer
Li-ion	Lithium-ion battery
MEA	Membrane electrode assembly
N117	Nafion 117
Na-S	Sodium-sulfur battery
NASA	National Aeronautic and Space Administration
OER	Oxygen evolution reaction
ORR	Oxygen reduction reaction
Pb-acid	Lead-acid battery

PEI	Polyethyleneimine
PEMFC	Proton exchange membrane fuel cell
PHS	Pumped hydro storage
PV	Photovoltaic
RFB	Redox flow battery
SEM	Scanning electron microscopy
SHE	Standard hydrogen electrode
TGA	Thermogravimetric analysis
URFC	Unitized regenerative fuel cell
VARFB	Vanadium/air redox flow battery
VOFC	Vanadium/oxygen fuel cell
VRFB	All-vanadium redox flow battery
XRD	X-ray diffraction

## **Symbols**

$c$	Concentration
$E^0$	Standard electrode potential
$\Delta E^0$	Standard cell potential
$I$	Current
$j$	Current density
$n$	Amount of substance
$Q$	Charge
$U$	Voltage
$V$	Volume
$W$	Electrical energy

$\eta_C$	Coulombic efficiency
$\eta_E$	Energy efficiency
$\eta_V$	Voltaic efficiency
$\oplus / (+)$	Positive electrode
$\ominus / (-)$	Negative electrode



# Publications



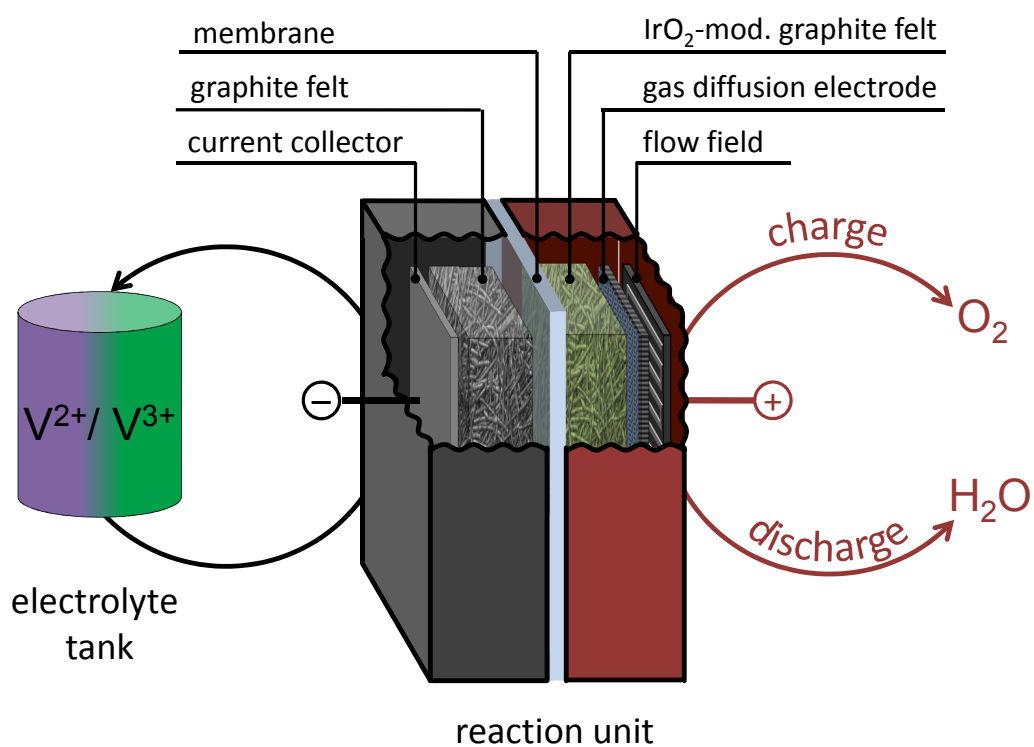
# Publication I



# Study of an unitesed bidirectional vanadium/air redox flow battery comprising a two-layered cathode

Authors: Jan grosse Austing, Carolina Nunes Kirchner, Eva-Maria Hammer, Lidiya Komsiyiska and Gunther Wittstock

Journal of Power Sources, 273, 2015, 1163-1170, DOI: 10.1016/j.jpowsour.2014.09.177







Contents lists available at ScienceDirect

## Journal of Power Sources

journal homepage: [www.elsevier.com/locate/jpowsour](http://www.elsevier.com/locate/jpowsour)

# Study of an unitesed bidirectional vanadium/air redox flow battery comprising a two-layered cathode



Jan grosse Austing<sup>a</sup>, Carolina Nunes Kirchner<sup>a</sup>, Eva-Maria Hammer<sup>a,1</sup>,  
Lidiya Komsijska<sup>a,\*</sup>, Gunther Wittstock<sup>b</sup>

<sup>a</sup> NEXT ENERGY – EWE Research Centre for Energy Technology, Carl-von-Ossietzky-Str. 15, 26129 Oldenburg, Germany

<sup>b</sup> Carl von Ossietzky University of Oldenburg, School of Mathematics and Natural Sciences, Centre of Interface Science, Department of Chemistry, 26111 Oldenburg, Germany

## H I G H L I G H T S

- We introduce a new concept for an unitesed vanadium/air redox flow battery.
- A novel bidirectional two-layered cathode setup was utilised in the battery.
- An energy efficiency of 42% was achieved at 21 °C and 20 mA cm<sup>-2</sup> current density.
- Overvoltage increase and species crossover are observed during consecutive cycling.

## A R T I C L E I N F O

### Article history:

Received 3 July 2014  
Received in revised form  
8 September 2014  
Accepted 29 September 2014  
Available online 6 October 2014

### Keywords:

Vanadium air redox flow battery  
Vanadium oxygen fuel cell  
Bidirectional oxygen/air electrode  
Air battery  
Unitized regenerative fuel cell

## A B S T R A C T

The performance of a unitesed bidirectional vanadium/air redox flow battery (VARFB) is described. It contains a two-layered cathode consisting of a gas diffusion electrode (GDE) with Pt/C catalyst for discharging and of an IrO<sub>2</sub> modified graphite felt for charging. A simple routine is shown for the modification of a graphite felt with IrO<sub>2</sub>. A maximum energy efficiency of 41.7% at a current density of 20 mA cm<sup>-2</sup> as well as an average discharge power density of 34.6 mW cm<sup>-2</sup> at 40 mA cm<sup>-2</sup> were obtained for VARFB operation at room temperature with the novel cathode setup. A dynamic hydrogen electrode was used to monitor half cell potentials during operation allowing to quantify the contribution of the cathode to the overall performance of the VARFB. Four consecutive cycles revealed that crossover of vanadium ions took place and irreversible degradation processes within the reaction unit lead to a performance decrease.

© 2014 Elsevier B.V. All rights reserved.

## 1. Introduction

Redox flow batteries (RFB) are electrochemical storage devices comprising a reaction unit and two electrolyte tanks in which the fluidic electrochemical active material is stored externally. By circulating the electrolytes through the reaction unit and applying a DC source or load, conversion of chemical to electrical energy and vice versa can take place.

In the past years all-vanadium redox flow batteries (VRFB) gained increasing interest due to their potential application as stationary

energy storage device, e.g. for the compensation of the fluctuating electricity production of renewables [1–4]. Promising properties of redox flow batteries are the independence of power and capacity, high cycle life (>12,000 [2]) and competitive round-trip efficiencies (≈80% [4]). The VRFB utilises two vanadium-containing aqueous electrolytes and therefore issues due to the crossover of species from one half cell to the other are reduced. However, one major drawback of VRFB is the low energy density and specific energy of 25–30 Wh kg<sup>-1</sup> [5] being similar to lead-acid batteries (30–50 Wh kg<sup>-1</sup> [2]). The low energy density has its origin in the solubility limitations of the vanadium species and the low standard cell potential of  $\Delta E_{\text{VRFB}}^0 = 1.25$  V. The low energy density can be an obstruction in electrical storage applications with limited space.

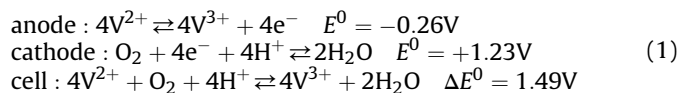
There are different attempts proposed in literature for increasing the vanadium solubility and thus the energy density by using various electrolyte additives [6–8]. However, these attempts again show limits determined by the maximal soluble amount of

\* Corresponding author. Tel.: +49 441 99906 418; fax: +49 441 99906 109.

E-mail addresses: [jan.austing@next-energy.de](mailto:jan.austing@next-energy.de) (J. grosse Austing), [carolina.nunes-kirchner@next-energy.de](mailto:carolina.nunes-kirchner@next-energy.de) (C. Nunes Kirchner), [e.hammer@fz-juelich.de](mailto:e.hammer@fz-juelich.de) (E.-M. Hammer), [lidiya.komsijska@next-energy.de](mailto:lidiya.komsijska@next-energy.de) (L. Komsijska), [gunther.wittstock@uni-oldenburg.de](mailto:gunther.wittstock@uni-oldenburg.de) (G. Wittstock).

<sup>1</sup> Present address: Forschungszentrum Jülich GmbH, Institute of Energy and Climate Research (IEK-1), Materials Synthesis and Processing, Wilhelm-Johnen-Str., 52428 Jülich, Germany.

the electroactive species. Another approach for increasing the energy density is the replacement of the positive (cathode) redox couple,  $\text{VO}_2^+/\text{VO}^{2+}$ , by  $\text{O}_2/\text{H}_2\text{O}$  (Eq. (1)). This vanadium/air redox flow battery (VARFB) was first proposed and disclosed in a patent by Kaneko et al., in 1992 [9].



The anodic reactions are the same as in a conventional VRFB and occur readily on activated carbon materials. Carbon-based electrodes are well suited for redox flow batteries as they offer a wide operation potential windows, chemical stability as well as reasonable costs [10]. Different carbon materials (e.g. graphite felts or carbon paper) have been investigated concerning their properties in redox flow battery application [10,11], including several routines to improve redox kinetics by surface treatments such as thermal treatment [12], catalyst deposition [13] or plasma activation [14].

The oxygen source for the cathodic discharge reaction can be the ambient air while the water for the charging process needs to be stored in a tank. Although the system still needs a cathodic container for the water, a significant increase in the energy density is expected due to the fact that the mass and the volume of the cathodic container is decreased. Based on a vanadium concentration of 1.5 M and assuming that all water in the container can be consumed, the volume of the water tank is approx. 1% of the volume of the original  $\text{VO}_2^+/\text{VO}^{2+}$  containing tank. Therefore, a significant decrease in system weight and volume is achieved, resulting in an increased energy density. Depending on the ratio of reaction unit to tank sizes, the energy density of the VARFB is roughly doubled [1]. Likewise, the standard potential of the VARFB is approx. 20% higher than that of the VRFB ( $\Delta E_{\text{VRFB}}^0 = 1.25\text{V}$ ) which leads to an additional enhancement of energy density.

A big challenge for such a system is the design of the electrode setup on the cathode side. During charging when water is split (oxygen evolution reaction; OER), a hydrophilic electrode is preferable to allow the reactant water to wet the electrode surface and to repel produced oxygen out of the electrode. Additionally, this substrate should contain a suitable OER catalyst (e.g.  $\text{IrO}_2$ ). For the discharging reaction (oxygen reduction reaction; ORR) a hydrophobic electrode is required to remove the produced water and avoid flooding of the electrode, as accumulated water hinders mass transport of the reactant oxygen to the catalytic sites. Again a suitable catalyst to support the ORR is needed (e.g. Pt). As the requirements for OER and ORR are contrary concerning hydrophobicity and adequate catalyst, the design of such a bidirectional air electrode generally implies compromises. There are different approaches how to engineer these electrode (e.g. single electrode/single catalytic layer, separate electrodes/single catalytic layer or single electrode/multiple catalytic layers [15]).

Hosseiny et al. [16] published results about a modular VARFB using two different membrane electrode assemblies (MEA) for charging and discharging, respectively. Between charging and discharging they exchanged the MEA used for charging by a different MEA for the discharging process. They reported energy efficiencies of 26.67% at 40 °C operating temperature and at a current density of 2.4 mA cm<sup>-2</sup> for both charging and discharging.

Menictas et al. [17] investigated a vanadium-oxygen fuel cell (VOFC). This system permits the discharging process only, i.e. oxidising  $\text{V}^{2+}$  to  $\text{V}^{3+}$  while reducing oxygen. They examined the influence of different materials and operation conditions on the performance of a 5-cell VOFC stack. One major challenge discussed in their study is the detachment of the GDE from the membrane due to swelling caused by water uptake. By optimising the bonding

of the GDE to the membrane, they were able to operate the stack for over 120 h.

Recently, Noack et al. [18] published results of a 280 cm<sup>2</sup> VOFC. The setup consisted of two membranes to avoid crossover of  $\text{V}^{2+}$  to the Pt catalyst on the cathode side. They investigated the influence of air flow rates on the discharging potentials and on power densities. For a better understanding of the factors causing losses, they conducted several electrochemical impedance measurements. The maximum average power density was 19.6 mW cm<sup>-2</sup>. However, the VOFC can only be used for discharging the electrolyte, charging has to be done in a different device.

In this work we report a novel unitised bidirectional vanadium/air redox flow battery comprising a two-layered cathode and its behaviour. This system is, in contrast to fuel cells, rechargeable. Driven by the motivation to decrease the system weight and volume, we created a unitised bidirectional system, i.e. charging and discharging process can be conducted in the same reaction unit. The cathode of this system is comparable to the one used in unitised regenerative fuel cells (URFC). In URFC a PEM water electrolyser is combined with a proton-exchange membrane (PEM) fuel cell resulting in a closed-loop device.

For a better understanding of the processes, the VARFB is investigated with a dynamic hydrogen reference electrode (DHE) to monitor separately half cell potentials. Finally, we discuss remaining drawbacks and possible approaches to improve the performance of the system.

## 2. Experimental

### 2.1. $\text{IrO}_2$ -modified graphite felt

The  $\text{IrO}_2$ -modified graphite felt was prepared by the thermal decomposition of an iridium compound similar to procedures described elsewhere [19,20] First, a graphite felt of 2 cm × 2 cm (GFD5, SGL Carbon GmbH, Germany) was activated at 400 °C for 18 h in air atmosphere. This hydrophilic felt was immersed in a solution of 18.6 mg  $(\text{NH}_4)_2\text{IrCl}_6$  (99.994%; Alfa Aesar, GmbH & Co KG, Germany) in 5.5 mL ultrapure water (>18 MΩ cm at 25 °C). Subsequently, the felt was dried in a vacuum oven at 60 °C for 30 min and then calcinated for 15 min at 450 °C in air atmosphere. The soaking/drying/calcinating sequence was repeated two times, with the only modification that the third calcination step was conducted for 1 h. The complete volume of the  $(\text{NH}_4)_2\text{IrCl}_6$  solution was consumed.

The modified felt was investigated using XRD (scan step 0.05°; X-Pert Pro MPD diffractometer with copper tube, PANalytical B.V., Netherlands) and SEM/EDX (NEON 40, Zeiss, Germany).

### 2.2. GDE preparation and membrane pretreatment

The GDE was prepared by airbrushing a suspension of an ORR catalyst and Nafion<sup>®</sup> ionomer on a gas diffusion layer (GDL). The GDL was a carbon cloth material (ELAT HT 1400-W, BASF fuel cell GmbH, Germany). A suspension of Pt/C (40 mass % Pt on carbon black; Alfa Aesar GmbH & Co KG, Germany) in 1:100 (w/w) 2-propanol (99.9%; VWR International GmbH, Germany) was ultrasonicated for 20 min, then 1:20 (w/w, based on Pt/C) of a Nafion<sup>®</sup> perfluorinated resin solution (5 mass % in lower aliphatic alcohols and water; Sigma–Aldrich, Germany) was added and again ultrasonicated for 45 min. This suspension was airbrushed on the GDL. By differential weighing of the GDL substrate before and after the airbrushing process a loading of approx. 0.8 mg cm<sup>-2</sup> Pt was determined.

Prior to use in the VARFB a Nafion<sup>®</sup> 117 membrane (Ion Power GmbH, Germany) was pretreated. The membrane was cleaned in 5%

H<sub>2</sub>O<sub>2</sub> (30%; Carl Roth GmbH & Co. KG, Germany) in deionised water for 30 min at 80 °C. After rinsing it with deionised water it was protonated in 1 M H<sub>2</sub>SO<sub>4</sub> (95–97%; Fischer Scientific GmbH, Germany) for 30 min at 80 °C and finally it was boiled in deionised water for 10 min.

### 2.3. V<sup>3+</sup> electrolyte production

The V<sup>3+</sup> electrolyte was produced electrolytically in a VRFB setup similar to a routine described elsewhere [21]. Briefly, a solution of 1.13 M VOSO<sub>4</sub>·xH<sub>2</sub>O (97%; Sigma Aldrich, Germany) and 2.0 M H<sub>2</sub>SO<sub>4</sub> (95–97%; Fischer Scientific GmbH, Germany) in deionised water was prepared. For preparing a defined concentration, the amount of crystal water in VOSO<sub>4</sub>·xH<sub>2</sub>O was determined as  $x \approx 3$  with ICP-MS (XSERIES 2 ICP-MS, Thermo Scientific, USA). This solution was electrolysed up to 1.8 V with two consecutive current densities (80 mA cm<sup>-2</sup> and 40 mA cm<sup>-2</sup>, respectively) in a VRFB setup, using twice the volume on the cathode as on the anode. After reaching 1.8 V, half of the catholyte was disposed and the electrolytes were discharged up to 0.8 V (again 80 mA cm<sup>-2</sup> and 40 mA cm<sup>-2</sup>, respectively). The anolyte was used as V<sup>3+</sup> electrolyte for the VARFB operation experiments. The concentration of vanadium in this electrolyte was determined as 1.2 mol L<sup>-1</sup> by ICP-MS.

### 2.4. Operating VARFB

For the investigation of the VARFB performance, a test cell with 4 cm<sup>2</sup> geometric area was constructed. The cell consisted of two half cells, separated by a membrane. The sealing between the two half cells was achieved with Viton<sup>®</sup> O-rings (Dichtelemente arcus GmbH, Germany). The body of each half cell consisted of a polycarbonate block with manifolds for the electrolyte and cavities (2 cm × 2 cm) for the current collector and the electrodes. The anodic current collector was made of a graphite-based bipolar plate material (PPG 86, Eisenhuth GmbH Co. KG, Germany) and the anode was a thermally activated graphite felt (GFD5, SGL Carbon GmbH, Germany; activation: 400 °C/18 h/air atmosphere). The cathodic current collector was made of titanium (grade 2) with an integrated serpentine flow field (Keil Feinwerktechnik GmbH, Germany). The GDE was placed on top of the flow field, followed by the IrO<sub>2</sub>-modified graphite felt (Fig. 2). The GDE, the IrO<sub>2</sub>-modified graphite felt and the anodic graphite felt were replaced by new ones for each experiment, except for those where the subsequent cycles were recorded. The hydraulic connections were made from Tygon<sup>®</sup> tubings. The electrolytes were pumped through the reaction unit by

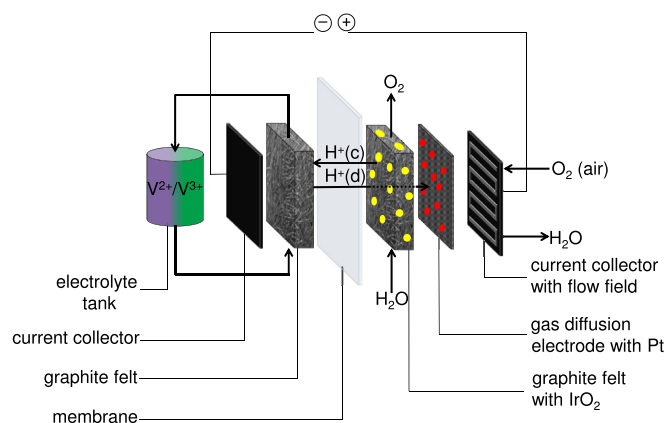


Fig. 2. Setup for a unidirectional bidirectional VARFB comprising a two-layered cathode (H<sup>+</sup>(c) = H<sup>+</sup> transport during charge; H<sup>+</sup>(d) = H<sup>+</sup> transport during discharge).

membrane pumps (KNF Neuberger dosing pumps SIMDOS 10, Germany).

12 mL of the V<sup>3+</sup> anolyte was used (renewed for each experiment, except for those with consecutive cycles) and purged permanently with N<sub>2</sub> to prevent contact of the electrolyte with air. The small volume of anolyte was chosen to be able to perform charging and discharging in reasonable time. To avoid operational limitations, an excess catholyte volume of 50 mL was employed. 2 M H<sub>2</sub>SO<sub>4</sub> was used as catholyte instead of pure water to achieve a higher conductivity and reduce osmotic pressure with respect to the anolyte. Mass transport limitations should be avoided by pumping the electrolytes through the cell with flow rates of 100 mL min<sup>-1</sup> while charging the VARFB. During discharging the 2 M H<sub>2</sub>SO<sub>4</sub> was not pumped but remained in the IrO<sub>2</sub>-modified graphite felt, whereas air with 267 mL min<sup>-1</sup> was pumped through the flow field to the GDE (anolyte circulated as in charging mode with 100 mL min<sup>-1</sup>). All experiments were carried out at room temperature (21 °C ± 1 °C). The operation of the VARFB was conducted with a potentiostat/galvanostat (Solartron Analytical Modulab Pstat potentiostat/galvanostat, UK).

In parallel to charging and discharging, half cell potentials were recorded versus a dynamic hydrogen reference electrode (DHE). The DHE was integrated into the cell as described by Li and Pickup [22] for fuel cell application and similar as Sun et al. [23] reported for redox flow batteries. The DHE consisted of two thin Pt wires (Ø = 0.175 mm) placed between membrane and cathodic half cell body close to the edge of the cathode. A constant current source (5–30 µA) was adjusted to produce small quantities of H<sub>2</sub> until a potential of -0.197 V vs. Ag/AgCl/KCl(sat.), i.e. 0 V vs. standard hydrogen electrode (SHE), was measured. In order to achieve this, the Pt wires were placed on the cathodic half cell of the VARFB test cell, covered with a Nafion<sup>®</sup> 117 membrane and the latter was pressed onto the half cell with a cover sheet. This sheet had an opening in the region where the DHE was placed. Via this hole the Ag/AgCl reference electrode was coupled ionically to the membrane. After the current was adjusted, the cover sheet was removed and the cell was assembled. The current of the DHE remained constant during the following experiment. A scheme of the overall setup for the operation experiments of the VARFB is depicted in Fig. 1.

## 3. Results & discussion

### 3.1. Concept of the unidirectional bidirectional VARFB

The VARFB can be regarded as a combination of the negative half cell of VRFB and with a bidirectional air electrode as the positive

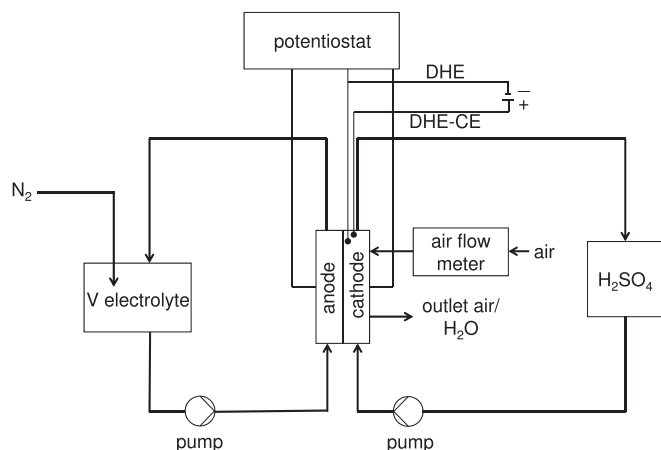


Fig. 1. Scheme of the VARFB test cell operation system; DHE = dynamic hydrogen electrode, DHE-CE = counter electrode for DHE.

half cell. The anode of the VARFB is similar as in a VRFB, consisting of an activated graphite felt that is electrically connected to a graphite-based current collector, and the electrolyte being circulated through the felt. As already mentioned, the cathode (= positive half cell) implies challenges due to the different requirements for the charging reaction (ORR) and discharging reaction (OER).

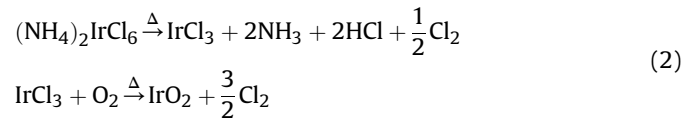
In order to the contradictory requirements, two different electrode layers were used as cathode, one layer was optimised for the ORR and the other for the OER. The ORR electrode was a hydrophobised, Pt/C and Nafion<sup>®</sup> ionomer loaded GDE similar to PEM fuel cells, the OER electrode consisted of an IrO<sub>2</sub>-modified graphite felt. The two layers were assembled in direct contact to each other, the IrO<sub>2</sub>-modified graphite felt pressed against the membrane while the GDE was in direct contact with the current collector (Fig. 2).

For charging, H<sub>2</sub>O/H<sup>+</sup> as the reactant for the OER was circulated through the IrO<sub>2</sub>-modified graphite felt in parallel to the membrane. The produced H<sup>+</sup> can be transported to the anode to achieve charge balance. The IrO<sub>2</sub>-modified graphite felt was electrically contacted to the current collector via the GDE. In discharging mode, the GDE was supplied with oxygen from air by the flow field that is integrated in the current collector. The protons that are necessary for the ORR were conducted from the anode through the membrane and the OER layer which was flooded with H<sub>2</sub>O/H<sup>+</sup> during discharging. On the surface of the GDE, oxygen and protons reacted on the Pt/C catalyst particles to form water. In addition to the individual optimisation of the two electrode layers, the advantage of this cathode design is that hot-pressing of a GDE onto a fully wetted membrane is avoided together with the related detachment problems described in Ref. [17].

### 3.2. IrO<sub>2</sub>-modified graphite felt

The thermal decomposition of (NH<sub>4</sub>)<sub>2</sub>IrCl<sub>6</sub> on graphite felt yielded IrO<sub>2</sub> particles on the surface of the fibres. Graphite felts were chosen as substrate for the IrO<sub>2</sub> catalyst as this material is also successfully used as positive electrode material in VRFB due to high

porosity and surface area as well as adequate chemical stability. The pristine graphite felts are hydrophobic due to a lack of surface functionalities. These functional groups on the surface can be created by a mild thermal oxidation [12]. After this treatment the felts were hydrophilic allowing wetting them with the iridium-containing aqueous solution. The thermal decomposition reactions of (NH<sub>4</sub>)<sub>2</sub>IrCl<sub>6</sub> as described in Eq. (2) are proposed to take place [19].



Differential weighing of the felt before and after the treatment to determine mass differences as proposed in Ref. [19] was not successful. This was related to the harsh annealing conditions of 450 °C under which the graphite fibres themselves can react with oxygen from the air to form CO<sub>2</sub>. Therefore, the mass of the modified felt was often less than the mass of the pristine felt. The maximum iridium loading per geometric area can be calculated as 1.98 mg cm<sup>-2</sup> (calculated as IrO<sub>2</sub>) from the iridium content of the solution that was completely consumed during the modification process.

The IrO<sub>2</sub>-modified graphite felt was investigated with SEM to provide information about the coverage with the deposit (Fig. 3). Thermally treated non-modified graphite felt showed a plain surface (Fig. 3A, B). EDX analysis (not shown here) confirmed the presence of Ir in the deposits shown in Fig. 3C, D. These iridium-containing deposits were well distributed over the sample. The higher magnification image (Fig. 3D) shows agglomerates of deposits with size in the micrometer range.

Wang et al. [19] proposed a further reduction of the IrO<sub>2</sub> to Ir by graphite (IrO<sub>2</sub> + C → Ir + CO<sub>2</sub>). We did not observe metallic Ir but IrO<sub>2</sub>. This was shown by XRD measurements (Fig. 4). XRD diffractograms were recorded of the IrO<sub>2</sub>-modified graphite felt and of a graphite felt treated under the same thermal conditions but

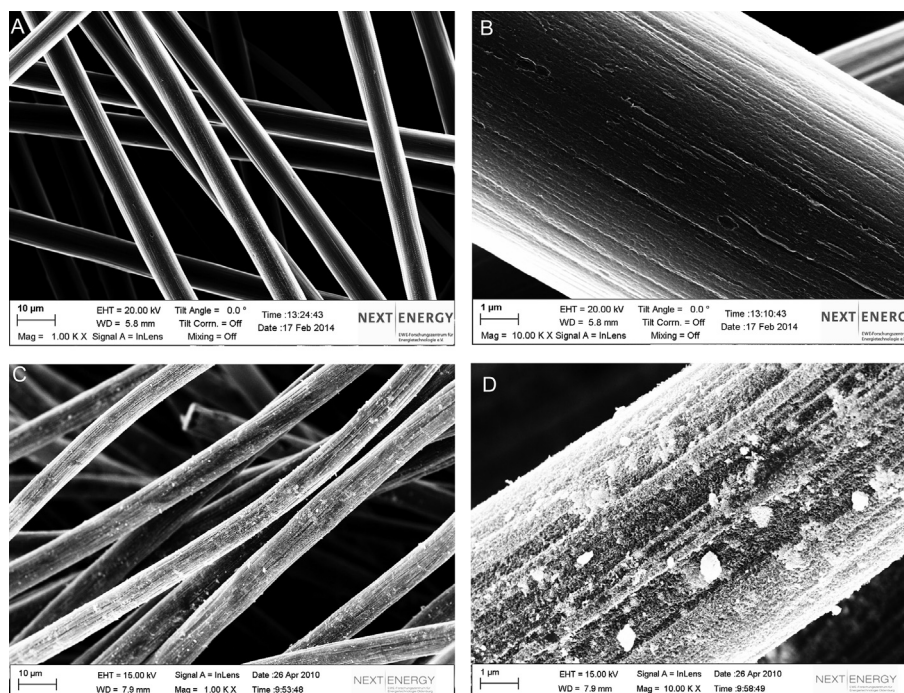


Fig. 3. SEM images of non-modified (but thermally treated under same conditions as the IrO<sub>2</sub>-modified fibres) graphite fibres (A,B) and IrO<sub>2</sub>-modified graphite fibres (C,D).

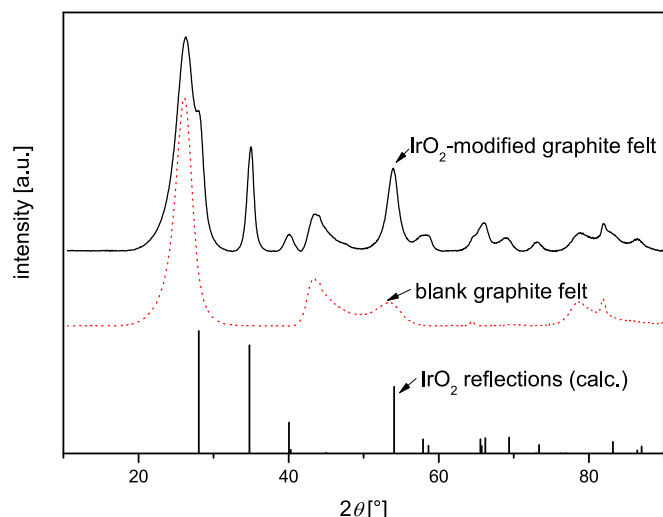


Fig. 4. XRD pattern of IrO<sub>2</sub>-modified graphite felt (solid line), a blank but thermally treated graphite felt (dashed line) and calculated IrO<sub>2</sub> reflections (vertical lines; [24]).

without immersion in (NH<sub>4</sub>)<sub>2</sub>IrCl<sub>6</sub> solution. Besides the graphite-related reflections (i.e. reflections at  $2\theta \approx 26^\circ$ ;  $43^\circ$ ;  $53.5^\circ$ ;  $79^\circ$  and  $82^\circ$ ), the pattern of the IrO<sub>2</sub>-modified graphite felt shows additional reflections (e.g.  $2\theta \approx 28^\circ$ ;  $35^\circ$  or  $40^\circ$ ). These reflections are related to IrO<sub>2</sub> as calculated in Ref. [24].

The modification routine did not allow influencing the morphology of IrO<sub>2</sub>. This would be desirable for the formation of higher surface area to volume ratio but is beyond the scope of this paper. The described method is a simple and straightforward routine to load a graphite felt with IrO<sub>2</sub> which was used here to test the proposed two-layered cathode design for the VARFB.

### 3.3. Operation of the VARFB

The performance of the constructed unitised bidirectional VARFB was examined with current densities of  $15 \text{ mA cm}^{-2}$ ,  $20 \text{ mA cm}^{-2}$  and  $40 \text{ mA cm}^{-2}$  at room temperature (Fig. 5). As the system is new and therefore no information about an adequate end-of-charge voltage for the different current densities was available, the VARFB was charged in all experiments up to 93% of

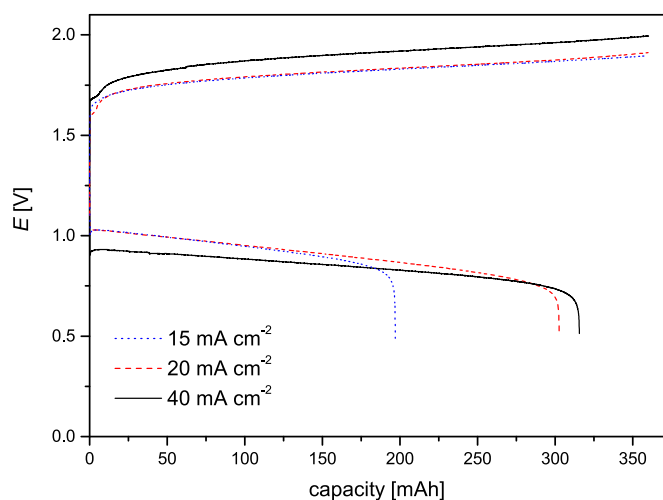


Fig. 5. Charge and discharge performance of the VARFB test cell at current densities of  $15 \text{ mA cm}^{-2}$  (dotted line),  $20 \text{ mA cm}^{-2}$  (dashed line) and  $40 \text{ mA cm}^{-2}$  (solid line).

the theoretical coulombic capacity of the anolyte. Based on the measurements shown in Fig. 5, cell efficiencies were calculated (Table 1).

The general shapes of charging and discharging curves were in good agreement with the curves shown in literature [16,18]. All curves exhibited significant overpotentials both in charging and discharging process which became more pronounced at higher current densities. This can be explained with increasing overpotentials of electrochemical reactions at higher current densities. Notably, the highest discharge capacity was achieved at the highest current density. This observation was in contrast to the experience with other battery technologies, as normally the discharge capacity increases with lowering the current density because of generally lower overpotentials. This phenomenon observed for the VARFB test cell indicated that probably crossover processes lead to a self-discharge of the electrolyte. These losses were more pronounced when operating with lower current density and therefore longer operation time during which crossover processes may proceed. The crossover is important for the performance of the VARFB and will be investigated in detail in future work. However, the charging and discharging curves show that a stable operation of the VARFB at different current densities was possible.

The obtained average discharge power density at  $40 \text{ mA cm}^{-2}$  was  $33.8 \text{ mW cm}^{-2}$ . The maximum average discharge power density reported in literature for a  $280 \text{ cm}^2$  VOFC was  $19.6 \text{ mW cm}^{-2}$  [18]. However, the larger geometric area of the VOFC presented in Ref. [18] may involve additional operational issues leading to the lower power density.

The maximum energy efficiency  $\eta_E$  of the VARFB operated at room temperature was 41.7% at a current density of  $20 \text{ mA cm}^{-2}$ . It was much higher than the efficiency of 26.6% reported by Hosseiny et al. [16] at  $2.4 \text{ mA cm}^{-2}$  and  $40^\circ \text{C}$  and comparable to the one they obtained at  $2.4 \text{ mA cm}^{-2}$  and  $80^\circ \text{C}$  ( $\eta_E = 45.7\%$ ). Higher temperature enhances the kinetics of ORR and OER leading to lower charging and higher discharging cell potentials, respectively. Thus further improvement of the efficiency is expected at elevated operation temperatures.

Table 1 shows clearly that both, low  $\eta_C$  and  $\eta_V$ , contribute to the limited energy efficiency  $\eta_E$ . As known from conventional VRFB ([25]), a trend concerning the coulombic efficiencies  $\eta_C$  and voltaic efficiencies  $\eta_V$  was observed: With increasing current densities,  $\eta_C$  increased whereas  $\eta_V$  decreases. Due to crossover processes the  $\eta_C$  may be lowered. At higher current densities, side reactions (such as hydrogen evolution on the anode side or oxidative corrosion on the cathode side) can be promoted due to diffusion limitations or the higher potentials, thus leading to lower coulombic efficiencies. At moderate current densities, the described negative effect on  $\eta_C$  due to side-reactions was not so pronounced compared to the crossover-related effect.

Taking into account the Butler–Volmer equation it is clear that  $\eta_V$  increased with lowering the current density. In order to obtain more information about the underlying processes, we investigated the VARFB operation with an integrated DHE reference electrode to resolve the single contributions of the two half cells to the overall cell performance. A charge and discharge curve of the VARFB at  $40 \text{ mA cm}^{-2}$  together with the anode and cathode half cell potentials vs. DHE are shown in Fig. 6. As common for battery charging curves, the cell voltage increased during the charging process. This was caused by the change in the  $\text{V}^{2+}:\text{V}^{3+}$  ratio during charging that resulted in an increase of the Nernst potential and therefore lead to a rising anode half cell potential. The concentrations ratio of the redox pair  $\text{H}_2\text{O}/\text{O}_2$  in the catholyte did not change significantly during charging, therefore the cathode half cell potential remained nearly constant. A similar behaviour was recognized during discharging.

**Table 1**

Efficiencies of VARFB at 15 mA cm<sup>-2</sup>, 20 mA cm<sup>-2</sup> and 40 mA cm<sup>-2</sup>;  $\eta_c$  = coulombic efficiency,  $\eta_v$  = voltaic efficiency,  $\eta_E$  = energy efficiency.

$i$ [mA cm <sup>-2</sup> ]	$\eta_c$	$\eta_v$	$\eta_E$
15	55.0%	51.6%	28.4%
20	84.2%	49.5%	41.7%
40	87.6%	44.5%	39.0%

The major reason for the observed low  $\eta_v$  were the high cathodic overpotentials (Fig. 6) The difference in average cathodic voltage between charging and discharging was  $\Delta E_{\text{cathode}} = 0.7$  V while the corresponding difference of the average anode potentials was  $\Delta E_{\text{anode}} = 0.1$  V. The two cathode (= positive half cell) reactions, ORR and OER, are well known to be kinetically slow and therefore accompanied with relatively high overpotentials leading to reduced  $\eta_v$ . This observation is in agreement with experiences gained with unitised regenerative fuel cells (URFC). For URFC, in which the ORR and OER are also the half cell reactions on the positive electrode, energy efficiencies of 49% [26] or 53% [27] were reported.

Enhancing ORR and OER kinetics, e.g. by operating the battery at higher temperatures (as shown by Hosseiny et al. [16]) or using other catalysts, could improve the voltaic efficiency. Moreover, optimisation of the cell design may minimise internal resistances and therefore increasing the voltaic efficiency as well. Another factor that influences the voltaic efficiency is the degradation of the electrodes, the catalyst support and the catalyst itself. To gain information about the contribution of these processes and of crossover reactions on the performance of the VARFB, the test cell was operated for consecutive cycles.

Four consecutive cycles of the VARFB at a current density of 20 mA cm<sup>-2</sup> are shown in Fig. 7. During the first three cycles (charging up to 93% of the theoretical coulombic capacity of the anolyte) the VARFB cell components including peripherals (e.g. electrolytes) were not exchanged, for the fourth cycle only the anolyte (1.2 M V<sup>3+</sup> + 2 M H<sub>2</sub>SO<sub>4</sub>) and the catholyte (2 M H<sub>2</sub>SO<sub>4</sub>) were exchanged by new, fresh solutions. Table 2 summarises performance data of the four consecutive cycles operation of the VARFB.

The average charging potential and especially the potential at the end of the charging step increased from cycle one to three. In the fourth cycle (conducted after exchange of electrolytes) the average charging potential is less than in the third cycle and the

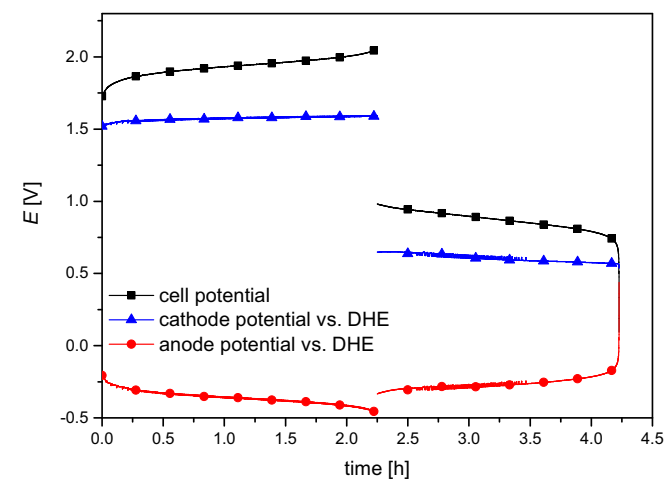


Fig. 6. Charge and discharge performance of VARFB at 40 mA cm<sup>-2</sup> with additional anode and cathode potentials vs. DHE.

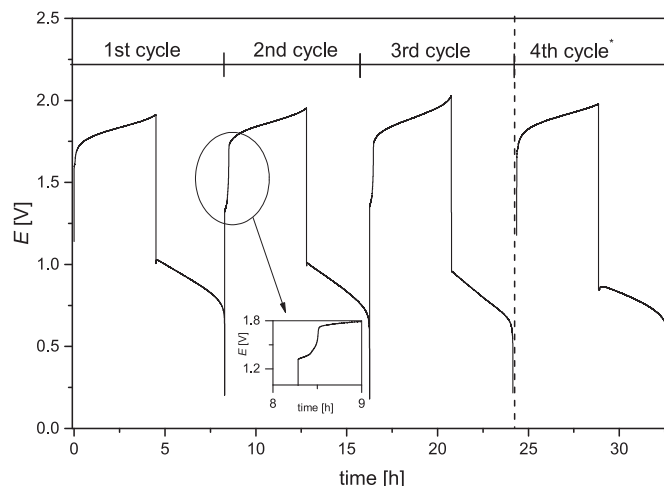


Fig. 7. Four subsequent cycles of VARFB operation at 20 mA cm<sup>-2</sup>. The inset shows a magnification of the beginning of the second charging sequence. The fourth cycle was recorded with fresh anolyte and catholyte.

exponential potential increase at the end of the step is missing. These observations can be explained with crossover of V<sup>2+</sup>/V<sup>3+</sup> from the anode to the cathode in combination with the fact that the VARFB was charged in all cycles with the constant charge of 93% of the initial anolyte capacity. The loss of vanadium on the anode side leads to a loss of the anolyte capacity. Different V<sup>2+</sup>:V<sup>3+</sup> ratio results in different electrode potentials and higher charging potential.

Additionally, with decreasing total amount of vanadium in the anolyte the share of side reactions may increase. After all V<sup>3+</sup> is converted to V<sup>2+</sup>, the reaction on the anode will be the evolution of hydrogen (2H<sup>+</sup> + 2e<sup>-</sup> → H<sub>2</sub>) [28]. This reaction is known to proceed with relatively high overpotentials on a graphite felt electrode [19], therefore the charging potential increased at the end of the charging step. In the fourth cycle the original anolyte capacity was recovered due to an exchange of the electrolyte. The potential did not increase at the end of the charging step as it was the case in the second and third cycle. This explanation is also reflected in the coulombic efficiencies  $\eta_c$  and the discharge capacity  $Q_{\text{discha}}$  for the four cycles (Table 2). A decrease of  $\eta_c$  and  $Q_{\text{discha}}$  with each of the first three cycles was observed, in the fourth cycle both values were approximately the same as in the first cycle. The produced hydrogen lead to a loss of charge and therefore a reduction of the coulombic efficiency. In the third cycle the anolyte capacity was the lowest, the side reaction (hydrogen evolution) became more significant and therefore the coulombic efficiency was the lowest of all cycles.

Despite of that, the continuous crossover of vanadium to the cathode side can also be noticed by comparing the beginning of the charging curves. The second and the third cycle showed a small potential step in the beginning of the charging reaction, while the first and fourth cycle did not show this feature (see inset in Fig. 7).

**Table 2**

Performance data of subsequent cycles of VARFB operation at 20 mA cm<sup>-2</sup> (Q = charge; W = electrical energy,  $\eta_c$  = coulombic efficiency,  $\eta_v$  = voltaic efficiency,  $\eta_E$  = energy efficiency).

Cycle	$Q_{\text{discha}}$ [mAh]	$\eta_c$	$W_{\text{cha}}$ [mWh]	$W_{\text{discha}}$ [mWh]	$\eta_E$	$\eta_v$
1st	302.4	83.9%	654.9	272.6	41.6%	49.6%
2nd	277.0	76.7%	661.5	240.0	36.3%	47.3%
3rd	269.8	74.7%	674.5	216.2	32.1%	43.0%
4th <sup>a</sup>	307.9	85.4%	680.3	239.7	35.2%	41.2%

<sup>a</sup> The fourth cycle was recorded with fresh anolyte and catholyte.

This potential step was most probably related to the oxidation of  $\text{VO}^{2+}$  to  $\text{VO}_2^+$  on the cathode side, since the oxidation of  $\text{VO}^{2+}$  takes place at potentials lower than those necessary for OER.  $\text{VO}^{2+}$  was present on the cathode side due to crossover of  $\text{V}^{2+}/\text{V}^{3+}$  which were immediately oxidised to  $\text{VO}^{2+}$  under the existing potential conditions.

Although the increase of charging potential caused by the capacity loss was suppressed by exchanging the electrolytes, an additional irreversible potential increase can be noticed. The sharp increase at the end of the charging step vanished in the fourth cycle after the electrolytes were exchanged but the average charging potential was higher than in the first cycle. This was also represented by the increasing energy consumption in the charging steps ( $W_{\text{cha}}$  in Table 2) for all four cycles. Even after the electrolyte exchange higher charging potentials were still observed. Therefore, it can be concluded that the system additionally underwent degradation processes that were not related to crossover reactions. The same, even more pronounced, was observed for the discharging curves. The discharge overpotentials increased with each cycle and therefore the average discharge potential decreased. The general increase of overpotentials for both charging and discharging with each of the four cycles was also reflected by the continuous decrease of the voltaic efficiency  $\eta_V$  shown in Table 2.

A general increase of overpotentials that can not be suppressed by electrolyte exchange indicates that the cell resistances (ohmic resistances, but also charge-transfer resistances) increased during operation. There are several factors that can contribute to this irreversibly increased resistances. Firstly, corrosion of conducting materials in the cell such as the electrodes or current collectors may raise the internal resistance of the cell and/or hinder the diffusion of reactants leading to increased mass transport resistances. Secondly, the degradation and/or agglomeration of the catalyst particles may lead to a loss of catalytically active surface area resulting in an increase of charge-transfer resistances. The average discharging potential decreased with each cycle much more than the average charging potential increased. Accordingly, it can be assumed that the degradation of the GDE (the active electrode during discharging) was more pronounced than that of the  $\text{IrO}_2$ -modified graphite felt. This could be attributed to the less graphitic nature of the GDL compared to the graphite felt. From PEM fuel cells it is known that electrochemical oxidation of the GDL leads to a loss of hydrophobicity [29]. This in turn promotes the flooding of the GDL with water hindering the oxygen transport to the catalytic sites and thus leading to performance loss. Additionally, it is known that the carbon support of the catalyst might undergo corrosion and platinum particles might agglomerate in PEM fuel cells when operated at high potentials [30–32]. The GDE seems to be prone to corrosion under the severe potential conditions. Further investigations of alternative GDL and different supports for the platinum catalyst which could reduce corrosion effects have to be performed.

The degradation of the  $\text{IrO}_2$ -modified graphite felt electrode seems to be less pronounced. On one hand, this can be attributed to the stability of  $\text{IrO}_2$  even under severe oxidative conditions [33]. On the other hand, the graphite felt support was shown to undergo some degradation in VRFB under certain operating conditions [34–36] but it was also reported that the presence of  $\text{IrO}_2$  on carbon surface reduces carbon corrosion under oxidative conditions [37]. Further investigations on the stability of the  $\text{IrO}_2$ -modified graphite felt under VARFB operation conditions are necessary to detail specific degradation mechanisms.

#### 4. Conclusion

In this paper the design of a VARFB comprising a novel two-layered cathode was presented and its performance was

investigated. We showed a straightforward and simple routine to modify a graphite felt with  $\text{IrO}_2$  which performed well as electrode for the reaction in the positive half cell during charging (OER). With the proposed layer arrangement and materials which were used for the positive half cell reactions (ORR in discharging and OER in charging), a better performance in terms of efficiency, discharge power density and employable current density could be obtained in comparison to existing reports on VARFB [16] and VOFC [17,18]. At a current density of  $20 \text{ mA cm}^{-2}$  and room temperature, the VARFB was operated with a coulombic efficiency of  $\eta_C = 84.2\%$ , a voltaic efficiency of  $\eta_V = 49.5\%$  and an energy efficiency of  $\eta_E = 41.7\%$ . An average discharge power density of  $34.6 \text{ mW cm}^{-2}$  at  $40 \text{ mA cm}^{-2}$  was achieved.

Half cell potentials showed that energy and voltaic efficiency were mainly limited by slow OER and ORR kinetics. Higher operation temperatures are promising to enhance the cathodic reactions and increase efficiency.

The operation of the VARFB for four subsequent cycles revealed a performance decrease with each cycle which was not only related to loss of active material due to crossover, but also due to irreversible degradation processes taking place during operation. Therefore, crossover-minimising membranes are needed to reduce coulombic losses and alternative corrosion-resistant GDL as well as other catalyst support strategies would be promising to achieve a higher stability.

#### Acknowledgements

The authors would like to thank Andrea Ballarin, Benedikt Berger and Frank Bättermann for assisting with the experimental work. Likewise we appreciate the contributions of Martin Knipper (XRD measurements), Dana Schonvogel (ICP-MS measurements), Hayo Seeba and Dietmar Piehler (construction of the test cell). Jan grosse Austing thanks the Reiner Lemoine-Stiftung, Berlin, Germany for a Ph.D. scholarship.

#### References

- [1] P. Alotto, M. Guarnieri, F. Moro, *Renewable Sustainable Energy Rev.* 29 (2014) 325–335.
- [2] H. Chen, T.N. Cong, W. Yang, C. Tan, Y. Li, Y. Ding, *Prog. Nat. Sci.* 19 (2009) 291–312.
- [3] C. Ponce de León, a. Frías-Ferrer, J. González-García, D. Szánto, F. Walsh, *J. Power Sources* 160 (2006) 716–732.
- [4] M. Skyllas-Kazacos, M.H. Chakrabarti, S.a. Hajimolana, F.S. Mjalli, M. Saleem, *J. Electrochem. Soc.* 158 (2011) R55.
- [5] P. Leung, X. Li, C. Ponce de León, L. Berlouis, C.T.J. Low, F.C. Walsh, *RSC Adv.* 2 (2012) 10125.
- [6] L. Li, S. Kim, W. Wang, M. Vijayakumar, Z. Nie, B. Chen, J. Zhang, G. Xia, J. Hu, G. Graff, J. Liu, Z. Yang, *Adv. Energy Mater.* 1 (2011) 394–400.
- [7] M. Skyllas-Kazacos, *J. Power Sources* 124 (2003) 299–302.
- [8] S. Peng, N. Wang, C. Gao, Y. Lei, X. Liang, S. Liu, Y. Liu, *Int. J. Electrochem. Sci.* 7 (2012) 4388–4396.
- [9] H. Kaneko, A. Negishi, K. Nozaki, K. Sato, M. Nakajima, EU Patent 0517217A1, 1992.
- [10] M. Chakrabarti, N. Brandon, S. Hajimolana, F. Tariq, V. Yufit, M. Hashim, M. Hussain, C. Low, P. Aravind, *J. Power Sources* 253 (2014) 150–166.
- [11] H.-S. Kim, *Bull. Korean Chem. Soc.* 32 (2011) 571–575.
- [12] B. Sun, M. Skyllas-Kazacos, *Electrochim. Acta* 37 (1992) 1253–1260.
- [13] B. Sun, M. Skyllas-Kazacos, *Electrochim. Acta* 36 (1991) 513–517.
- [14] E.-M. Hammer, B. Berger, L. Komsyiska, *Int. J. Renewable Energy Dev.* 3 (2014) 7–12.
- [15] L. Jörissen, *J. Power Sources* 155 (2006) 23–32.
- [16] S. Hosseiny, M. Saakes, M. Wessling, *Electrochem. Commun.* 13 (2011) 751–754.
- [17] C. Menictas, M. Skyllas-Kazacos, *J. Appl. Electrochem.* 41 (2011) 1223–1232.
- [18] J. Noack, C. Cremers, D. Bayer, J. Tübke, K. Pinkwart, *J. Power Sources* 253 (2014) 397–403.
- [19] W. Wang, X. Wang, *Electrochim. Acta* 52 (2007) 6755–6762.
- [20] L. Ouattara, S. Fierro, O. Frey, M. Koudelka, C. Comninellis, *J. Appl. Electrochem.* 39 (2009) 1361–1367.
- [21] Q.H. Liu, G.M. Grim, A.B. Papandrew, A. Turhan, T.A. Zawodzinski, M.M. Mench, *J. Electrochem. Soc.* 159 (2012) A1246–A1252.

- [22] G. Li, P.G. Pickup, *Electrochim. Acta* 49 (2004) 4119–4126.
- [23] C.-N. Sun, F.M. Delnick, D.S. Aaron, A.B. Papandrew, M.M. Mench, T.A. Zawodzinski, *ECS Electrochem. Lett.* 2 (2013) A43–A45.
- [24] ICDD, PDF-2 Database Release 2009, Code: 03-065-2822, International Centre for Diffraction Data, Newtown Square, PA, USA, 2009.
- [25] J. Xi, Z. Wu, X. Teng, Y. Zhao, L. Chen, X. Qiu, *J. Mater. Chem.* 18 (2008) 1232.
- [26] H.-Y. Jung, P. Ganesan, B. Popov, *ECS Trans.* 25 (2009) 1261–1269.
- [27] S.-D. Yim, W.-Y. Lee, Y.-G. Yoon, Y.-J. Sohn, G.-G. Park, T.-H. Yang, C.-S. Kim, *Electrochim. Acta* 50 (2004) 713–718.
- [28] M. Skyllas-Kazacos, M. Kazacos, *J. Power Sources* 196 (2011) 8822–8827.
- [29] S. Yu, X. Li, S. Liu, J. Hao, Z. Shao, B. Yi, *RSC Adv.* 4 (2014) 3852.
- [30] N. Linse, L. Gubler, G.G. Scherer, A. Wokaun, *Electrochim. Acta* 56 (2011) 7541–7549.
- [31] R.L. Borup, J.R. Davey, F.H. Garzon, D.L. Wood, M.a. Inbody, *J. Power Sources* 163 (2006) 76–81.
- [32] S. Maass, F. Finsterwalder, G. Frank, R. Hartmann, C. Merten, *J. Power Sources* 176 (2008) 444–451.
- [33] S. Trasatti, *Electrochim. Acta* 45 (2000) 2377–2385.
- [34] A. Parasuraman, T.M. Lim, C. Menictas, M. Skyllas-Kazacos, *Electrochim. Acta* 101 (2013) 27–40.
- [35] M. Rychcik, M. Skyllas-Kazacos, *J. Power Sources* 19 (1987) 45–54.
- [36] H. Liu, Q. Xu, C. Yan, *Electrochem. Commun.* 28 (2013) 58–62.
- [37] S.-E. Jang, H. Kim, *J. Am. Chem. Soc.* 132 (2010) 14700–14701.

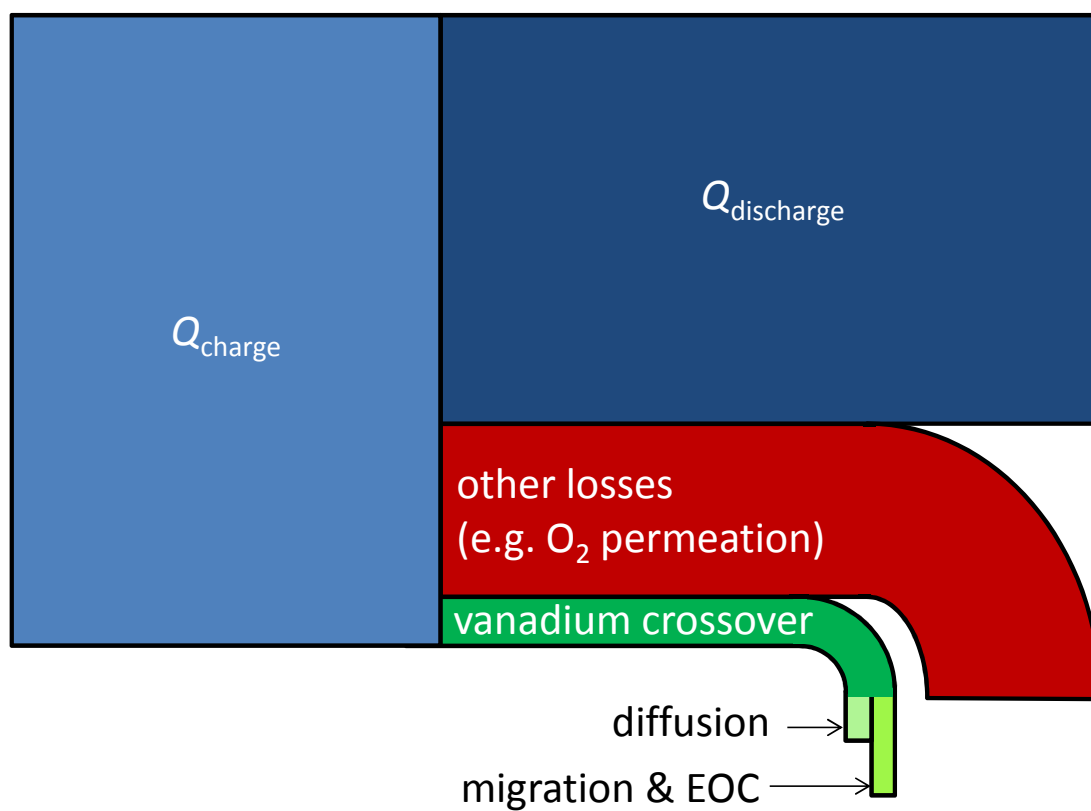
# Publication II



# Investigation of crossover processes in a unitized bidirectional vanadium/air redox flow battery

Authors: Jan grosse Austing, Carolina Nunes Kirchner, Lidiya Komsiyka and Gunther Wittstock

Journal of Power Sources, 306, 2016, 692-701, DOI: 10.1016/j.jpowsour.2015.12.052







# Investigation of crossover processes in a unitized bidirectional vanadium/air redox flow battery



Jan grosse Austing<sup>a</sup>, Carolina Nunes Kirchner<sup>a</sup>, Lidiya Komsiyiska<sup>a</sup>, Gunther Wittstock<sup>b,\*</sup>

<sup>a</sup> NEXT ENERGY EWE Research Centre for Energy Technology, 26129 Oldenburg, Germany

<sup>b</sup> Carl von Ossietzky University of Oldenburg, Faculty of Mathematics and Natural Sciences, Center of Interface Science, Institute of Chemistry, 26111 Oldenburg, Germany

## HIGHLIGHTS

- Crossover in a VARFB is investigated using ICP-MS and *in situ* UV/Vis spectroscopy.
- Coulombic efficiency of a VARFB is lowered by crossover (mainly O<sub>2</sub> permeation).
- Vanadium crossover which limits the cycle life of VARFB is quantified.
- Diffusion coefficients of V<sup>2+</sup> and V<sup>3+</sup> through Nafion<sup>®</sup> 117 are determined.

## ARTICLE INFO

### Article history:

Received 9 September 2015

Received in revised form

27 November 2015

Accepted 15 December 2015

Available online xxx

### Keywords:

Vanadium-air redox flow battery

Crossover redox flow battery

Vanadium oxygen fuel cell

Bidirectional oxygen/air electrode

Unitized regenerative fuel cell

Diffusion coefficient vanadium Nafion

## ABSTRACT

In this paper the losses in coulombic efficiency are investigated for a vanadium/air redox flow battery (VARFB) comprising a two-layered positive electrode. Ultraviolet/visible (UV/Vis) spectroscopy is used to monitor the concentrations  $c_{V^{2+}}$  and  $c_{V^{3+}}$  during operation. The most likely cause for the largest part of the coulombic losses is the permeation of oxygen from the positive to the negative electrode followed by an oxidation of V<sup>2+</sup> to V<sup>3+</sup>. The total vanadium crossover is followed by inductively coupled plasma mass spectroscopy (ICP-MS) analysis of the positive electrolyte after one VARFB cycle. During one cycle 6% of the vanadium species initially present in the negative electrolyte are transferred to the positive electrolyte, which can account at most for 20% of the coulombic losses. The diffusion coefficients of V<sup>2+</sup> and V<sup>3+</sup> through Nafion<sup>®</sup> 117 are determined as  $D_{V^{2+}, N117} = 9.05 \cdot 10^{-6} \text{ cm}^2 \text{ min}^{-1}$  and  $D_{V^{3+}, N117} = 4.35 \cdot 10^{-6} \text{ cm}^2 \text{ min}^{-1}$  and are used to calculate vanadium crossover due to diffusion which allows differentiation between vanadium crossover due to diffusion and migration/electroosmotic convection. In order to optimize coulombic efficiency of VARFB, membranes need to be designed with reduced oxygen permeation and vanadium crossover.

© 2015 Elsevier B.V. All rights reserved.

## 1. Introduction

In the past years, redox flow batteries (RFB) have gained increasing attention as promising candidates for stationary electricity storage applications. They show advantageous characteristics such as high cycle life (>12,000 [1]) and good round-trip efficiencies ( $\eta_E \approx 80\%$  [2]). However, as redox flow batteries are generally based on electroactive materials (e.g. metal cations) dissolved in a solvent (e.g. water) with a limited solubility, the energy density of RFB is low compared to other battery systems (e.g.

25–30 Wh kg<sup>-1</sup> for the all-vanadium redox flow battery (VRFB) [3]).

Different approaches have been proposed to enhance the energy density of RFB including increasing the solubility of the electrolytes by using additives [4,5] or following alternative concepts such as solid/liquid hybrid redox flow batteries [6,7]. The substitution of the positive half cell (i.e. the VO<sup>2+</sup>/VO<sub>2</sub><sup>+</sup> redox couple) by a bidirectional air electrode was disclosed in a patent in 1992 [8] and holds the potential for roughly doubling the energy density in relation to a VRFB. A modular VARFB system (i.e. two separate reaction units for charging and discharging) was described by Hosseiny et al. [9] and a system for discharging only was reported by Noack et al. [10] and Menictas et al. [11].

In our previous paper [12] we introduced a concept for a

\* Corresponding author.

E-mail address: [gunther.wittstock@uni-oldenburg.de](mailto:gunther.wittstock@uni-oldenburg.de) (G. Wittstock).

unitised bidirectional VARFB utilising a two-layered positive electrode. Figure 1a depicts the setup of the VARFB. The negative electrode of the battery comprises a current collector (②) and a graphite felt electrode (③) through which the  $V^{2+}/V^{3+}$  containing electrolyte (①) is circulated. For brevity we denote the electrolyte in the negative electrode as “negative electrolyte” (analogous for the “positive electrolyte”). The positive electrode is composed of two electrodes that are pressed together: An  $IrO_2$ -modified graphite felt (⑤) serves as electrode for the charging reaction (oxygen evolution reaction, OER;  $2H_2O \rightarrow O_2 + 4e^- + 4H^+$ ), while a platinum-containing gas diffusion layer (⑥) which is fed with air through the flow-field/current collector (⑦) supports the discharging reaction (oxygen reduction reaction, ORR;  $O_2 + 4e^- + 4H^+ \rightarrow 2H_2O$ ). Negative and positive electrode are separated from each other by a Nafion® 117 membrane (④). The VARFB was operated for several cycles and an energy efficiency  $\eta_E = 39\%$  at  $21^\circ C$  and  $40\text{ mA cm}^{-2}$  was achieved [12].

However, comparably low coulombic efficiencies ( $\eta_C = 55.0\%$  at  $15\text{ mA cm}^{-2}$  and  $\eta_C = 87.6\%$  at  $40\text{ mA cm}^{-2}$ ) were obtained which also decreased with each consecutive cycle. The coulombic efficiency  $\eta_C$  is the ratio of the amount of electric charge delivered during discharging ( $Q_{\text{discharge}}$ ) to the charge consumed during charging ( $Q_{\text{charge}}$ ):

$$\eta_C = \frac{Q_{\text{discharge}}}{Q_{\text{charge}}} \quad (1)$$

The capacity of the VARFB depends exclusively on the capacity of the negative electrolyte because the reagents of the positive electrode are  $O_2$  and  $H_2O$  which are not limiting in our setup (Fig. 1b). Therefore, a decrease of  $\eta_C$  must only consider all side reactions that influence the capacity of the negative electrolyte. Fig. 2b shows the cell reactions occurring in a VARFB. The main

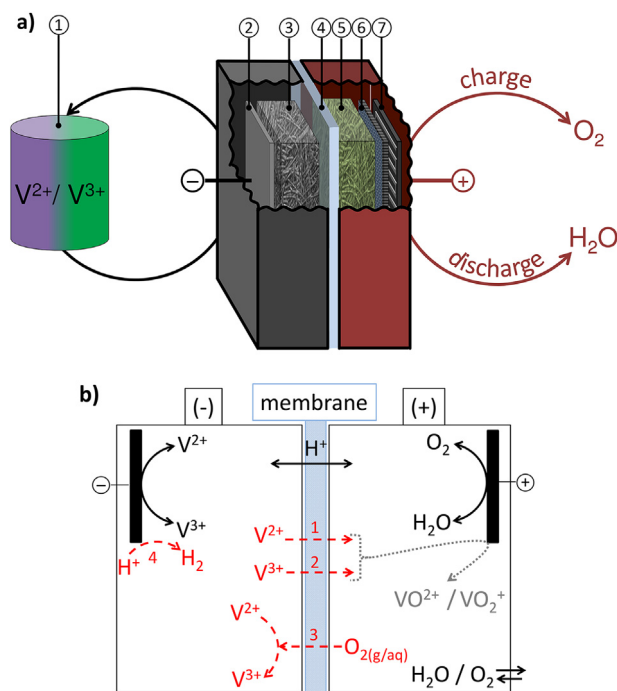


Fig. 1. a) The VARFB test cell comprising a two-layered positive electrode. ① = negative electrolyte tank; ② = current collector; ③ = graphite felt; ④ = membrane; ⑤ =  $IrO_2$ -mod. graphite felt; ⑥ = gas diffusion electrode; ⑦ = current collector with flow field. b) Possible chemical reactions in the VARFB. Main reactions (—),  $\eta_C$  reducing crossover and side reactions (---) and subsequent chemical reaction (···). 1, 2 = vanadium crossover; 3 = oxygen crossover; 4 = hydrogen evolution.

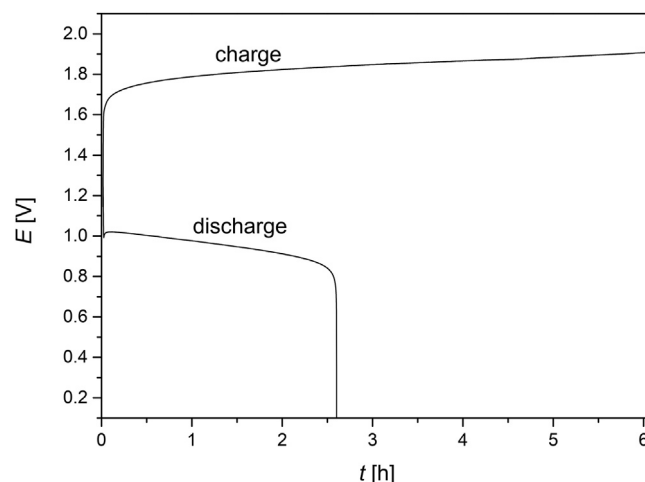


Fig. 2. Charge/discharge curve of the VARFB test cell ( $j = 15\text{ mA cm}^{-2}$ ,  $21^\circ C \pm 1^\circ C$ ).

reactions are shown as black solid line, side reactions reducing  $\eta_C$  are numbered and highlighted by red dashed lines. Processes 1 and 2 illustrate the crossover of  $V^{2+}$  and  $V^{3+}$  from the negative to the positive electrode. After crossing the membrane,  $V^{2+}$  and  $V^{3+}$  can be oxidized at the positive electrode to  $VO^{2+}$  (“ $V^{4+}$ ”) and/or  $VO_2^+$  (“ $V^{5+}$ ”) due to the potential of the positive electrode or due to oxygen present in the positive electrode chamber. This reaction (gray dotted arrow) does not influence  $\eta_C$  because the capacity is determined by the capacity of the negative electrolyte. Process 3 depicts the oxygen crossover and the subsequent homogeneous oxidation of  $V^{2+}$  to  $V^{3+}$  by  $O_2$  which reduces  $\eta_C$  because  $V^{2+}$  is consumed. Hydrogen evolution reaction (HER; process 4) would also lower  $\eta_C$ . The chemical follow-up reaction has no influence on  $\eta_C$  and thus depicted as gray dotted line.

For conventional VRFB the crossover of vanadium species through the membrane has been reported to contribute to  $\eta_C$  losses and was investigated in several studies [13–18]. This crossover (i.e. the transport of ions through the membrane) is caused by one or more of the three processes: migration (in the electric field during battery operation), electroosmotic convection (EOC; caused by electroosmotic flow of water through the membrane) and/or diffusion [19]. Recently, these processes were studied in detail for VRFB by Darling et al. [20] and Yang et al. [19] by modeling approaches. Yang et al. [19] found that  $V^{3+}$  net transfer from the negative to the positive electrode is much more pronounced during discharging than during charging due to superposition of the three processes. During charging the direction of the diffusive part (negative to positive) is opposite to the direction of migration and EOC (positive to negative).

The transport of vanadium cations through the cation exchange membrane is influenced by the interactions of the cations with the negatively charged sulfonate groups of the membrane [21,22]. The transport mechanisms of vanadium ions through a Nafion® membrane on a molecular level have been investigated and discussed in several publications [22–25]. Vijayakumar et al. [22] reported about two fouling mechanisms of Nafion® membranes due to vanadium cations that blocked the sulfonic acid groups. Recently, the interaction between triflic acid ( $F_3C-SO_3H$ ) as a reference system for Nafion® and vanadium cations was investigated with hybrid density functional theory [21]. The influence of absorbed  $V^{2+}$  and  $V^{3+}$  on the local structure of Nafion® was examined by molecular dynamics [26].

Diffusion coefficients for vanadium species through diverse (pristine and modified) membranes were investigated in several

studies [13–17,27–29] and used in detailed modeling and simulation studies of VRFB [30–33]. For Nafion® 115 membranes diffusion coefficients for  $V^{2+}$  and  $V^{3+}$  were reported [13,14], for Nafion® 117 membranes values for  $V^{3+}$  were published [15,16]. In a VARFB, the crossover of  $V^{2+}$  and  $V^{3+}$  from the negative to the positive electrode leads to a decreased amount of vanadium ions in the negative electrolyte and therefore to an irreversible decrease in battery capacity because the negative electrolyte is the capacity limiting factor. No “back-crossover” from the (diluted) positive electrolyte to the (concentrated) negative electrolyte is assumed to occur.

Hosseiny et al. [9] suspected crossover of oxygen as a possible cause for additional  $\eta_C$  reduction. Oxygen could permeate from the positive to the negative electrode followed by oxidation of  $V^{2+}$  to  $V^{3+}$ . However, this assumption has not been investigated experimentally yet.

Furthermore, the HER which might occur on the negative electrode would lower  $\eta_C$  as well. Unwanted side reactions on the positive electrode (e.g. carbon corrosion) have no influence on the loss of  $\eta_C$  as the cathodic reactants ( $H_2O$  and  $O_2$ , respectively) are supplied in excess.

In the current contribution, losses of  $\eta_C$  in a VARFB were investigated with the aim to identify and quantify the different loss processes. UV/Vis spectroscopy was applied to investigate the concentrations of the vanadium species in VRFB [34–41]. In the negative electrolyte exists a linear relationship between absorption and  $c_{V^{2+}}$  and  $c_{V^{3+}}$  at least up to 1.6 M when using a cuvette with a maximum path length of  $d = 1$  mm [36,39]. Due to dimer formation between  $VO_2^+$  and  $VO^{2+}$  species, the monitoring of the positive electrolyte would require a non-linear calibration [36,37,39,42]. Using a flow-through cuvette with  $d \leq 1$  mm avoids on the one hand the necessity of diluting solutions before UV/Vis analysis [34,38] and avoids on the other hand the contact of the negative electrolyte with air ( $O_2$  easily oxidizes  $V^{2+}$  to  $V^{3+}$ ) allowing UV/Vis spectroscopy to be applied *in situ*. The monitoring of  $c_{V^{2+}}$  and  $c_{V^{3+}}$  during VARFB operation allowed conclusion on occurring loss mechanisms.

Inductively coupled plasma mass spectroscopy (ICP-MS) measurements was used to determine the overall vanadium crossover occurring during charging and discharging by measuring the vanadium concentration in the positive electrolyte. Diffusion coefficients of  $V^{2+}$  and  $V^{3+}$  through Nafion® 117 were determined to estimate the contribution of fickian diffusion on the vanadium crossover. This information allows relating the crossover processes 1, 2 and 3 in Fig. 1b to each other. Finally, recommendations are discussed for future membrane development to improve  $\eta_C$ .

## 2. Experimental

### 2.1. $V^{2+}$ and $V^{3+}$ electrolyte preparation

The  $V^{2+}$  and  $V^{3+}$  electrolytes used in this work were prepared electrolytically in a conventional VRFB setup similar as described elsewhere [43] and as reported in our previous publication [12].

Briefly, a solution of 1.2 M  $VOSO_4 \cdot x H_2O$  ( $x \approx 3$ ; 97%; Sigma Aldrich, Germany) and 2.0 M  $H_2SO_4$  (95–97%; Fischer Scientific GmbH, Germany) in deionized water was prepared and appropriately electrolyzed in a VRFB setup using a potentiostat/galvanostat (Solartron Analytical Modulab Pstat potentiostat/galvanostat, UK).

The  $V^{2+}$  and  $V^{3+}$  electrolytes are analysed using ICP-MS (XSERIES 2 ICP-MS, Thermo Scientific, USA) to determine the total vanadium concentration, as it can deviate from the initial vanadium concentration of 1.2 mol  $L^{-1}$  due to crossover processes during the electrolyte preparation [13,44]. Scandium was used as an internal standard. For these and all following ICP-MS-analysed samples the concentration of vanadium was determined in three subsequent

runs and the average value was used. The relative standard deviations (RSD) between the runs was less than 1.2%.

### 2.2. Components for the VARFB test cell and operation

The components for the VARFB test cell were fabricated and the VARFB operated as described in our previous paper [12]. The general setup of the VARFB test cell with the different layers of the reaction unit is shown in Fig. 1a.

Carbon felts (GFD5, SGL Carbon GmbH, Germany) were thermally activated at 400 °C for 18 h in air. The  $IrO_2$ -modified graphite felt was prepared by thermal decomposition of  $(NH_4)IrCl_6$  (99.994%; Alfa Aesar, GmbH & Co KG, Germany). The gas diffusion electrode (GDE) was loaded with Nafion® and Pt/C (approx. 0.96 mg  $cm^{-2}$  Pt) via airbrushing. Nafion® 117 (Ion Power GmbH, Germany) was used as membrane after protonation [(1) 5%  $H_2O_2$ /80 °C/30 min; (2) 1.0 M  $H_2SO_4$ /80 °C/30 min; (3) deionized water/100 °C/10 min]. Nafion membranes with the equivalent weight of 1100 are a benchmark material used in VRFB research. Although having a higher ohmic resistance, the thicker Nafion® 117 in comparison to the thinner Nafion® 115 was chosen because lower vanadium crossover and oxygen permeation fluxes can be expected. The negative current collector was made from a graphite bipolar plate material (PPG 86, Eisenhuth GmbH Co. KG, Germany), the positive one was manufactured from titanium (grade 2).

A previously [12] described test cell with 4  $cm^2$  geometric electrode area was used for VARFB operation. The negative electrolyte was 12 mL of a  $V^{3+}$  electrolyte which was permanently purged with humidified  $N_2$  to avoid contact with air. 50 mL of 2 M  $H_2SO_4$  were employed as positive electrolyte. Both electrolytes were circulated with 100  $mL\ min^{-1}$ . During discharging the positive electrolyte was not circulated but the GDE on the positive electrode was fed with air (267  $mL\ min^{-1}$ ). The experiments were carried out at room temperature (21 °C  $\pm$  1 °C). After charging and discharging, a sample of the positive electrolyte was taken for ICP-MS measurements.

### 2.3. UV/Vis calibration and *in situ* UV/Vis spectroscopy of the negative electrolyte during VARFB operation

A calibration curve was obtained by measuring the UV/Vis absorption (LAMBDA XLS + UV/Vis Spectrophotometer, PerkinElmer, USA) of a dilution series of  $V^{2+}$  and  $V^{3+}$  in 2 M  $H_2SO_4$ . Diluted  $V^{2+}$  and  $V^{3+}$  electrolytes were derived from electrolytically prepared  $V^{2+}$  and  $V^{3+}$  electrolytes (section 2.1). The concentrations as determined by ICP-MS were  $c_{V^{2+}} = 1.06$  mol  $L^{-1}$  and  $c_{V^{3+}} = 1.09$  mol  $L^{-1}$ , respectively. The UV/Vis measurements were conducted by circulating the electrolyte through a flow-through cuvette with 1 mm path length (137-QS, Quartz SUPRASIL®, Hellma GmbH & Co. KG, Germany). The electrolyte was blanketed with humidified nitrogen to avoid contact with air.

During VARFB operation the flow-through cuvette was integrated in the hydraulic circuit of the negative electrolyte which was pumped through the cuvette before entering the VARFB test cell. Approx. every 15 min a UV/Vis spectrum was recorded and the  $V^{2+}$  and  $V^{3+}$  concentrations were calculated based on the calibration data.

### 2.4. Determination of diffusion coefficients of $V^{2+}$ and $V^{3+}$ through Nafion® 117

For the determination of the permeability of  $V^{2+}$  and  $V^{3+}$  through a Nafion® 117 membrane, a similar routine is used as described by other authors [13,14,16,45]. The membrane was sandwiched between the compartments of a separable H-cell with

an exposed membrane area of 5.391 cm<sup>2</sup>. The thickness of the pretreated, wetted Nafion® 117 membrane was measured as  $x = 207 \mu\text{m}$ . One side of the H-cell was filled with 130 mL of a V<sup>2+</sup> or V<sup>3+</sup> electrolyte (denoted as excess side). The initial concentration of vanadium in the V<sup>2+</sup> electrolyte was  $c_{V^{2+}} = 1.08 \text{ mol L}^{-1}$ , the concentration in the V<sup>3+</sup> electrolyte was  $c_{V^{3+}} = 1.12 \text{ mol L}^{-1}$  as determined by ICP-MS.

The other side (denoted as deficiency side) was filled with 130 mL of a 1.2 M MgSO<sub>4</sub> and 2 M H<sub>2</sub>SO<sub>4</sub> solution. MgSO<sub>4</sub> was used to reduce the difference in ionic strengths between the two solutions and therefore to reduce the osmotic pressure [45]. Both solutions were permanently kept under a blanket of humidified nitrogen to avoid the oxidation of the V<sup>2+</sup> or V<sup>3+</sup> species by oxygen from the ambient air. The deficiency side was stirred for 1 min with a magnetic stir bar (to achieve a homogeneous vanadium concentration in the solution) before taking a sample. Approx. every 60 min samples of the solution in the deficiency side were taken for the determination of the vanadium concentration by ICP-MS.

### 3. Results & discussion

A typical charge/discharge cycle at room temperature with a current density of  $j = 15 \text{ mA cm}^{-2}$  is shown in Fig. 2. A substantial amount of the charge from the charging process cannot be recovered during discharging ( $Q_{\text{charge}} = 361 \text{ mAh}$ ;  $Q_{\text{discharge}} = 156 \text{ mAh}$ ). Possible causes for this observation are the processes 1 (V<sup>2+</sup> crossover), 3 (oxygen permeation) and 4 (HER) depicted in Fig. 1b. All these processes have the consequence that  $\eta_C$  of the battery is reduced. The processes 1, 3 and 4 have a direct or an indirect influence on the vanadium concentration in the negative electrolyte: Process 1 decreases  $c_{V^{2+}}$ , process 3 decreases  $c_{V^{2+}}$  and increases  $c_{V^{3+}}$  and process 4 consumes charge that would be used to oxidize V<sup>2+</sup> to V<sup>3+</sup> (therefore indirectly decreases  $c_{V^{2+}}$  and  $c_{V^{3+}}$  in comparison to the stoichiometrically calculated value). It should be noted that  $\eta_C$  of the presented cycles in this contribution ( $\eta_C, 15 \text{ mA cm}^{-2} = 43\%$ ,  $\eta_C, 20 \text{ mA cm}^{-2} = 65\%$ ) differ from the values obtained in our previous publication ( $\eta_C, 15 \text{ mA cm}^{-2} = 55\%$ ,  $\eta_C, 20 \text{ mA cm}^{-2} = 84\%$ ) [12]. As all other experimental parameters were the same except the vanadium concentration in the negative electrolyte was 20% higher in the former publication (1.2 M vs. 0.96 M), it is assumed that the low vanadium concentration in the negative electrolyte could lead to faster depletion of convertible species and therefore more pronounced side reactions such as HER. This relationship between vanadium concentration and coulombic efficiency was also reported for VRFB [46]. As a possible explanation for this correlation the authors suggested gas evolution such as HER and OER which can be promoted due to depletion of species caused by low vanadium concentrations or low flow rates [46,47].

#### 3.1. Investigation of vanadium concentration in the negative electrolyte during VARFB operation with *in situ* UV/Vis spectroscopy

In order to gain insight into the loss mechanisms during VARFB which affect  $\eta_C$ , UV/Vis spectroscopy with a flow-through cuvette was used to determine  $c_{V^{2+}}$  and  $c_{V^{3+}}$  in the negative electrolyte during operation. As the vanadium species all have different visible spectrum, UV/Vis spectroscopy can be applied for their determination. The additivity of absorption  $A(\lambda)$  allows the determination of  $c_{V^{2+}}$  and  $c_{V^{3+}}$  by measuring the absorption  $A(\lambda_1)$  and  $A(\lambda_2)$  of the mixture at two different wavelengths  $\lambda_1$  and  $\lambda_2$  and using the Beer–Lambert law. The concentrations can be calculated by solving the following system of linear equations:

$$\begin{aligned} A(\lambda_1) &= \varepsilon_{V^{2+}}(\lambda_1) \cdot c_{V^{2+}} \cdot d + \varepsilon_{V^{3+}}(\lambda_1) \cdot c_{V^{3+}} \cdot d \\ A(\lambda_2) &= \varepsilon_{V^{2+}}(\lambda_2) \cdot c_{V^{2+}} \cdot d + \varepsilon_{V^{3+}}(\lambda_2) \cdot c_{V^{3+}} \cdot d \end{aligned} \quad (2)$$

The spectra of the electrolytes are shown in Fig. 3 for either 1.06 M V<sup>2+</sup> or 1.09 M V<sup>3+</sup> in 2 M H<sub>2</sub>SO<sub>4</sub>. V<sup>2+</sup> has absorption maxima at approximately 370 nm, 570 nm and 850 nm and V<sup>3+</sup> at 400 nm and 605 nm. The absorptions at 605 nm and 850 nm were used for the *in situ* UV/Vis spectroscopic monitoring of  $c_{V^{2+}}$  and  $c_{V^{3+}}$  in the negative electrolyte during VARFB operation. Calibration curves, obtained by measuring UV/Vis absorption of appropriately diluted V<sup>2+</sup> and V<sup>3+</sup> electrolytes, are shown in Fig. 3b with good linearity in the entire investigated concentration range allowing the simultaneous determination of  $c_{V^{2+}}$  and  $c_{V^{3+}}$  using Eq. (2).

Following Beer–Lambert law ( $A(\lambda) = \varepsilon(\lambda) \cdot c \cdot d$ ), the slope of the fitted lines in Fig. 3b is used to calculate the molar absorptivities:  $\varepsilon(\lambda) = \text{slope}/d$  ( $d = 1 \text{ mm}$ ). The molar absorptivities  $\varepsilon(\lambda)$  of V<sup>2+</sup> and V<sup>3+</sup> at 375 nm, 405 nm, 570 nm, 605 nm and 850 nm are compiled in Table 1.

The voltage,  $c_{V^{2+}}$  and  $c_{V^{3+}}$  obtained from UV/Vis spectroscopy are plotted as a function of time during the constant current charging (Fig. 4a) and discharging (Fig. 4b) at  $j = 15 \text{ mA cm}^{-2}$ . Assuming the absence of any loss mechanism and any transfer process through the membrane except H<sup>+</sup> permeation,  $c_{V^{2+}}$  should increase linearly and  $c_{V^{3+}}$  should decrease linearly (as schematically shown in

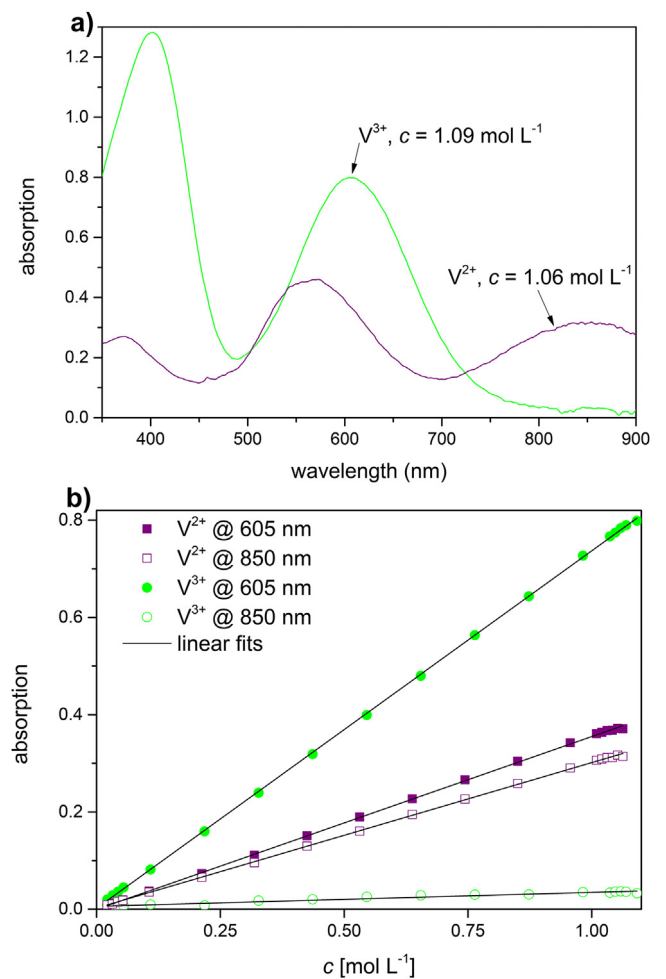
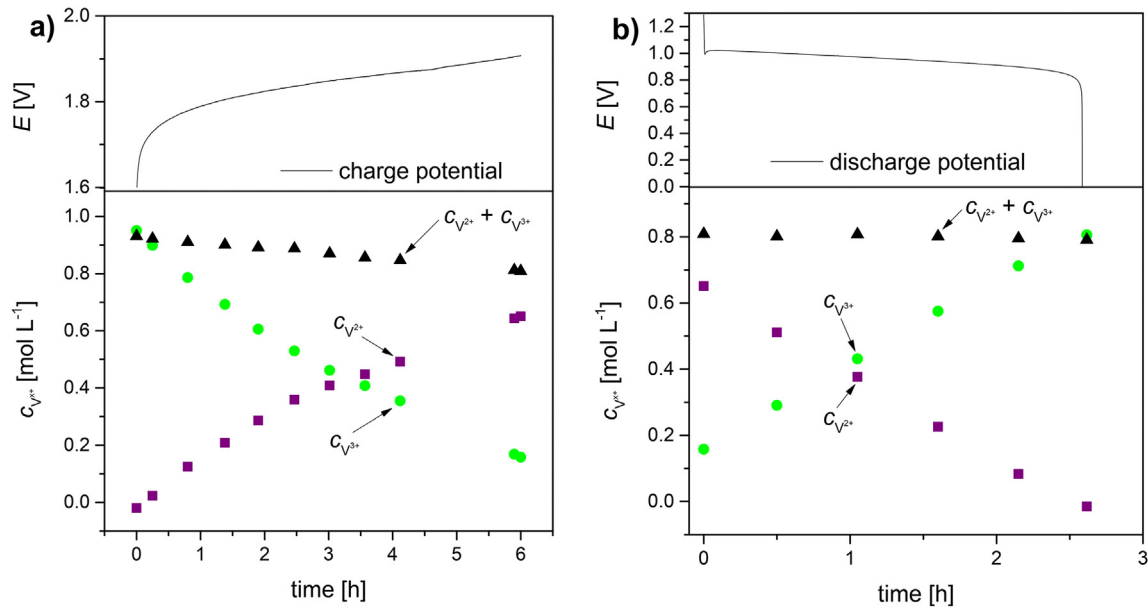


Fig. 3. Calibration of UV/Vis absorption of V<sup>2+</sup> and V<sup>3+</sup> electrolytes in 2 M H<sub>2</sub>SO<sub>4</sub>. a) UV/Vis spectra of concentrated V<sup>2+</sup> and V<sup>3+</sup> electrolytes. b) UV/Vis absorptions of V<sup>2+</sup> and V<sup>3+</sup> solutions with different concentrations at 605 nm and 850 nm and linear fits.

**Table 1**  
Molar absorptivities  $\epsilon(\lambda)$  [ $\text{L mol}^{-1} \text{cm}^{-1}$ ] of  $\text{V}^{2+}$  and  $\text{V}^{3+}$  in 2 M  $\text{H}_2\text{SO}_4$  at specific wavelengths  $\lambda$ .

	$\epsilon(375 \text{ nm})$	$\epsilon(405 \text{ nm})$	$\epsilon(570 \text{ nm})$	$\epsilon(605 \text{ nm})$	$\epsilon(850 \text{ nm})$
$\text{V}^{2+}$	2.51	1.72	4.34	3.56	2.99
$\text{V}^{3+}$	10.09	11.73	6.04	7.35	0.29



**Fig. 4.** In-situ UV/Vis monitoring of vanadium concentrations in the negative electrolyte during VARFB operation at  $j = 15 \text{ mA cm}^{-2}$ . a) Charging; b) Discharging.

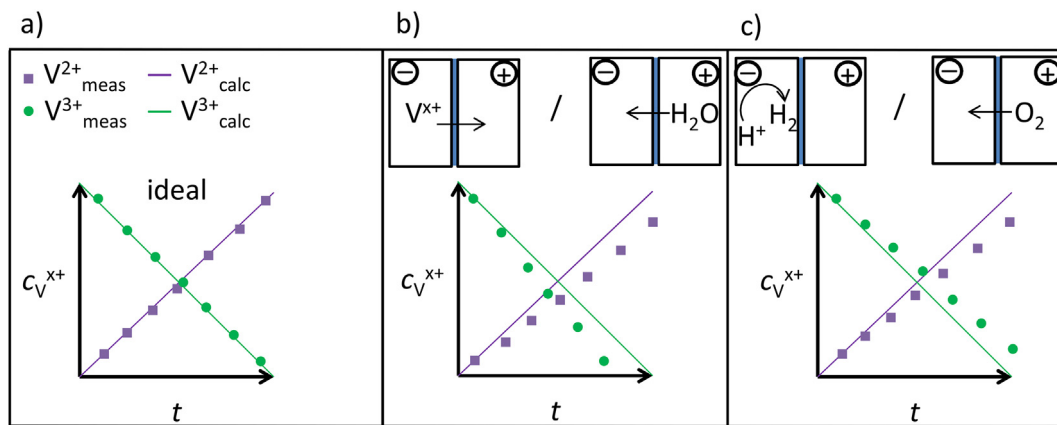


**Fig. 5.** Development of calculated concentrations  $c_{\text{V}^{2+}, \text{calc}}$  and  $c_{\text{V}^{3+}, \text{calc}}$  based on Eq. (3) in comparison to  $c_{\text{V}^{2+}, \text{meas}}$  and  $c_{\text{V}^{3+}, \text{meas}}$  during VARFB charging with no side reactions (a), influenced by water transfer and/or vanadium crossover (b) or by hydrogen evolution and/or oxygen permeation (c).

Fig. 5a). During the charging process (Fig. 4a) is clearly recognizable an asymptotic increase of  $c_{\text{V}^{2+}}$  above 60% state of charge (SOC), whereas the concentration of  $c_{\text{V}^{3+}}$  decreases in similar manner. The total vanadium concentration  $c_{\text{V}^{2+}} + c_{\text{V}^{3+}}$  is continuously decreasing during the charging. This could be caused by water transfer and/or vanadium crossover (Fig. 5b). During the discharge process in Fig. 4b,  $c_{\text{V}^{2+}}$  decreases linearly and  $c_{\text{V}^{3+}}$  increases. The total vanadium concentration remains constant during discharging. Since the vanadium concentrations change linearly during the discharge process, the asymptotic change of the concentrations during charging is most likely due to the HER taking place only during

charging. In general, at higher SOC the electrolyte is depleted of convertible species and the side reactions become more dominant. This effect is expected to be more noticeable at high current densities. However, the decrease of the total vanadium concentration in Fig. 4a contributes to the depletion of the active species in the electrolyte, which might be the reason for the asymptotic behavior

also at moderate SOC values. The diffusional vanadium crossover through the membrane due to concentration gradient is expected to be more pronounced at low current densities due to the longer charging time, since the amount of vanadium ions transferred by diffusion is independent of current density but increases with time. Therefore, the following studies were performed at a moderate current density of  $j = 20 \text{ mA cm}^{-2}$ .

To monitor the deviation between measured and calculated concentration, the volume  $V_{(-)}$  of the negative electrolyte needs to be known. However, the used experimental setup does not allow to monitor the negative electrolyte volume *in situ*. Therefore,  $V_{(-)}$  was

determined after charging and after discharging (Table 2). This approach is justified since the volume changes of negative electrolyte were not substantial. The theoretical  $c_{V^{2+}, calc}$  and  $c_{V^{3+}, calc}$  are obtained from Eq. (3) which is based on Faraday's law of electrolysis ( $I$  is the current,  $n_{V^{x+}}$  is the amount of  $V^{x+}$  and  $F$  is the Faraday constant) under the assumption that no side reactions take place and, therefore, concentration changes of  $c_{V^{2+}}$  and  $c_{V^{3+}}$  are exclusively due to their mutual interconversion by electron transfer at the negative electrode. The initial concentrations  $c_{V^{x+}}(t = 0)$  before charging and discharging were determined with UV/Vis spectroscopy. The “+” and “-” are used in appropriate manner (e.g. during charging the “+” is used for  $c_{V^{2+}}$  as this concentration increases).

$$c_{V^{x+}, calc}(t) = c_{V^{x+}}(t = 0) \pm \frac{\Delta n_{V^{x+}}(t)}{V_{(-)}} = c_{V^{x+}}(t = 0) \pm \frac{I \cdot t}{F \cdot V_{(-)}} \quad (3)$$

Taking into account the possible side reactions shown in Fig. 1b, the time evolution of  $c_{V^{2+}, meas}$  and  $c_{V^{3+}, meas}$  is shown schematically in Fig. 5a during charging in comparison to the expected evolution in the absence of any side reaction. If water is transferred from the positive electrode to the negative electrode and/or both vanadium species undergo crossover from the negative to the positive electrode,  $c_{V^{2+}, meas}$  and  $c_{V^{3+}, meas}$  should be lower than  $c_{V^{2+}, calc}$  and  $c_{V^{3+}, calc}$  (Fig. 5b). In case of parallel hydrogen evolution and/or oxygen permeation with subsequent chemical oxidation of  $V^{2+}$  to  $V^{3+}$ , the SOC of the battery is always lower than theoretically expected from the charge measured in the external circuit. The occurrence of these side reactions is indicated if  $c_{V^{2+}, meas}$  is lower than  $c_{V^{2+}, calc}$  and  $c_{V^{3+}, meas}$  is higher than  $c_{V^{3+}, calc}$  (Fig. 5c). However, during real operation of the VARFB a combination of the individual loss mechanisms is expected. Therefore, real values for  $c_{V^{2+}, meas}$  and  $c_{V^{3+}, meas}$  will most probably result from a superposition of the effects shown in Fig. 5a–c.

From the values in Table 2 it is evident that water is transferred through the membrane from the positive electrode to the negative electrode during charging and vice versa during discharging. The transfer of water is also known from VRFB [13,48,49] and is caused by osmotic pressure between the electrolytes and by water transfer concerted with proton transport due to charge balancing.

The potential during charging and discharging and  $c_{V^{2+}, meas}$  and  $c_{V^{3+}, meas}$  in the negative electrolyte at  $j = 20 \text{ mA cm}^{-2}$  are shown in Fig. 6. A significant deviation between the measured and calculated concentrations during charging can be seen at the end of the charging process for  $c_{V^{2+}}$  (Fig. 6a). As also discussed in section 3.2 and indicated by the amount of vanadium determined in the positive electrolyte by ICP-MS  $n_{V^{x+}, (+)}$ , ICP-MS in Table 3 diffusion of vanadium species occurs from the negative to positive electrode during the whole cycle. Thus,  $c_{V^{2+}, meas}$  and  $c_{V^{3+}, meas}$  lower than  $c_{V^{2+}, calc}$  and  $c_{V^{3+}, calc}$  are expected as schematically depicted in Fig. 5b. However, in Fig. 6a only  $c_{V^{2+}, meas}$  is lower than  $c_{V^{2+}, calc}$ , while  $c_{V^{3+}, meas}$  is close to  $c_{V^{3+}, calc}$ . This observation corresponds to a combination of the two scenarios shown in Fig. 5b and c. Three possible reactions that cause the deviation described in Fig. 5c are:

1. Hydrogen evolution (hydrogen evolution reaction; HER) at the negative electrode (process 4 in Fig. 1b).
2. Contact of oxygen with the negative electrolyte (and subsequent oxidation of  $V^{2+}$  to  $V^{3+}$ ).
3. Oxygen permeation from the positive to the negative electrode (process 3 in Fig. 1b).

The negative electrolyte was permanently purged with  $N_2$  to prevent contact of negative electrolyte with ambient air and therefore the explanation 2 can be neglected. Although relatively low potentials are present at the negative electrode during charging and HER could take place as a side reaction [50,51], the overpotential for HER is very high on graphite electrodes ( $\eta_{HER, graphite} = 0.977 \text{ V}$  at  $100 \text{ mA cm}^{-2}$  and  $25 \text{ }^\circ\text{C}$  [52]) and no bubble formation on the negative electrode was observed during charging. Therefore, we suppose that HER is not the dominant reaction. The permeation of oxygen through the membrane and subsequent oxidation of  $V^{2+}$  to  $V^{3+}$  was also suspected by Hosseiny et al. [9] to take place in a VARFB and is assumed to contribute most significantly to the deviation of  $c_{V^{2+}, meas}$  and  $c_{V^{3+}, meas}$  from  $c_{V^{2+}, calc}$  and  $c_{V^{3+}, calc}$ .

All possible explanations 1–3 would have the consequence that  $c_{V^{2+}, meas}$  would be lower than  $c_{V^{2+}, calc}$  and  $c_{V^{3+}, meas}$  would be higher than  $c_{V^{3+}, calc}$  (Fig. 5c). Taking into account that in parallel to oxygen permeation (or HER) the crossover of vanadium species from the negative to the positive electrode takes place which lowers  $c_{V^{2+}, meas}$  and  $c_{V^{3+}, meas}$ , measured  $c_{V^{2+}, meas}$  should fall below the values predicted by Eq. (3). The measured  $c_{V^{3+}, meas}$  value can be higher or lower than  $c_{V^{3+}, calc}$ , depending on whether oxygen permeation or vanadium crossover is more dominant. The observation concerning  $c_{V^{2+}, meas}$  (decreasing) and  $c_{V^{3+}, meas}$  (more or less constant) is reflected by Fig. 6a. One possible interpretation for this is that  $V^{2+}$  and  $V^{3+}$  crossover take place as well as  $O_2$  permeation and subsequent oxidation of  $V^{2+}$  to  $V^{3+}$ . As  $c_{V^{3+}, meas}$  remains nearly constant, the amount of “lost”  $V^{3+}$  due to crossover needs to be approximately equal to the amount of  $V^{3+}$  “gained” due to oxidation of  $V^{2+}$  by permeated  $O_2$ . Nevertheless, the observed deviation of the  $c_{V^{2+}, meas}$  at the end of the charging process is likely to be caused by simultaneous hydrogen evolution since at high SOC the amount of  $V^{2+}$  depletes and therefore side reactions (such as HER) are more pronounced. The deviation of  $c_{V^{2+}}$  at the end of the charging step is similar to the observation in the VARFB charging with  $j = 15 \text{ mA cm}^{-2}$  (Fig. 4).

In the discharging process (Fig. 6b) a more pronounced deviation between measured and calculated concentrations is observed.  $c_{V^{2+}, meas}$  is much lower than calculated, whereas  $c_{V^{3+}, meas}$  is much higher than calculated. This observation cannot be explained by vanadium crossover only (Fig. 5b). HER is not likely to dominate galvanic discharging. Thus, the observation concerning  $c_{V^{2+}, meas}$  and  $c_{V^{3+}, meas}$  during discharging indicates indirectly the occurrence of  $O_2$  permeation. In the discharging process significant loss mechanisms like oxygen permeation, which lower  $c_{V^{2+}, meas}$  and raise  $c_{V^{3+}, meas}$  in comparison to  $c_{V^{2+}, calc}$  and  $c_{V^{3+}, calc}$ , occur in parallel to vanadium crossover (lowering both  $c_{V^{2+}, meas}$  and  $c_{V^{3+}, meas}$ ). In contrast to the charging process, the GDE is supplied with compressed air for the oxygen reduction reaction. This air is in excess (to avoid VARFB performance limitation due to insufficient  $O_2$  supply and to facilitate the removal of product water out of the GDE). The increased partial pressure of oxygen facilitates permeation to the negative half cell resulting in more pronounced deviation of vanadium concentrations from the calculated values during the discharge process (Fig. 6b).

Overall, significant differences between charging and discharging are observed in the VARFB cycle at  $j = 20 \text{ mA cm}^{-2}$ . First, the deviations between  $c_{V^{2+}, meas}$  and  $c_{V^{3+}, meas}$  and  $c_{V^{2+}, calc}$  and

**Table 2**

Volume  $V_{(-)}$ , total vanadium concentration measured by UV/Vis spectroscopy  $(c_{V^{2+}} + c_{V^{3+}})_{(-)}$ , UV/Vis and total amount of vanadium  $(n_{V^{2+}} + n_{V^{3+}})_{(-)}$ , UV/Vis of the negative electrolyte before and after charging and discharging, respectively, during the VARFB cycle at  $j = 20 \text{ mA cm}^{-2}$ .

	$V_{(-)}$ [mL]	$(c_{V^{2+}} + c_{V^{3+}})_{(-)}$ , UV/Vis [mol L <sup>-1</sup> ]	$(n_{V^{2+}} + n_{V^{3+}})_{(-)}$ , UV/Vis [mmol]
Before charging	12.0	0.96	12
After charging	13.6	0.85	12
After discharging	13.0	0.83	11

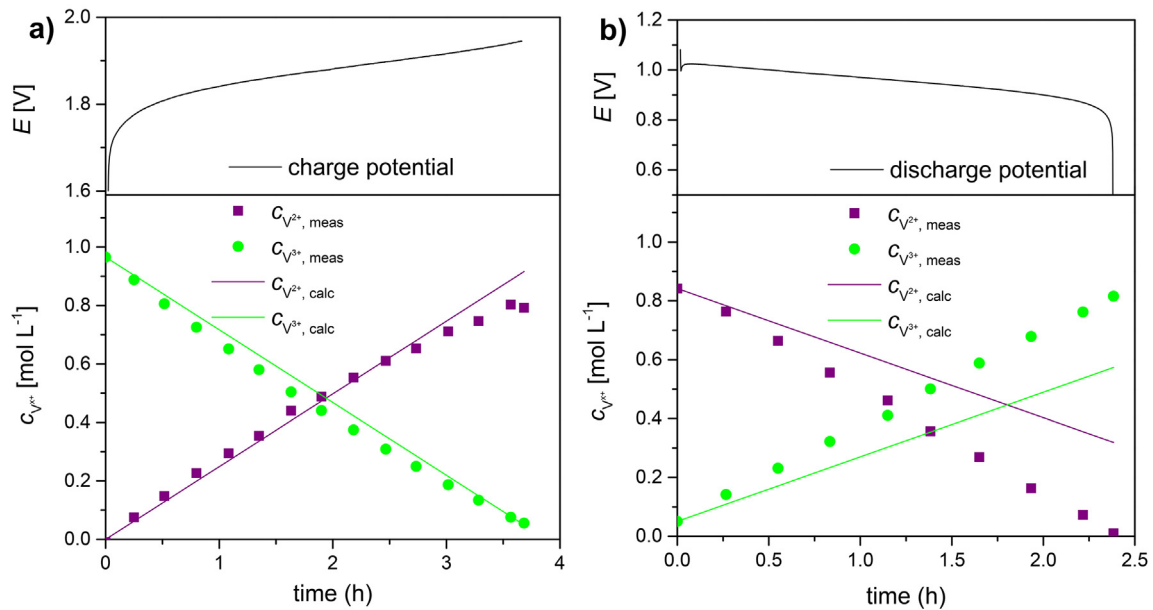


**Fig. 6.** In-situ UV/Vis monitoring of vanadium concentrations in the negative electrolyte during VARFB operation at  $j = 20 \text{ mA cm}^{-2}$  in comparison to calculated concentrations based on Faraday's law. a) Charging; b) Discharging.

**Table 3**

Volume  $V_{(+)}$ , total vanadium concentration  $c_{V^{x+}, (+), \text{ICP-MS}}$  and total amount of vanadium  $n_{V^{x+}, (+), \text{ICP-MS}}$  of the positive electrolyte before and after charging and discharging, respectively, during the VARFB cycle at  $j = 20 \text{ mA cm}^{-2}$ .

	$V_{(+)}$ [mL]	$c_{V^{x+}, (+), \text{ICP-MS}}$ [mol L <sup>-1</sup> ]	$n_{V^{x+}, (+), \text{ICP-MS}}$ [mmol]
Before charging	50.0	—	—
After charging	49.0	0.0079	0.395
After discharging	47.0	0.0165	0.776

$c_{V^{3+}, \text{calc}}$  are much more pronounced during discharging. In the charging process  $c_{V^{2+}, \text{meas}}$  deviates from  $c_{V^{2+}, \text{calc}}$  only towards the end of the charging and start to show asymptotic behavior at SOC above 80%.  $c_{V^{3+}, \text{meas}}$  is always close to  $c_{V^{3+}, \text{calc}}$ . Supported also by the values for the total amount of vanadium measured in the anolyte via UV/Vis spectroscopy ( $n_{V^{2+}} + n_{V^{3+}})_{(-), \text{UV/Vis}}$  before and after charging (Table 2), it is concluded that the vanadium crossover during charging is less pronounced than during discharging. This finding can be explained by the electric-field dependent transfer processes through the membrane: migration and EOC. While diffusion takes place from negative to the positive electrode due to concentration gradient during charging and discharging, transfer of vanadium ions from negative electrode to the positive electrode due to migration and EOC can occur only during discharging. Therefore, the total vanadium crossover is expected to be higher during discharging than during charging. Indeed, this is observed here and was also reported for VRFB [19].

The crossover of oxygen through Nafion® membranes and possible transport mechanisms have been studied intensively, a comparison of diffusion coefficients for oxygen through Nafion determined with different methods is given in Ref. [53]. However, it does not seem to be appropriate to use these values for oxygen permeation calculations due to several reasons. First, the context of the studies are fuel cells in which gaseous reactants are in direct contact to the membrane, whereas the membrane is in contact with liquid water/acid in VARFB. Second, it was stated that all conventional techniques to determine the oxygen permeation are *ex situ* techniques and therefore their results have limited transferability

to membrane-containing systems working under real conditions [54]. Additionally, in VARFB operation an electric field is present which could cause EOC flux of water and dissolved oxygen transport through the membrane [55].

The *in situ* monitoring of the negative electrolyte with UV/Vis spectroscopy during VARFB operation shows indication for the overlapping effects of all loss mechanisms ( $V^{2+}/V^{3+}$  crossover, oxygen permeation, HER) that prevented a quantitative disentanglement of the individual processes. Therefore, the total vanadium crossover was quantified with ICP-MS analysis of the positive electrolyte after charging and discharging.

### 3.2. Vanadium crossover during VARFB operation determined with ICP-MS

The total vanadium crossover after charging and after discharging the VARFB at  $j = 20 \text{ mA cm}^{-2}$  was determined by measuring the vanadium concentration in the positive electrolyte using ICP-MS and the volumes of the positive electrolyte (Table 3). The volume of the positive electrolyte is decreasing during the cycle due to water transfer from the positive to the negative electrode (charging), water consumption due to oxygen evolution reaction (charging) and evaporation due to the stream of compressed air (discharging).

The differences in  $n_{V^{x+}, (+), \text{ICP-MS}}$  are similar after charging and after discharging (Table 3). This is in contrast to the findings from UV/Vis measurements. However, the positive electrolyte was not pumped during discharging. Consequently,  $V^{2+}$  and  $V^{3+}$  accumulated in the small volume inside the cell and reduced the concentration difference across the membrane. This leads to an overall decreased diffusional flux of  $V^{2+}$  and  $V^{3+}$  from the negative to the positive electrolyte during discharging.

The vanadium concentration during the whole cycle decreases in the negative electrolyte and increases in the positive electrolyte. The amount of vanadium found in the positive electrolyte by ICP-MS after the complete cycle ( $n_{(+), \text{ICP-MS}} = 0.776 \text{ mmol}$ ; Table 3) is comparable to the loss of  $(n_{V^{2+}} + n_{V^{3+}})_{(-), \text{UV/Vis}}$  in the negative electrolyte  $\Delta(n_{V^{2+}} + n_{V^{3+}})_{(-), \text{UV/Vis}} = -1 \text{ mmol}$ ; Table 2). The

difference is explained with the accuracy limits of the UV/Vis measurements and of the volume determination.

Albeit not determined in this study, the “backward” vanadium crossover is assumed to be negligible in comparison to the crossover from the negative electrolyte to the positive electrolyte. This was estimated to be adequate as the maximal concentration of vanadium species in the positive electrolyte is 0.0165 mol L<sup>-1</sup> which is less than 2% of the total vanadium concentration in the negative electrolyte (0.96 mol L<sup>-1</sup>) even though the concentrations of vanadium species in the oxidation state 4 + and 5 + is zero in the negative electrolyte due to the potentials occurring on the negative electrode. Despite of this assumption, the differentiation between the simultaneously occurring “backward” and “forward” crossover is difficult as each diffusing species is immediately converted to a different oxidation state when reaching the other electrode.

The total amount of vanadium that underwent crossover (0.776 mmol) represents 6% of the initial vanadium amount in the negative electrolyte (12 mmol).  $\eta_c$  losses due to vanadium crossover are related to V<sup>2+</sup> crossover only. Even if the amount of 0.776 mmol of vanadium was V<sup>2+</sup> only, it would represent a charge of 74.9 C (via Faraday’s law). However,  $\Delta Q = Q_{\text{charge}} - Q_{\text{discharge}} = 370.6$  C, thus the vanadium crossover cannot be the only cause for  $\eta_c$  losses and can account at most for 20% of  $\Delta Q$ . It has to be concluded that the other loss mechanisms such as oxygen permeation as described above play an important role. The ICP-MS measurements of the positive electrolyte give information only about the total amount of vanadium that was transferred through the membrane, but the data do not allow distinguishing between V<sup>2+</sup> and V<sup>3+</sup>. In general, V<sup>2+</sup> and V<sup>3+</sup> cannot be distinguished in the positive electrolyte at the operation potentials of the positive electrode because both species are immediately oxidized to the oxidation states +4 or +5 when reaching the positive electrode. Since the crossover of V<sup>2+</sup> can only be given as an upper boundary (0.776 mmol), the fraction of  $\eta_c$  losses caused by vanadium crossover can only be given by an upper limit of 20%.

For the differentiation of vanadium crossover due to diffusion in contrast to electric-field induced migration and EOC, diffusion coefficients of V<sup>2+</sup> and V<sup>3+</sup> through Nafion® 117 were determined.

### 3.3. V<sup>2+</sup> and V<sup>3+</sup> diffusion coefficients through Nafion® 117

Vanadium cation crossover from negative to positive electrolyte occurs during VARFB operation driven by several processes. The total flux  $J_i$  of vanadium species  $i$  through a membrane in an electric field (as it is the case in VARFB operation) in one direction ( $x$ ) is described by the Nernst-Planck-Equation (Eq. (4)) [56]. The first term on the right side describes the diffusion, the second one the migration and the third describes the contribution of EOC.  $A$  is the diffusion area,  $n_i$  is the amount of substance and  $c_i$  the concentration of species  $i$ , respectively,  $t$  is the time,  $z_i$  is the charge of species  $i$ ,  $F$  is Faraday constant,  $R$  is the gas constant,  $T$  is the temperature,  $D_i$  is the diffusion coefficient of species  $i$ ,  $\phi$  is the potential and  $v_{eo}$  is the solute velocity due to EOC:

$$J_i = A \frac{dn_i}{dt} = -D_i \frac{dc_i(x)}{dx} - \frac{z_i F}{RT} D_i c_i(x) \frac{d\phi}{dx} + c_i(x) v_{eo}(x) \quad (4)$$

The diffusion coefficients of V<sup>2+</sup> and V<sup>3+</sup> through a Nafion® 117 membrane (denoted as N117) were needed to be able to quantify the amount of vanadium crossover caused by diffusion. There was no value reported yet for the diffusion coefficient of V<sup>2+</sup> through a Nafion® 117 membrane.

The diffusion coefficients  $D_{V^{2+}}$  and  $D_{V^{3+}}$  were determined using the H-cell setup as described in sec 2.4. The vanadium concentration in the deficiency side was probed in regular time intervals

(approx. every hour) by ICP-MS analysis.

The calculation of the diffusion coefficients  $D_{V^{x+}}$  follows a derivation of Fick’s first law in a one-dimensional form (Eq. (5)) reported elsewhere [13,14]:

$$\frac{1}{A} \frac{dn(t)}{dt} = -D \frac{dc(t)}{dx} \quad (5)$$

With  $V_e$  and  $V_d$  being the electrolyte volume of the excess and the deficiency side, transitioning from gradient  $dc/dx$  to difference  $\Delta c/\Delta x$ , assuming that the concentration of the excess side  $c_e$  remains nearly constant over time,  $c_d$  being the concentration in the deficiency side and  $\Delta x$  being the thickness of swollen membrane, Eq. (5) gives Eq. (6) and rearranging leads to the differential equation Eq. (7):

$$\frac{V_d dc_d(t)}{dt} = DA \frac{c_e - c_d(t)}{x} \quad (6)$$

$$\frac{dc_d(t)}{c_e - c_d(t)} = \frac{DA}{xV_d} dt \quad (7)$$

Assuming that  $D$ ,  $A$ ,  $x$  and  $V_d$  are independent of  $t$ , integration of Eq. (7) leads to:

$$\ln\left(\frac{c_e}{c_e - c_d(t)}\right) = \frac{DA}{xV_d} t \quad (8)$$

By plotting  $\ln(c_e/(c_e - c_d(t)))$  vs.  $t$ , the slope of the linear fit equals  $DA/xV_d$  which was used to obtain the diffusion coefficient of V<sup>2+</sup> and V<sup>3+</sup> through Nafion® 117 membranes (Fig. 7) as  $D_{V^{2+}, N117} = 9.05 \cdot 10^{-6} \text{ cm}^2 \text{ min}^{-1}$  ( $= 1.51 \cdot 10^{-7} \text{ cm}^2 \text{ s}^{-1}$ ) and  $D_{V^{3+}, N117} = 4.35 \cdot 10^{-6} \text{ cm}^2 \text{ min}^{-1}$  ( $= 7.25 \cdot 10^{-8} \text{ cm}^2 \text{ s}^{-1}$ ). There are no previously reported values for  $D_{V^{2+}, N117}$ . The value for V<sup>3+</sup> fits well to reported values ( $D_{V^{3+}, N117} = 3.56 \cdot 10^{-6} \text{ cm}^2 \text{ min}^{-1}$  [15] or  $D_{V^{3+}, N117} = 3.8 \cdot 10^{-6} \text{ cm}^2 \text{ min}^{-1}$  [16]). The value for  $D_{V^{2+}, N117}$  is approximately double the value of  $D_{V^{3+}, N117}$ . A similar ratio for  $D_{V^{2+}}/D_{V^{3+}}$  was reported for a Nafion® 115 membrane ( $D_{V^{2+}, N115} = 2.6 \cdot 10^{-6} \text{ cm}^2 \text{ min}^{-1}$  and  $D_{V^{3+}, N115} = 1.1 \cdot 10^{-6} \text{ cm}^2 \text{ min}^{-1}$  [14];  $D_{V^{2+}, N115} = 5.261 \cdot 10^{-6} \text{ cm}^2 \text{ min}^{-1}$  and  $D_{V^{3+}, N115} = 1.933 \cdot 10^{-6} \text{ cm}^2 \text{ min}^{-1}$  [13]). This membrane consists of the same polymer as Nafion® 117 but has a different thickness. However, for a true comparability, the swelling behavior of both membranes needs to be the same. Slade et al. [57] reported an unequal thickness increase of Nafion® 117 and Nafion® 115 in relation to their nominal thickness (+17% for Nafion® 117 and +27%

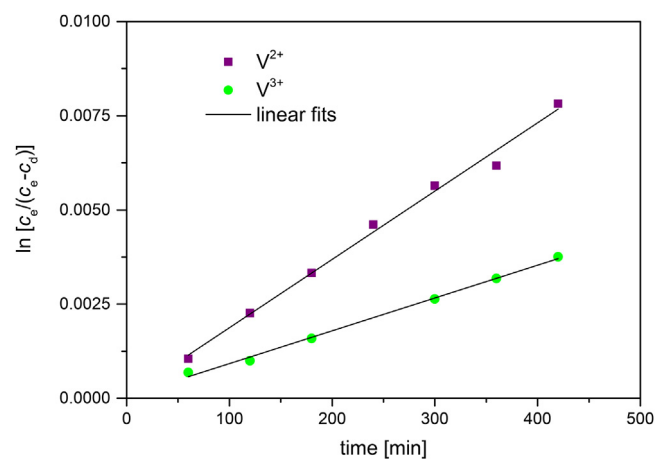


Fig. 7. Plot of  $\ln(c_e/(c_e - c_d))$  vs.  $t$  and linear fits for determination of diffusion coefficients of V<sup>2+</sup> and V<sup>3+</sup> through a Nafion® 117 membrane.

for Nafion® 115) due to a similar protonation routine as we used. Therefore, it seems to be advisable to determine the diffusion coefficients for each membrane although data might be available for the same polymer material processed to a membrane with different thickness.

Logette et al. proposed that the diffusion coefficient of cations through a cation exchange membrane is affected by the affinity of the ion for functional groups of the membrane and the mobility within the membrane [58]. Higher valency of the cation results in higher affinity for the membrane and in lower mobility due to stronger electrostatic interaction of the cation with the negative groups of the membrane. Depending on which of these opposed effects is more dominant, a higher valent cation can have a higher or lower diffusion coefficient than a lower valent cation. In the case of  $V^{2+}$  and  $V^{3+}$  with  $D_{V^{3+}, N117} \approx 0.5 \cdot D_{V^{2+}, N117}$ ,  $V^{3+}$  is either interacting stronger with the sulfonate groups than  $V^{2+}$  so that it becomes less mobile within the membrane or the interactions are so poor that  $V^{3+}$  only reaches a low concentration within the membrane. In aqueous solution,  $V^{2+}$  and  $V^{3+}$  both exist as hexaaquations [22,24,59,60]. It was shown that in sulfuric acid media  $SO_4^{2-}$  can substitute a water molecule in the inner hydration shell of  $V^{3+}$  yielding  $[V(SO_4)(H_2O)_5]^+$  [21,59], whereas this is not the case for  $V^{2+}$  which exists as  $[V(H_2O)_6]^{2+}$  [21,24]. The  $V^{3+}$  complex with the sulfate ion carries a lower positive charge than the  $V^{2+}$  complex. Another effect that was reported is that  $V^{3+}$  carries a more tightly bound hydration shell which screens effectively the electrostatic charge of the  $V^{3+}$  in comparison to  $V^{2+}$  [26]. Both effects would decrease the interaction of  $V^{3+}$  with the sulfonate groups in comparison to  $V^{2+}$ . Therefore, it could be deduced that  $V^{3+}$  probably has a low affinity to the membrane (weak interaction with membrane) and therefore reaches only a lower concentration within the membrane. The lower affinity of  $V^{3+}$  to the sulfonate groups of a Nafion® membrane in comparison to  $V^{2+}$  was also reported by Cui et al. by means of molecular dynamics [26]. The different affinity of  $V^{2+}$  and  $V^{3+}$  to the membrane could also be investigated experimentally by determining the concentration of vanadium cations in a membrane equilibrated in  $V^{2+}$  and  $V^{3+}$  solutions, respectively.

However, a detailed study of the interaction of vanadium species with the sulfonate groups in the channels of the Nafion® membrane is needed for a correlation of diffusivity of the vanadium species through the membrane to the interaction mechanisms of the diffusing species inside of the membrane. However, this was beyond the scope of this work.

For the estimation of the diffusional flux during VARFB operation at  $j = 20 \text{ mA cm}^{-2}$  it was assumed that the initial vanadium concentration in the negative electrolyte ( $0.96 \text{ mol L}^{-1}$ ) remains constant and an (arithmetic) average diffusion coefficient for  $V^{2+}$  and  $V^{3+}$  was used ( $D_{V^{2+/3+}} = 6.7 \cdot 10^{-6} \text{ cm}^2 \text{ min}^{-1}$ ). With these assumptions  $0.451 \text{ mmol}$  of  $V^{2+/3+}$  could have crossed the membrane during one VARFB cycle at  $j = 20 \text{ mA cm}^{-2}$  by diffusion only. The total amount of vanadium that crossed over during the VARFB cycle at  $j = 20 \text{ mA cm}^{-2}$  determined with ICP-MS was  $0.776 \text{ mmol}$  (Table 3), therefore the amount of vanadium crossover through the membrane by migration and/or EOC would be  $0.325 \text{ mmol}$ . That means that approximately 58% of the vanadium crossover is diffusion-related and therefore 42% result from migrational and/or EOC. The discussion above assumes independent permeation of oxygen and vanadium. However, this is an approximation as any oxygen can oxidize diffusing  $V^{2+}$  to  $V^{3+}$  (or even  $VO^{2+}$  (“ $V^{4+}$ ”)) inside the membrane. This not only would influence the overall transport properties of vanadium species but  $VO^{2+}$  can lead to fouling of the membrane [22]. A similar fouling process could also be imagined for  $V^{2+}$  and/or  $V^{3+}$  species. More theoretical and experimental investigations are necessary to fully unravel these coupled processes.

### 3.4. Combined crossover analysis

A Sankey diagram (Fig. 8) summarizes the findings concerning the coulombic losses in the VARFB in one cycle at  $j = 20 \text{ mA cm}^{-2}$ . Only 65% of  $Q_{\text{charge}}$  could be recovered during discharging ( $Q_{\text{discharge}}$ ). In Fig. 8 the vanadium crossover determined with ICP-MS is given by its maximum share of 20% of the coulombic losses which is 7% of  $Q_{\text{charge}}$ . Based on the calculations in section 3.3, the vanadium crossover is subdivided into diffusion (4% of  $Q_{\text{charge}}$ ) and the remaining quantity that relates to migration and/or EOC (3% of  $Q_{\text{charge}}$ ). The remaining part is related to HER and/or oxygen permeation and is depicted as “other losses (e.g. oxygen permeation)” as its minimal fraction. It accounts for 28% of  $Q_{\text{charge}}$ .

## 4. Conclusion

As the vanadium/air redox flow battery could theoretically double the energy density versus an all-vanadium redox flow battery, it is a promising technology especially for applications where energy density does matter (e.g. stationary electricity storage application with limited space). However,  $\eta_c$  need to be improved for practical applications.

In this paper the causes for  $\eta_c$  losses of a vanadium/air redox flow battery were investigated. We integrated successfully a UV/Vis spectrometer in the hydraulic circuit of the negative electrolyte for the *in situ* monitoring of  $c_{V^{2+}}$  and  $c_{V^{3+}}$  during VARFB operation at  $j = 15 \text{ mA cm}^{-2}$  and at  $j = 20 \text{ mA cm}^{-2}$ . This analysis revealed that  $\eta_c$  losses are caused by side reactions such as oxygen permeation through the membrane and subsequent oxidation of  $V^{2+}$  to  $V^{3+}$ . In general, the application of UV/Vis spectroscopy for analysing negative electrolyte concentrations is a powerful and convenient technique to monitor the battery operation *in situ* if appropriate cuvettes are used. The method is not limited to the VARFB.

Furthermore, the vanadium crossover during VARFB operation at  $j = 20 \text{ mA cm}^{-2}$  was quantified by analysing the positive electrolyte by ICP-MS. The vanadium crossover causes at most 20% of  $\eta_c$  losses. Although the vanadium crossover is not the main reason for low  $\eta_c$ , it is strongly undesired as it reduces the cycle life of the VARFB. The amount of vanadium in the negative electrolyte is the capacity-determining part of the VARFB, therefore the continuous crossover of vanadium species from the negative to the positive electrode leads to an ongoing capacity decay of the VARFB. Hence a strongly reduced vanadium crossover is essential for an increased cycle life of the VARFB which is necessary for practical applications.

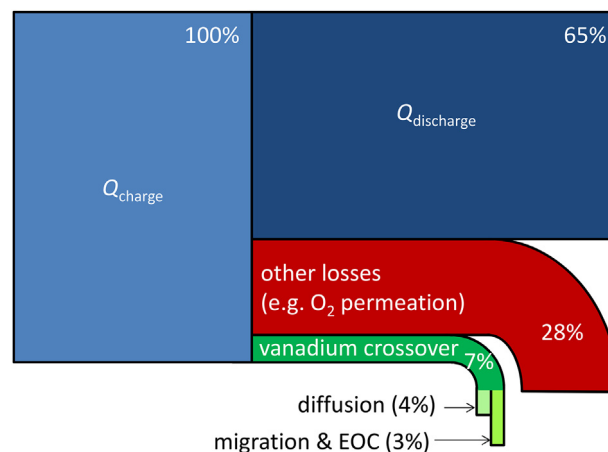


Fig. 8. Sankey diagram quantifying loss mechanisms during the VARFB operation cycle at  $j = 20 \text{ mA cm}^{-2}$ . See text for explanation.

The diffusion coefficients of  $V^{2+}$  and  $V^{3+}$  through Nafion<sup>®</sup> 117 were determined to differentiate vanadium crossover caused by diffusion and migration/electroosmotic convection (EOC). The diffusion coefficients can also be valuable for detailed simulation and modeling of all-vanadium redox flow batteries.

However, as the vanadium species that underwent crossover are immediately oxidized at the positive electrode to vanadium in the oxidation state 4 + and 5 + and cannot be distinguished after the crossover, the share of vanadium crossover on  $\eta_C$  losses can only be determined as upper limit (20%). Likewise, a more detailed understanding of the transport processes in the membrane requires an examination of the interactions between the diffusing species and the membrane on a molecular level unraveling the influence of the mutual interaction between the transferred species ( $V^{2+}$ ,  $V^{3+}$  and  $O_2$ ).

For future studies in an optimized system it would be interesting to investigate the influences of electrolyte flow rates and current densities on the overall  $\eta_C$  and the fractions of the individual loss mechanisms on the global losses.

For a more efficient VARFB operation, an optimized membrane is needed. Our study reveals that oxygen permeation is severely reducing  $\eta_C$ . Therefore, a membrane with low oxygen permeation is recommended for the VARFB. On the other hand, a membrane with low vanadium crossover is needed to enhance  $\eta_C$  and cycle life of the VARFB. A membrane combining both requirements seems to be most appropriate for an efficient and durable VARFB. Besides other possible approaches, existing membranes could be modified to reduce both vanadium crossover and oxygen permeation. A promising routine is the layer-by-layer deposition of polyelectrolytes thin films which could reduce vanadium crossover [61–63] and oxygen permeation [64–68] while maintaining proton conductivity of the membrane.

## Acknowledgments

The authors would like to thank Timo di Nardo for assisting in the experimental work. Likewise the contributions of Dana Schonvogel (ICP-MS measurements) are appreciated. The work was supported by the Reiner Lemoine-Stiftung, Berlin, Germany by supplying a PhD scholarship to J. grosse Austing.

## References

- [1] H. Chen, T.N. Cong, W. Yang, C. Tan, Y. Li, Y. Ding, *Prog. Nat. Sci.* 19 (2009) 291–312.
- [2] M. Skyllas-Kazacos, M.H. Chakrabarti, S. a. Hajimolana, F.S. Mjalli, M. Saleem, *J. Electrochem. Soc.* 158 (2011) R55.
- [3] P. Leung, X. Li, C. Ponce de León, L. Berlouis, C.T.J. Low, F.C. Walsh, *RSC Adv.* 2 (2012) 10125.
- [4] M. Skyllas-Kazacos, *J. Power Sources* 124 (2003) 299–302.
- [5] L. Li, S. Kim, W. Wang, M. Vijayakumar, Z. Nie, B. Chen, J. Zhang, G. Xia, J. Hu, G. Graff, J. Liu, Z. Yang, *Adv. Energy Mater.* 1 (2011) 394–400.
- [6] Y. Lu, J.B. Goodenough, Y. Kim, *J. Am. Chem. Soc.* 133 (2011) 5756–5759.
- [7] Q. Huang, Q. Wang, *Chempluschem* 80 (2015) 312–322.
- [8] H. Kaneko, A. Negishi, K. Nozaki, K. Sato, M. Nakajima, (1992) EU Patent 0517217A1.
- [9] S. Hosseiny, M. Saakes, M. Wessling, *Electrochem. Commun.* 13 (2011) 751–754.
- [10] J. Noack, C. Cremers, D. Bayer, J. Tübke, K. Pinkwart, *J. Power Sources* 253 (2014) 397–403.
- [11] C. Menictas, M. Skyllas-Kazacos, *J. Appl. Electrochem.* 41 (2011) 1223–1232.
- [12] J. grosse Austing, C. Nunes Kirchner, E.-M. Hammer, L. Komsiyka, G. Wittstock, *J. Power Sources* 273 (2015) 1163–1170.
- [13] C. Sun, J. Chen, H. Zhang, X. Han, Q. Luo, *J. Power Sources* 195 (2010) 890–897.
- [14] P. Leung, Q. Xu, T. Zhao, L. Zeng, C. Zhang, *Electrochim. Acta* 105 (2013) 584–592.
- [15] X. Luo, Z. Lu, J. Xi, Z. Wu, W. Zhu, *J. Phys. Chem. B* 109 (2005) 20310–20314.
- [16] J. Xi, Z. Wu, X. Qiu, L. Chen, *J. Power Sources* 166 (2007) 531–536.
- [17] Q. Luo, L. Li, Z. Nie, W. Wang, X. Wei, B. Li, B. Chen, Z. Yang, *J. Power Sources* 218 (2012) 15–20.
- [18] Q. Luo, L. Li, W. Wang, Z. Nie, X. Wei, B. Li, B. Chen, Z. Yang, V. Sprenkle, *ChemSusChem* 6 (2013) 268–274.
- [19] X.-G. Yang, Q. Ye, P. Cheng, T.S. Zhao, *Appl. Energy* 145 (2015) 306–319.
- [20] R.M. Darling, a. Z. Weber, M.C. Tucker, M.L. Perry, *J. Electrochem. Soc.* 163 (2016) A5014–A5022.
- [21] F. Sepehr, S.J. Paddison, *J. Phys. Chem. A* (2015), 150518095410002.
- [22] M. Vijayakumar, M.S. Bhuvanewari, P. Nachimuthu, B. Schwenzer, S. Kim, Z. Yang, J. Liu, G.L. Graff, S. Thevuthasan, J. Hu, *J. Memb. Sci.* 366 (2011) 325–334.
- [23] S. Quezado, J.C.T. Kwak, M. Falk, *Can. J. Chem.* 62 (1984) 958–966.
- [24] M. Benmelouka, S. Messaoudi, E. Furet, R. Gautier, E. Le Fur, J.Y. Pivan, *J. Phys. Chem. A* 107 (2003) 4122–4129.
- [25] K.M. Cable, K. a. Mauritz, R.B. Moore, *J. Polym. Sci. Part B Polym. Phys.* 33 (1995) 1065–1072.
- [26] S. Cui, S.J. Paddison, *J. Phys. Chem. C* (2015), 150521065237001.
- [27] X. Teng, Y. Zhao, J. Xi, Z. Wu, X. Qiu, L. Chen, *J. Power Sources* 189 (2009) 1240–1246.
- [28] J. Qiu, L. Zhao, M. Zhai, J. Ni, H. Zhou, J. Peng, J. Li, G. Wei, *J. Power Sources* 177 (2008) 617–623.
- [29] J. Xi, Z. Wu, X. Teng, Y. Zhao, L. Chen, X. Qiu, *J. Mater. Chem.* 18 (2008) 1232.
- [30] K.W. Knehr, E. Agar, C.R. Dennison, a. R. Kalidindi, E.C. Kumbur, *J. Electrochem. Soc.* 159 (2012) A1446–A1459.
- [31] D. You, H. Zhang, J. Chen, *Electrochim. Acta* 54 (2009) 6827–6836.
- [32] M. Skyllas-Kazacos, L. Goh, *J. Memb. Sci.* 399–400 (2012) 43–48.
- [33] R. Badrinarayanan, J. Zhao, K. Tseng, M. Skyllas-Kazacos, *J. Power Sources* 270 (2014) 576–586.
- [34] N.H. Choi, S.-k. Kwon, H. Kim, *J. Electrochem. Soc.* 160 (2013) A973–A979.
- [35] M. Skyllas-Kazacos, M. Kazacos, *J. Power Sources* 196 (2011) 8822–8827.
- [36] Z. Tang, D. Aaron, A.B. Papandrew, T.A. Zawodzinski, *ECS Trans.* 41 (2012) 1–9.
- [37] L. Liu, J. Xi, Z. Wu, W. Zhang, H. Zhou, W. Li, X. Qiu, *J. Appl. Electrochem.* 42 (2012) 1025–1031.
- [38] H.J. Lee, N.H. Choi, H. Kim, *J. Electrochem. Soc.* 161 (2014) A1291–A1296.
- [39] D.N. Buckley, X. Gao, R.P. Lynch, N. Quill, M.J. Leahy, *J. Electrochem. Soc.* 161 (2014) A524–A534.
- [40] D.C. Sing, J.P. Meyers, *ECS Trans.* (2013).
- [41] R.P. Brooker, C.J. Bell, L.J. Bonville, H.R. Kunz, J.M. Fenton, *J. Electrochem. Soc.* 162 (2015) A608–A613.
- [42] N. Quill, C. Petchsingh, R.P. Lynch, X. Gao, D. Oboroceanu, D.N. Eidihin, M.O. Mahony, C. Lenihan, D.N. Buckley, *ECS Trans.* 64 (2015) 23–39.
- [43] Q.H. Liu, G.M. Grim, a. B. Papandrew, A. Turhan, T. a. Zawodzinski, M.M. Mench, *J. Electrochem. Soc.* 159 (2012) A1246–A1252.
- [44] J. Sun, X. Li, X. Xi, Q. Lai, T. Liu, H. Zhang, *J. Power Sources* 271 (2014) 1–7.
- [45] T. Sukkar, M. Skyllas-Kazacos, *J. Appl. Electrochem* 34 (2004) 137–145.
- [46] A.A. Shah, M. Watt-Smith, F. Walsh, *Electrochim. Acta* 53 (2008) 8087–8100.
- [47] M.J. Watt-Smith, P. Ridley, R. G. a. Wills, a. a. Shah, F.C. Walsh, *J. Chem. Technol. Biotechnol.* 88 (2013) 126–138.
- [48] T. Sukkar, M. Skyllas-Kazacos, *J. Memb. Sci.* 222 (2003) 235–247.
- [49] T. Mohammadi, *J. Memb. Sci.* 133 (1997) 151–159.
- [50] C.-N. Sun, F.M. Delnick, L. Baggetto, G.M. Veith, T. a. Zawodzinski, *J. Power Sources* 248 (2014) 560–564.
- [51] a.a. Shah, H. Al-Fetlawi, F. Walsh, *Electrochim. Acta* 55 (2010) 1125–1139.
- [52] E. W. Washburn, N. R. C. (U.S.), C. West, International Council of Scientific Unions National Academy of Sciences (U.S.), International Critical Tables of Numerical Data, Physics, Chemistry and Technology, number Vol. 6 in International Critical Tables of Numerical Data, Physics, Chemistry and Technology, National Research Council, 1929.
- [53] V. a. Sethuraman, S. Khan, J.S. Jur, A.T. Haug, J.W. Weidner, *Electrochim. Acta* 54 (2009) 6850–6860.
- [54] P. Gode, G. Lindbergh, G. Sundholm, *J. Electroanal. Chem.* 518 (2002) 115–122.
- [55] P. Millet, R. Ngameni, S. a. Grigoriev, N. Mbemba, F. Brisset, a. Ranjbari, C. Etievant, *Int. J. Hydrogen Energy* 35 (2010) 5043–5052.
- [56] B. Bath, H. White, E. Scott, *Anal. Chem.* 72 (2000) 433–442.
- [57] S. Slade, S. Campbell, T. Ralph, F. Walsh (2002) 1556–1564.
- [58] S. Logette, C. Eysseric, G. Pourcelly, A. Lindheimer, C. Gavach, *J. Memb. Sci.* 144 (1998) 259–274.
- [59] M. Vijayakumar, L. Li, Z. Nie, Z. Yang, J. Hu, *Phys. Chem. Chem. Phys.* 14 (2012) 10233.
- [60] J. Krakowiak, D. Lundberg, I. Persson, *J. Inorg. Chem.* (2012) 9598–9609.
- [61] J. Xi, Z. Wu, X. Teng, Y. Zhao, L. Chen, X. Qiu, *J. Mater. Chem.* 18 (2008) 1232.
- [62] W. Xu, X. Li, J. Cao, H. Zhang, H. Zhang, *Sci. Rep.* 4 (2014) 4016.
- [63] S. Lu, C. Wu, D. Liang, Q. Tan, Y. Xiang, *RSC Adv.* 4 (2014) 24831.
- [64] Y.H. Yang, M. Haile, Y.T. Park, F. a. Malek, J.C. Grunlan, *Macromolecules* 44 (2011) 1450–1459.
- [65] Y.-H. Yang, L. Bolling, M. Haile, J.C. Grunlan, *RSC Adv.* (2012) 12355–12363.
- [66] D. a. Hagen, C. Box, S. Greenlee, F. Xiang, O. Regev, J.C. Grunlan, *RSC Adv.* 4 (2014) 18354.
- [67] D. a. Hagen, B. Foster, B. Stevens, J.C. Grunlan, *ACS Macro Lett.* 3 (2014) 663–666.
- [68] B.E. Stevens, P.K. Odenborg, M.A. Priolo, J.C. Grunlan, *J. Polym. Sci. Part B Polym. Phys.* 52 (2014) 1153–1156.

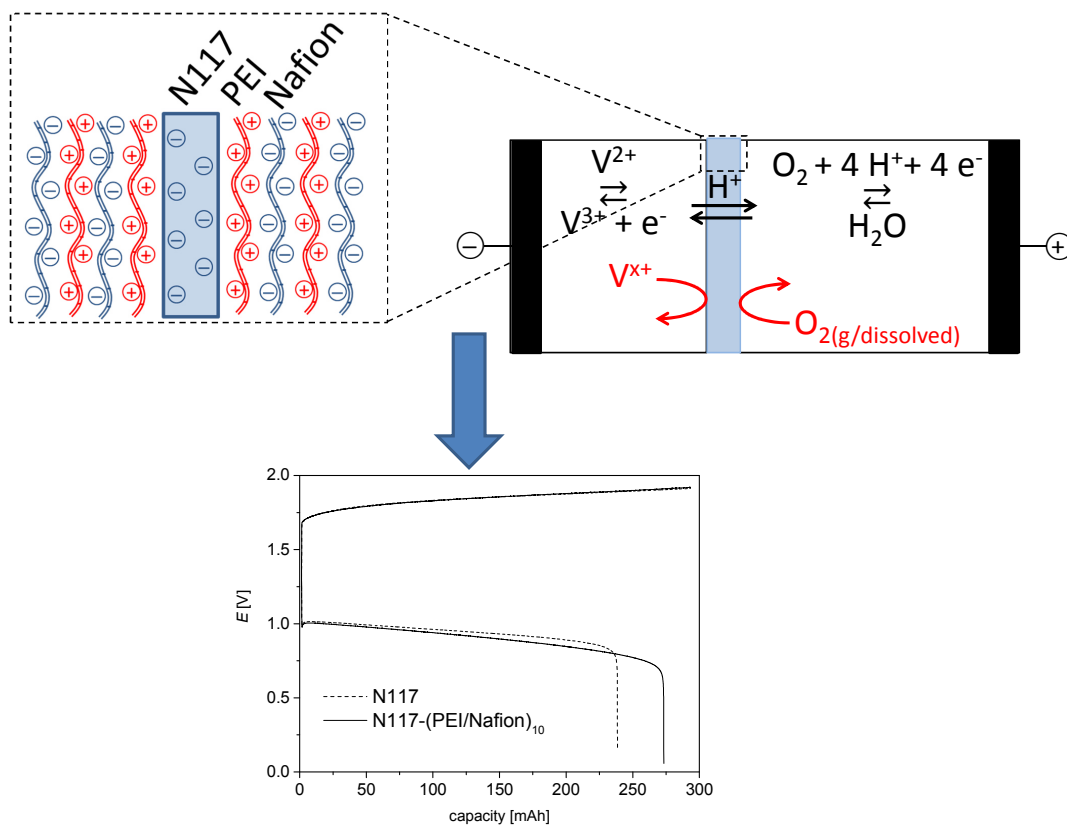
# Publication III



# Layer-by-layer modification of Nafion membranes for increased life-time and efficiency of vanadium/air redox flow batteries

Authors: Jan grosse Austing, Carolina Nunes Kirchner, Lidiya Komsiyaska and Gunther Wittstock

Journal of Membrane Science, 510, 2016, 259-269, DOI: 10.1016/j.memsci.2016.03.005







# Layer-by-layer modification of Nafion membranes for increased life-time and efficiency of vanadium/air redox flow batteries



Jan grosse Austing<sup>a</sup>, Carolina Nunes Kirchner<sup>a</sup>, Lidiya Komsijska<sup>a</sup>, Gunther Wittstock<sup>b,\*</sup>

<sup>a</sup> NEXT ENERGY EWE Research Centre for Energy Technology, 26129 Oldenburg, Germany

<sup>b</sup> Carl von Ossietzky University of Oldenburg, Faculty of Mathematics and Natural Sciences, Center of Interface Science, Institute of Chemistry, 26111 Oldenburg, Germany

## ARTICLE INFO

### Article history:

Received 4 January 2016

Received in revised form

26 February 2016

Accepted 1 March 2016

Available online 8 March 2016

### Keywords:

Vanadium–air redox flow battery

Crossover redox flow battery

Vanadium oxygen fuel cell

Layer-by-layer deposition

## ABSTRACT

Vanadium/air redox flow batteries (VARFB) promise higher energy densities compared to all-vanadium redox flow batteries (VRFB). However, VARFB suffer from crossover processes through the membrane, i.e. vanadium crossover and oxygen permeation. The vanadium crossover causes ongoing capacity losses and therefore reduces the lifetime of the battery. Additionally, the coulombic efficiency is reduced due to vanadium crossover and oxygen permeation. In this contribution we propose a straightforward routine for Nafion 117 (N117) membrane modification to reduce both vanadium crossover and oxygen permeation. Layer-by-layer (LbL) deposited films of polyethylenimine (PEI) and Nafion ionomer are build up on the membrane by dipping the membrane alternatingly in solutions of the polyelectrolytes. The modification of the membranes is characterized with infrared (IR) spectroscopy, scanning electron microscopy (SEM), thermogravimetric analysis (TGA) and film thickness measurements. The properties of the modified membranes are investigated by determining the proton conductivity, vanadium crossover and oxygen permeation. By the application of a LbL film of PEI/Nafion obtained after 10 LbL deposition repetitions, the selectivity ( $\sigma_{H^+}/P_{V^{2+}}$ ) of the membrane towards protons is increased by factor 21. Using this membrane in a VARFB reveals a strongly reduced vanadium crossover (approx. –70%) during a cycle as determined with inductively coupled plasma mass spectroscopy (ICP-MS) analysis of the positive electrolyte. The coulombic efficiency increases from 81% to 93% and the energy efficiency from 41.5% to 45.2%. TGA and IR measurements of the membrane after VARFB operation indicated a vanadium ion uptake into the membrane and the stability of the LbL film under conditions of VARFB operation.

© 2016 Elsevier B.V. All rights reserved.

## 1. Introduction

With increasing share of renewable electricity production, stationary energy storage is needed to harmonize the fluctuating electricity generation and the demand. Redox flow batteries are suitable candidates for this task due to their interesting properties such as independence of power and capacity, long cycle life and the good efficiency [1]. However, redox flow batteries generally exhibit a low specific energy in terms of mass and volume [1,2]. Although for most stationary installations irrelevant, low volumetric energy density can be an obstacle in applications with limited space (e.g. residential installation). A promising approach to increase the energy density of the all-vanadium redox flow battery (VRFB) is the vanadium/air redox flow battery (VARFB; Fig. 1) [3–7]. By substituting the positive redox couple ( $VO_2^+/VO^{2+}$ ) by the  $H_2O/O_2$  couple, the positive tank volume can be

reduced to approx. 1% of the initial volume [6]. The  $O_2$  for the discharging process is provided by the ambient air. Recently, we reported the successful operation of a unitized bidirectional VARFB using a two-layered positive electrode [6]. However, we observed a rapid capacity fading and reduced coulombic efficiency [6,8].

In a VARFB, vanadium crossover from the negative to the positive electrode (Fig. 1, process 1) can lead to reduced coulombic efficiency and lowers the cycle life due to irreversible loss of capacity. Additionally, the coulombic efficiency is decreased by oxygen permeation (Fig. 1, process 2) and the subsequent oxidation of  $V^{2+}$  to  $V^{3+}$  in the negative electrode. Vanadium crossover also occurs in conventional redox flow batteries, therefore several approaches were published to increase the coulombic efficiency of redox flow batteries by optimizing the membrane [9–20]. They include the use of new membranes based on polymer blends [13,14], organic/inorganic composite membranes (e.g. Nafion/SiO<sub>2</sub> or Nafion/(SiO<sub>2</sub> modified TiO<sub>2</sub>) [17,21]), alternative proton conducting polymers (e.g. sulfonated polyether ether ketone (SPEEK) [22]) or anion exchange polymers [15]. Despite these “bulk” modifications, it was shown that the surface modification of

\* Corresponding author.

E-mail address: [gunther.wittstock@uni-oldenburg.de](mailto:gunther.wittstock@uni-oldenburg.de) (G. Wittstock).

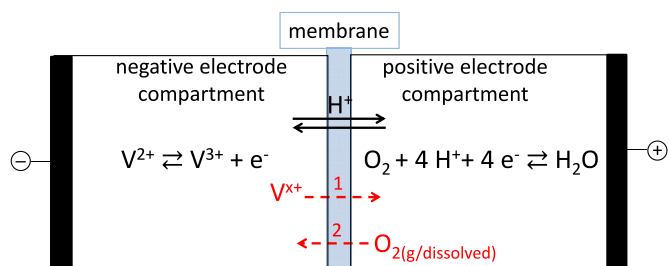


**Fig. 1.** Schematic of the vanadium/air redox flow battery, the main reactions (black solid lines) and undesired transfer processes through the membrane (numbered, red dashed lines).

conventional membranes is a viable approach to improve the performance of the redox flow battery. Covalently bonding and cross-linking polymers on the membrane surface [12], attaching polypyrrole [23] or assembling polyelectrolyte layers on the membrane surface using layer-by-layer (LbL) deposition are beneficial for reduced vanadium crossover [20,24].

The LbL deposition is a convenient and efficient surface modification routine for charged substrates [25–27]. By dipping the charged substrate alternately into oppositely charged polyelectrolyte solutions, a layered structure is built up on the substrate (Fig. 2a). By adjusting the deposition parameters (e.g. polyelectrolyte combination, deposition time, pH or ionic strength of

polyelectrolyte solutions), the growth behavior of the LbL film can be adjusted [28–30]. It was shown that a LbL film on the substrate membrane can increase the performance of a VRFB (e.g. poly(diallyldimethylammonium chloride) (PDADMAC)/PAA [31], PDADMAC/poly(sodium styrene sulfonate) (PSS) [24] or chitosan/phosphotungstic acid [20]).

Besides vanadium crossover, oxygen permeation is playing a significant role in reducing the performance of a VRFB (Fig. 1) [7,8]. During charging, oxygen is produced on the porous positive electrode which is in direct contact with the membrane. The produced oxygen can permeate in gaseous or dissolved form from the positive to the negative electrode. In the discharging process, the gas diffusion layer in the positive electrode is supplied with compressed air. To avoid mass transfer limitations, the supply is in surplus to the stoichiometric requirements. However, parts of this additional oxygen can also undergo permeation to the negative electrode.

In various applications (e.g. water electrolysis, food packaging or gas separation processes) the gas permeation properties of substrates were reduced via LbL deposition of polyelectrolytes [32]. For instance, oxygen permeability of PET substrates is reduced significantly by application of polyethylenimine (PEI) as polycation in multilayers (e.g. trilayers of PEI/montmorillonite clay/PAA [33], quadlayers of PEI/PAA/PEI/clay [34] or bilayer of PEI/PAA after cross-linking [35,32]). LbL films containing branched PEI

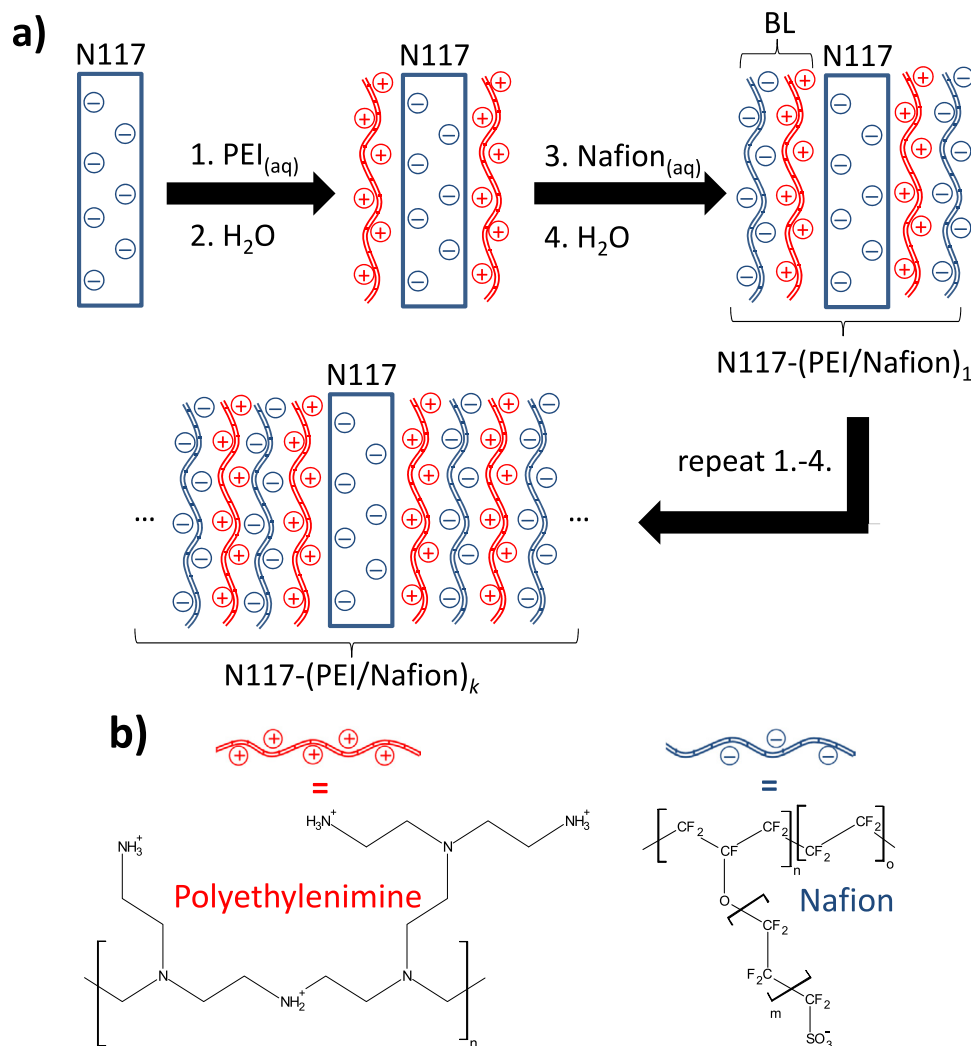


**Fig. 2.** (a) Principle of LbL deposition and the used nomenclature and (b) structure of the polyelectrolytes employed in this study.

were also proven to decrease multivalent ion crossover and increase the selectivity towards monovalent cations such as  $H^+$  [36–38].

The reduced vanadium crossover and reduced oxygen permeability are desired for VARFB operation for increased cycle life of the battery and better coulombic efficiency. In this contribution we applied LbL films containing the polycation PEI and the polyanion Nafion on Nafion 117 (N117) as a model substrate. PEI was chosen because of its barrier properties both to multivalent cations and oxygen. Nafion ionomer was chosen as polyanion because it was shown to be suitable in LbL deposition [39–41], due to its good proton conductivity and chemical stability and because it was also used as substrate material.

To our knowledge, there are no studies dealing with the improvement of membranes for VARFB application. In the current contribution, a membrane modification approach is presented which reduced both vanadium crossover and oxygen permeation, and hence enables the improvement of the VARFB efficiency. There are no reports about the simultaneous reduction of both multivalent ion crossover and oxygen permeation by application of a LbL film. Whereas the application of covalently bonded PEI on Nafion [12] as well as LbL deposition of polyelectrolytes [20,24,31] for improving VRFB membranes was described before, there is no report where LbL films of branched PEI/Nafion were applied on a membrane.

After an entire characterization of LbL deposited films of PEI and Nafion ionomer on N117 substrates, the modified membrane was mounted in a VARFB test cell to evaluate the battery performance. Furthermore, the stability of the modified membrane under VARFB operation conditions was investigated.

## 2. Experimental

### 2.1. Electrolyte preparation

The  $V^{2+}$  and  $V^{3+}$  electrolytes were prepared electrolytically as described elsewhere [6,8,42]. A solution of 1.2 M  $VOSO_4 \cdot x H_2O$  ( $x \approx 3$ ; 97%; Sigma Aldrich, Germany) and 2.0 M  $H_2SO_4$  (95–97%; Fischer Scientific GmbH, Germany) was electrolyzed in a VRFB setup using a potentiostat/galvanostat (Solartron Analytical Modulab Pstat potentiostat/galvanostat, UK). The vanadium concentration can change during the electrolyte preparation and was therefore determined with ICP-MS (XSERIES 2 ICP-MS, Thermo Scientific, USA). The prepared  $V^{2+}$  electrolyte had a vanadium concentration of 1.04 M, the  $V^{3+}$  electrolyte had a concentration of 1.10 M. Both electrolytes were kept under a blanket of humidified  $N_2$  to avoid oxidation by air.

### 2.2. Membrane modification

Initially, all Nafion 117 membranes were cleaned and protonated by subsequent treatment in 5%  $H_2O_2$  (30%; Carl Roth GmbH & Co. KG, Germany) at 80 °C for 30 min, followed by rinsing with deionized water, treatment in 1 M  $H_2SO_4$  for 30 min at 80 °C and finally boiling in deionized water for 10 min. The protonated membranes were modified with polyelectrolytes via a LbL deposition as depicted in Fig. 2a. The polyelectrolyte solutions consisted of 0.1 mass% PEI (branched, average molecular weight  $\sim 25\,000$  (by LS), Sigma Aldrich, Germany) and 0.1 mass% Nafion ionomer (Nafion perfluorinated resin solution, 5 mass% in lower aliphatic alcohols and water, 1100 EW; Sigma-Aldrich, Germany) in ultrapure water (Fig. 2b). The LbL film was build up on the membranes similar to the routine described by Yang et al. [32]. The membranes were repetitively immersed in the PEI solution for 5 min, rinsed thoroughly with ultrapure water, immersed in the

Nafion solution for 5 min followed by rinsing with ultrapure water. The polyelectrolyte layers are denoted as follows: substrate-(polycation/polyanion)<sub>k</sub>, where *k* denotes the number of deposition cycles (Fig. 2a). The modified membranes were stored in ultrapure water.

### 2.3. Membrane characterization

#### 2.3.1. Thickness

The thickness of the membranes was determined at five different positions of the membrane sample using a digital thickness dial gauge (Digital Foil Thickness Gauge FD 1000/30-3, Käfer Messuhrenfabrik GmbH & Co. KG, Germany). The membrane samples were carefully wiped dry with low-lint paper right before measuring the thickness.

#### 2.3.2. Infrared spectroscopy

The IR absorption spectra of the samples were recorded using an attenuated total reflection (ATR) equipment with an FTIR spectrometer (Spectrum 100, Perkin Elmer, USA). The membranes were investigated in a wetted condition, water on the surface was removed with low-lint paper.

#### 2.3.3. Scanning electron microscopy

Cross-sections of the membrane samples were prepared via a freeze-fracture routine, i.e. the samples were frozen in liquid nitrogen followed by snapping the sample into two parts using tweezers [43]. The samples were dried overnight at 60 °C in vacuum before imaging the cross-sections with SEM (NEON 40, Zeiss, Germany). The acceleration voltage was 5 kV and the maximal magnification was  $600 \times$ .

#### 2.3.4. Thermogravimetric analysis

Vacuum-dried samples (60 °C, overnight) were investigated in a thermogravimetric analyzer (TGA 4000, Perkin Elmer, USA) between 30 °C and 600 °C ( $10\text{ °C min}^{-1}$ ) in  $N_2$  atmosphere ( $40\text{ mL min}^{-1}$ ).

### 2.4. Membrane performance

#### 2.4.1. Vanadium permeability

The permeability of  $V^{2+}$  through the membranes was determined using a setup described elsewhere [8,17,44]. Briefly, the samples were pressed between the flanges of an H cell (active area:  $2.545\text{ cm}^2$ ), one compartment (excess side) was filled with 20 mL of  $V^{2+}$  electrolyte (preparation described above) and the other compartment (deficiency side) was filled with 1.2 M  $MgSO_4/2\text{ M }H_2SO_4$  solution and stirred (magnetic stir bar) during the experiment. Both solutions were maintained under a blanket of humidified  $N_2$  to prevent oxidation of  $V^{2+}$  to  $V^{3+}$  by oxygen from the ambient air. Five aliquotes of the “deficiency side” were taken within 24 h and the vanadium concentration was determined by ICP-MS. The same procedure was used to determine the permeability of  $V^{3+}$ . The permeability of  $VO^{2+}$  was determined analogously using 1.2 M  $VOSO_4/2\text{ M }H_2SO_4$  in the “excess side” and the vanadium concentration in the “deficiency side” was determined during the measurement by calibrated UV/Vis absorption at 765 nm.

#### 2.4.2. Conductivity measurements

The H cell setup with a reduced active area of  $0.785\text{ cm}^2$  and with a 4 electrode arrangement was used for through-plane conductivity measurements similar to the description in literature [45]. The membrane was sandwiched between the flanges and both compartments were filled with 2 M  $H_2SO_4$ . In each compartment a piece of Pt wire served as voltage sense which was

placed in a fixed position close to the membrane ( $\sim 1$  mm distance). A disk of activated graphite felt (GFD5, SGL Carbon, Germany; activation:  $400^\circ\text{C}/18$  h/air atmosphere) connected via a Pt wire was the working electrode in each compartment. As conductivity is strongly depending on temperature, the complete cell was maintained at  $(20 \pm 0.1)^\circ\text{C}$  during the measurements with a thermostat (F12, Julabo, Germany). The resistance was determined using linear sweep voltammetry between  $-0.1$  V and  $+0.1$  V with  $10$  mV  $\text{s}^{-1}$ . To obtain the membrane resistance only, the resistance of the H cell without membrane was subtracted from each measurement. The membrane resistance measurements were repeated three times and the average value was used.

#### 2.4.3. Oxygen permeation

The permeation of oxygen was determined with the so-called electrochemical monitoring technique described in the literature [46–48]. In this method the permeation of oxygen through membranes is determined by reducing the permeated oxygen on a Pt electrode under mass transfer conditions. Specifically, a thin Pt mesh was placed on one side of the membrane sample and the assembly was pressed between the flanges of the H cell (active area:  $2.545$  cm<sup>2</sup>), the Pt mesh facing the “liquid” compartment that was filled with  $2$  M  $\text{H}_2\text{SO}_4$ . The Pt mesh served as working electrode while a Ag/AgCl reference electrode and a Pt grid as counter electrode were also placed into the “liquid” compartment. The  $2$  M  $\text{H}_2\text{SO}_4$  was purged with humidified  $\text{N}_2$  for  $15$  min to remove any oxygen and afterwards kept under a  $\text{N}_2$  blanket while the “gas” compartment was also flushed with  $\text{N}_2$ . After purging, a potential of  $+0.1$  V vs. Ag/AgCl was applied to the Pt mesh which makes the oxygen reduction on the Pt mesh mass-transfer limited [46,48]. While still supplying  $\text{N}_2$  to the “gas” compartment, the background current was measured. After reaching a steady state current (approx.  $10$  min), the gas supply was changed from  $\text{N}_2$  to  $\text{O}_2$  while continuing the potentiostatic measurement and this was defined as  $t=0$ . The cathodic current increased as oxygen permeated from the “gas” compartment through the membrane reaching the Pt mesh till a steady-state was obtained and the experiment was stopped. The experiments were conducted at  $21 \pm 1^\circ\text{C}$ .

#### 2.5. Vanadium/air redox flow battery operation

The VARFB test cell described before [6] consisted of polycarbonate bodies with cavities in which the current collectors and electrodes were placed. The negative electrode consisted of a graphite current collector and an activated graphite felt, the positive electrode comprised a titanium current collector with integrated flow field, a gas diffusion electrode decorated with Pt/C and Nafion ionomer and an  $\text{IrO}_2$ -modified graphite felt. The membrane was placed between the two polycarbonate bodies, separating the negative and positive electrodes.  $12$  mL of the  $\text{V}^{3+}$  electrolyte were employed as negative electrolyte which was permanently purged with humidified  $\text{N}_2$  during the experiment. The positive electrolyte was  $50$  mL of  $2$  M  $\text{H}_2\text{SO}_4$ . The electrolytes were pumped through the electrodes with  $100$  mL  $\text{min}^{-1}$  during charging, during discharging the positive electrolyte was not pumped but the GDE was fed with  $267$  mL  $\text{min}^{-1}$  air through the flow field and the anolyte was pumped as in charging mode. As the reactants of the positive electrode are supplied in excess, the battery capacity is limited by the capacity of the anolyte. To minimize hydrogen evolution and to define comparable experimental conditions, the VARFB was always charged up to  $83\%$  of the anolyte capacity. The applied current density was  $20$  mA  $\text{cm}^{-2}$ . An ICP-MS sample was taken from the positive electrolyte after discharging to determine the vanadium crossover during one cycle. Operation of the VARFB was conducted at room temperature ( $21 \pm 1^\circ\text{C}$ ).

### 3. Results and discussion

#### 3.1. Membrane characterization

To verify the modification of the N117 substrate with the polyelectrolytes, ATR-FTIR spectra were recorded of the pure polyelectrolyte PEI, of an unmodified N117 and of  $\text{N117}-(\text{PEI}/\text{Nafion})_k$  with  $k=5, 10, 20$  (Fig. 3). The spectrum of PEI shows typical features of the C–H bond ( $\nu_a(\text{C-H})\sim 2930$   $\text{cm}^{-1}$ ;  $\nu_s(\text{C-H})\sim 2815$   $\text{cm}^{-1}$ ;  $\delta(\text{C-H})\sim 1460$   $\text{cm}^{-1}$ ) and the N–H bond ( $\delta(\text{N-H})\sim 1585$   $\text{cm}^{-1}$ ) [49,50]. The N117 shows absorption related to C–F bonds ( $\nu_a(\text{C-F})\sim 1200$   $\text{cm}^{-1}$ ;  $\nu_s(\text{C-F})\sim 1150$   $\text{cm}^{-1}$ ), the C–O–C group ( $\nu_{as}(\text{C-O-C})\sim 970$ – $985$   $\text{cm}^{-1}$ ) and S–O bonds ( $\nu_s(\text{S-O})\sim 1060$   $\text{cm}^{-1}$ ) as well as bending vibration of absorbed water ( $\delta(\text{O-H})\sim 1635$   $\text{cm}^{-1}$ ) in good agreement with the literature [51–54]. N117 does not show any C–H bond features because it is fully fluorinated. It is clearly visible in Fig. 3 that with increasing  $k$ , the PEI-related features of the C–H and N–H bond also increase which indicates an increased amount of PEI. Other features of the PEI than the C–H stretching/deformation and the N–H deformation cannot be used for identifying PEI on the substrate because these absorptions overlap with substrate features. The performed FTIR measurements show that the applied modification routine is suitable to modify N117 membranes with polyelectrolytes. However, the FTIR measurements only confirm qualitatively the deposition of PEI. Therefore, TGA measurements of the unmodified and modified samples were conducted to gain quantitative information on the modifications.

The TGA and negative derivatives of mass loss are shown in Fig. 4 for unmodified membranes and membranes modified with polyelectrolytes. The TGA of Nafion can be divided into three regions. Up to  $200^\circ\text{C}$  the Nafion membrane loses water [55–57], in the range of  $300$ – $400^\circ\text{C}$  C–S bonds are broken [56], the  $-\text{SO}_3\text{H}$  groups decompose [58] and/or the ether groups of the Nafion break down [55]. At temperatures above  $400^\circ\text{C}$ , the polytetrafluorethylene (PTFE) backbone of the Nafion is destructed [51,53]. The TGA of samples of differently modified membranes appear similar in the temperature range up to  $200^\circ\text{C}$ . It can be seen in Fig. 4 that the TGA of the investigated membranes differs especially in the region between  $300^\circ\text{C}$  and  $400^\circ\text{C}$ . PEI decomposes at temperatures up to  $350/400^\circ\text{C}$  [59,60]. The difference of TGA between  $300^\circ\text{C}$  and  $400^\circ\text{C}$  is most likely due to the different amount of PEI and Nafion on the membrane samples which are decomposed in that temperature range. The inset in Fig. 4 shows the

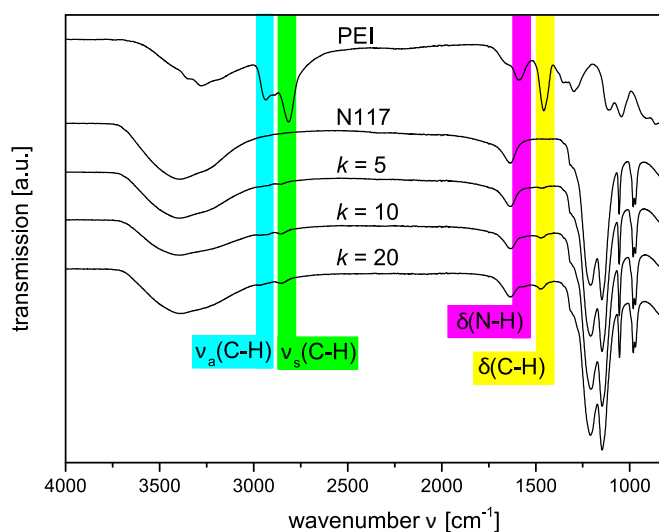
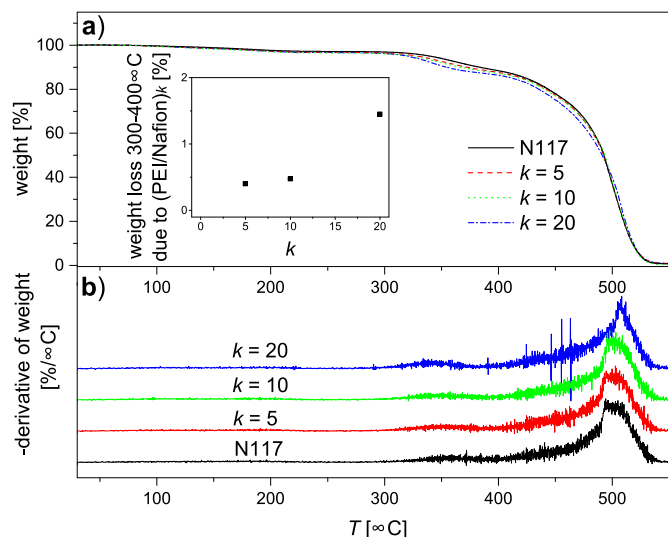


Fig. 3. ATR-FTIR spectra of PEI, N117 and  $\text{N117}-(\text{PEI}/\text{Nafion})_k$  with  $k=5, 10, 20$ .



**Fig. 4.** (a) TGA and (b) negative derivatives of N117 and N117-(PEI/Nafion)<sub>k</sub> with  $k=5, 10, 20$ . The inset in (a) shows the weight loss of membranes with  $k=5, 10, 20$  in % between 300 °C and 400 °C subtracted by the weight loss of N117 between 300 °C and 400 °C.

weight loss of the modified membranes between 300 °C and 400 °C subtracted by the weight loss of the unmodified membrane between 300 °C and 400 °C, i.e. the weight loss due to the LbL film. With increasing  $k$ , the weight loss increases as well. This increase is not linear but seems to be exponential which can be a hint that the growth of LbL film under the given deposition conditions is not linear. Exponential growth was found for PEI/PAA films assembled from polyelectrolytes with pH 9 for the PEI and pH 2.85 for the PAA solution [61]. After preparation without any pH adjustment, the PEI solution used in this work had a pH 10–11 and the Nafion solution pH 3.

To monitor the morphology and roughness of the LbL film, cross-sections were examined with SEM (Fig. 5). Both the cross-sections and the surface/main planes of the membranes which were modified with the PEI/Nafion LbL film are imaged. The surface of the non-modified N117 is smooth and even. The samples N117-(PEI/Nafion)<sub>k</sub> with  $k=5$  and  $k=10$  show features and have a slightly heterogeneous surface. The surface roughness of the modification increases with  $k$ . The difference between the sample  $k=10$  and  $k=20$  is the most distinct one; the  $k=10$  sample has a quite homogeneous surface structure while the membrane

modified with  $k=20$  has a spongy and porous structure. As discussed in several publications [25,62,63], surface roughness of the LbL film and exponential growth are linked to each other. McAloney et al. [64] investigated the growth of PDADMAC/PSS LbL films in dependence of the ionic strength of the polyelectrolyte solutions. They found via AFM measurements that in the regime with the strongest growth per bilayer, the surface roughness increases with  $k$ . Likewise, Choi et al. [63] observed for exponential buildup of poly(2-(dimethylamino)ethyl methacrylate) (PDMAEMA)/PAA multilayers a non-uniform surface with a higher surface roughness which is increasing with  $k$  as it is also observed here. It is assumed that exponential growth occurs due to the “in” and “out” diffusion of at least one of the polyelectrolytes within the whole film during each deposition step. This leads to exponential growth of the LbL film and to a rougher surface in comparison to a LbL film built up with “true” bilayer consisting of closed, homogeneous and equally thick layers on top of oppositely charged with the same morphological properties. Although exponential growth is desired for the fast buildup of thick LbL films [25], for well-defined film properties a homogeneous layer deposition is needed. In the case of the chosen polyelectrolyte system and deposition parameters, (PEI/Nafion)<sub>10</sub> can be deposited on N117 as comparatively compact, smooth and homogeneous film.

The TGA and SEM results suggested a non-linear LbL film growth. This hypothesis is verified by thickness measurements (Fig. 6). The film thickness increases non-linearly with  $k$  which is in agreement with the aforementioned results. A non-linear relationship between  $k$  and thickness was also found by Yang et al. for a (PEI/PAA)<sub>k</sub> system [35].

### 3.2. Membrane performance

For the application of the modified membranes in VARFB the proton conductivity, vanadium permeation and oxygen permeation are important and thus discussed in the following.

The relevant conductivity in membranes is in general the through-plane conductivity as this is the direction along which protons move. However, most conductivity values given in the literature are in-plane conductivities. This is probably due to its easier, reproducible determination [65]. However, there is no consensus in the literature whether Nafion has anisotropic conductivity [66,67] or not [65,68]. The conductivity of N117-(PEI/Nafion)<sub>k</sub> must be determined as through-plane conductivity as obviously the in-plane and through-plane conductivity cannot be equivalent due to the layered structure. Reported values for

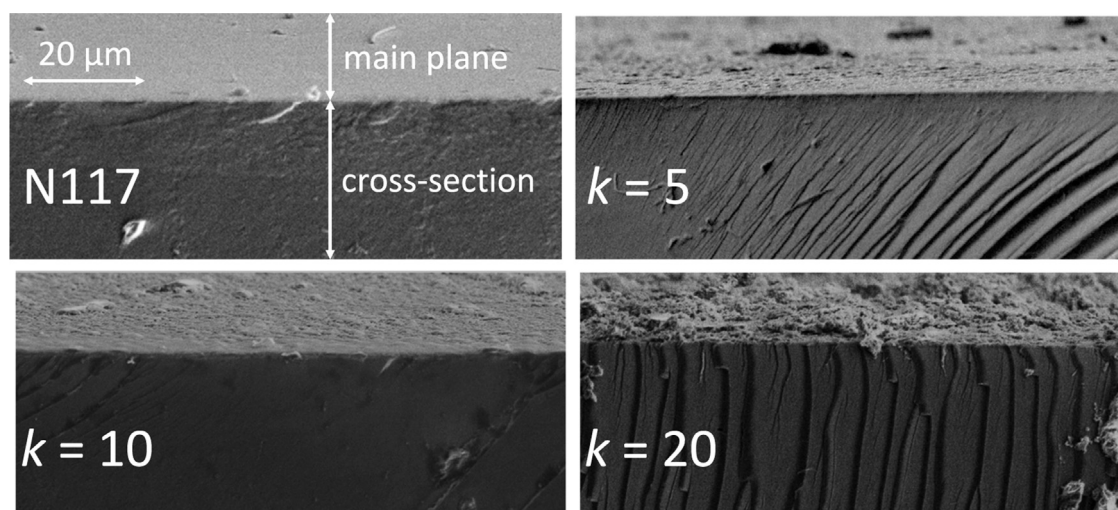


**Fig. 5.** SEM images of cross-sections of N117 and N117-(PEI/Nafion)<sub>k</sub> with  $k=5, 10, 20$ .

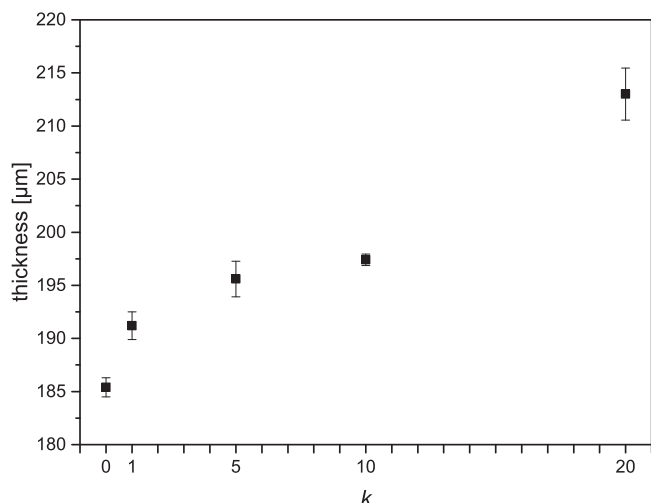


**Fig. 6.** Mean values of the thickness of N117 ( $k=0$ ) and N117-(PEI/Nafion) $_k$  with  $k=1, 5, 10, 20$  and standard deviations of the five measurements.

**Table 1**

Literature values and value determined in this work for Nafion conductivity in sulfuric acid media.

Conductivity [ $\text{S cm}^{-1}$ ]	Temperature [ $^{\circ}\text{C}$ ]	Medium	Method [reference]
0.088	20	1 M $\text{H}_2\text{SO}_4$	Through-plane [69]
0.085	20	3 M $\text{H}_2\text{SO}_4$	Through-plane [69]
0.11	22	2 M $\text{H}_2\text{SO}_4$	n/a [70]
0.076	25	1 M $\text{H}_2\text{SO}_4$	In-plane [71]
0.071	25	1 M $\text{H}_2\text{SO}_4$	Through-plane, cell 1 [72]
0.084	30	1 M $\text{H}_2\text{SO}_4$	Through-plane, cell 2 [72]
0.0899	20	2 M $\text{H}_2\text{SO}_4$	Through-plane (this study)

through-plane conductivity measurements of Nafion show substantial scatter depending on the design of the conductivity cell, the measurements conditions as well as the pretreatment of the membrane. Table 1 shows selected conductivity values of Nafion membranes obtained under different measurement conditions in sulfuric acid and the conductivity of N117 determined in this work which is in good agreement with most of the reported values given in Table 1.

With increasing  $k$  the conductivity decreases (Fig. 7a). The conductivity is decreased by 22% from  $0.0899 \text{ S cm}^{-1}$  for N117 to  $0.070 \text{ S cm}^{-1}$  for N117-(PEI/Nafion) $_{20}$ . This finding can be explained with higher resistance of the modified membrane due to lower cation conduction. The ion conduction and especially proton conduction mechanism in Nafion membranes is well described in the literature [73–75]. From a microstructural point of view, hydrated Nafion consists of interpenetrating hydrophilic and hydrophobic domains [73]. The hydrolyzed sulfonic acid groups of Nafion form water channels. Proton conduction through these channels occurs both via a hopping or Grotthus-like mechanisms and/or by a diffusion or “vehicular” mechanism [74]. The amine groups of PEI interact via hydrogen bonds or protonation with the sulfonic acid groups of the Nafion or with the dopant sulfuric acid, similarly as it was described for polybenzimidazole (PBI) interacting with acids [76,77]. Thus, proton conduction through the LbL film occurs via proton hopping between the amine groups and the acid (sulfonic acids groups of Nafion or  $\text{H}_2\text{SO}_4$ ). This was also reported for PEI doped with  $\text{H}_2\text{SO}_4$  [78].

A desired reduction of vanadium permeation typically comes

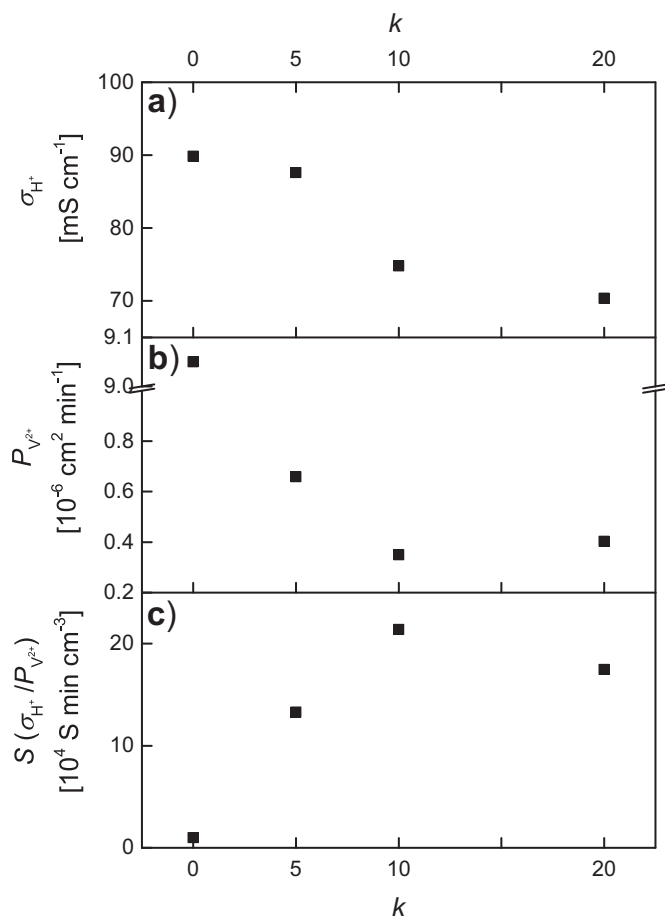


**Fig. 7.** (a)  $\text{H}^+$  conductivity  $\sigma_{\text{H}^+}$ , (b)  $\text{V}^{2+}$  permeability  $P_{\text{V}^{2+}}$  and (c) selectivity  $\sigma_{\text{H}^+}/P_{\text{V}^{2+}}$  of N117 ( $k=0$ ) and N117-(PEI/Nafion) $_k$  with  $k=5, 10, 20$ .

along with an unwanted decrease in proton conductivity as the LbL film reduces the overall cation permeation. For the determination of the optimal  $k$ , the permeation coefficient for vanadium cations  $P_{\text{V}^{x+}}$  through the membrane need to be measured and set in relation to the  $\text{H}^+$  conductivity. Following the routine described in the literature [8,17,44],  $P_{\text{V}^{x+}}$  through the membrane is determined by measuring the transport of vanadium species from a highly concentrated vanadium solution (excess side) with concentration  $c_e$  to an initially vanadium-free solution (deficiency side; vanadium concentration  $c_d = 0$  at time  $t=0$ ) of equal ionic strength. Assuming that  $c_e$ , the permeation coefficient  $P$ , the membrane area  $A$ , the membrane thickness  $x$  and the volume of the deficiency side  $V_d$  are independent of  $t$ , the permeation coefficient  $P$  can be deduced from the slope of the line  $\ln(c_e/(c_e - c_d(t)))$  vs.  $t$  [8,44].

$P_{\text{V}^{2+}}$  values were determined because  $\text{V}^{2+}$  permeates through a N117 membrane much faster than  $\text{V}^{3+}$  ( $P_{\text{V}^{2+}} = 9.05 \cdot 10^{-6} \text{ cm}^2 \text{ min}^{-1}$ ,  $P_{\text{V}^{3+}} = 4.35 \cdot 10^{-6} \text{ cm}^2 \text{ min}^{-1}$ ; Fig. 8). Consequently, the permeability for  $\text{V}^{2+}$  is more critical for the VARFB performance. The dependence of  $P_{\text{V}^{2+}}$  on  $k$  is shown in Fig. 7b.  $P_{\text{V}^{2+}} = 3.50 \cdot 10^{-7} \text{ cm}^2 \text{ min}^{-1}$  of the N117-(PEI/Nafion) $_{10}$  is more than one order of magnitude (or approx. –96%) lower than  $P_{\text{V}^{2+}}$  of N117. Interestingly, the N117-(PEI/Nafion) $_{20}$  membrane has a slightly higher  $P_{\text{V}^{2+}} = 4.03 \cdot 10^{-7} \text{ cm}^2 \text{ min}^{-1}$  compared to the N117-(PEI/Nafion) $_{10}$ . This observation might be the result of the porous, spongy structure of the LbL film which was observed with SEM. The more opened layer structure enables faster permeation by cations such as  $\text{V}^{2+}$ . However, the proton conductivity of the N117-(PEI/Nafion) $_{20}$  membrane is not higher than the conductivity of the N117-(PEI/Nafion) $_{10}$  sample.

Similar to the reduced proton conductivity (Fig. 7a), the lower

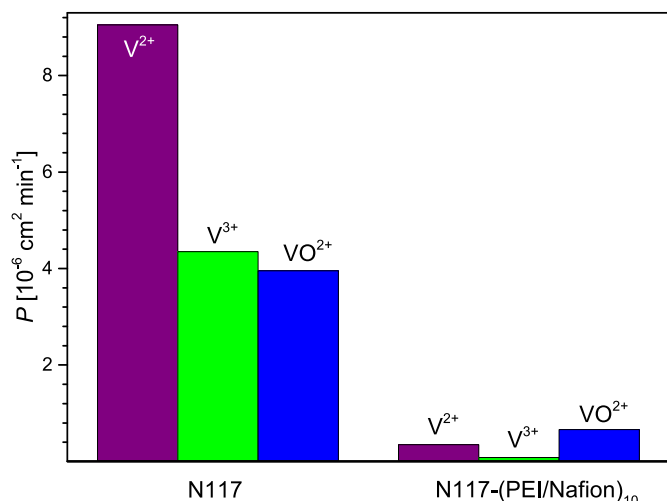


**Fig. 8.** Permeation coefficients of  $V^{2+}$ ,  $V^{3+}$  and  $VO^{2+}$  through N117 and N117-(PEI/Nafion)<sub>10</sub>.

vanadium permeation can be attributed to the repulsive forces due to the same charge of the cationic PEI layers and the vanadium cations. However, the reduction in vanadium permeation is much more pronounced than the reduction of proton conductivity (reduction of  $P_{V^{2+}}$  by approx. 92% due to (PEI/Nafion)<sub>5</sub> vs. reduction of  $\sigma_{H^+}$  by approx. 2.5% due to (PEI/Nafion)<sub>5</sub>). The reason for this is most probably that the proton conductivity in the LbL film can be maintained by proton hopping mechanism while other cations than protons are transferred only via the vehicular mechanism [79]. Additionally, due to the higher valency of the vanadium ions (+2 and +3, respectively) in comparison to the monovalent protons, the electrostatic repulsion and thus donnan exclusion of the positively charged  $V^{2+}$  and  $V^{3+}$  by the positively charged PEI is higher than to  $H^+$ , leading to a more pronounced decrease of  $V^{x+}$  conductivity compared to  $H^+$  [36,80].

For improving the overall performance of a membrane by a modification routine, the reduced vanadium permeation should prevail over the reduced proton conductivity. A common measure is the selectivity which is the ratio of proton conductivity to  $V^{2+}$  ion permeability  $S = \sigma_{H^+}/P_{V^{2+}}$  [13,14]. The higher the selectivity, the more efficient is the modification. In Fig. 7c the selectivity is shown for N117 ( $k=0$ ) and N117-(PEI/Nafion)<sub>k</sub> with  $k=5, 10, 20$ .  $S$  of N117 is approx.  $1 \cdot 10^4 \text{ S min cm}^{-3}$  (Fig. 7). It can be seen that  $S$  has a maximum at N117-(PEI/Nafion)<sub>10</sub> with approx.  $21 \cdot 10^4 \text{ S min cm}^{-3}$ , i.e. the modification with (PEI/Nafion)<sub>10</sub> is the most efficient one due to the best compromise between reduced  $V^{2+}$  permeation and reduced  $H^+$  conductivity. The achieved selectivity improvement by a factor of 21 is remarkable also in comparison to literature. Xi et al. [24] reported a maximum selectivity (concerning  $VO^{2+}$ ;  $\sigma_{H^+}/P_{VO^{2+}}$ ) increase factor of almost 7 due to (PDDA/PSS)<sub>5</sub> on a Nafion membrane and Lu et al. [20] observed a maximum selectivity ( $\sigma_{H^+}/P_{VO^{2+}}$ ) for (chitosan/phosphotungstic acid)<sub>3</sub> on a Nafion membrane which was about 2 times higher than that of the pristine membrane. The reduced vanadium permeation is crucial for the lifetime of the VARFB. Therefore, the following experiments, evaluation of  $V^{3+}$  and  $VO^{2+}$  permeability, investigation of oxygen permeation and performance in VARFB, are conducted with N117-(PEI/Nafion)<sub>10</sub> which was the membrane with the highest selectivity  $\sigma_{H^+}/P_{V^{2+}}$ .

The permeabilities of  $V^{2+}$ ,  $V^{3+}$  and  $VO^{2+}$  through unmodified N117 and N117-(PEI/Nafion)<sub>10</sub> are shown in Fig. 8. Although not relevant for VARFB, the permeability of  $VO^{2+}$  was determined in order to allow an estimation of the performance of N117-(PEI/Nafion)<sub>10</sub> in VRFB application. Overall, a significant reduction of permeability of all vanadium species is observed for the N117-(PEI/

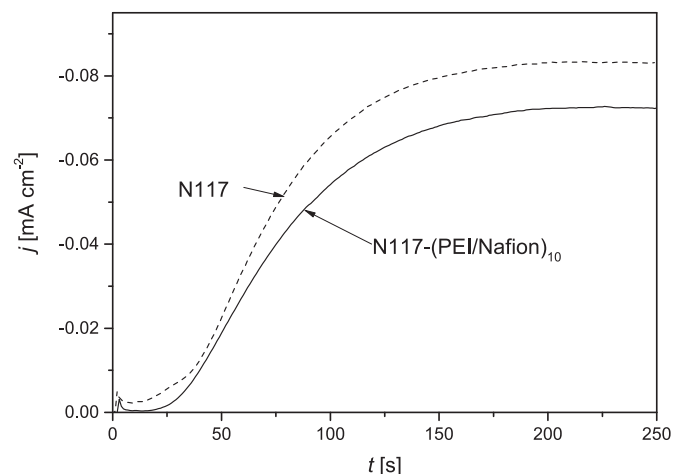


**Fig. 9.** Background-current corrected current transients due to oxygen reduction after permeation through unmodified N117 and N117-(PEI/Nafion)<sub>10</sub>.

Nafion)<sub>10</sub> in comparison to N117. By application of (PEI/Nafion)<sub>10</sub> on the N117 membrane the permeability of  $V^{3+}$  is reduced by nearly two orders of magnitude from  $4.35 \cdot 10^{-6} \text{ cm}^2 \text{ min}^{-1}$  to  $8.55 \cdot 10^{-8} \text{ cm}^2 \text{ min}^{-1}$ . For the unmodified N117, the permeability of  $VO^{2+}$  was determined as  $39.53 \cdot 10^{-7} \text{ cm}^2 \text{ min}^{-1}$  which is in good agreement with [81] ( $36.55 \cdot 10^{-7} \text{ cm}^2 \text{ min}^{-1}$ ). The permeability of  $VO^{2+}$  is reduced to  $6.62 \cdot 10^{-7} \text{ cm}^2 \text{ min}^{-1}$  by application of (PEI/Nafion)<sub>10</sub> on N117 whereas the modification of a N117 with a covalently bonded PEI layer proposed in [81] resulted in a slightly lower permeability of  $5.23 \cdot 10^{-7} \text{ cm}^2 \text{ min}^{-1}$ .

The oxygen permeation of N117 and N117-(PEI/Nafion)<sub>10</sub> were determined by electrochemical reduction of oxygen after the permeation through the membrane. The steady-state oxygen reduction current  $j_{\infty}$  (corrected by the background current) represents the steady-state oxygen permeation through the membrane (Fig. 9). This current is  $j_{\infty} = 82.1 \mu\text{A cm}^{-2}$  for the unmodified N117 and  $j_{\infty} = 71.57 \mu\text{A cm}^{-2}$  for the N117-(PEI/Nafion)<sub>10</sub> membrane, i.e. the permeation of oxygen is reduced by approx. 13% by the LbL film. However, the N117-(PEI/Nafion)<sub>10</sub> membrane is also thicker and therefore a comparison of the permeability which also accounts for the thickness of the membrane is advisable to draw a conclusion about the permeation resistance of the LbL film.

The permeability  $P$  is calculated as  $P = (j_{\infty} \cdot x)/(z \cdot F)$  with  $x$  being the membrane thickness,  $z=4$  the transferred electrons per species and  $F$  is the Faraday constant [47,82]. The permeability is  $3.94 \cdot 10^{-12} \text{ mol s}^{-1} \text{ cm}^{-1}$  for the unmodified N117. This value is in good agreement with literature values (Table 2), however, the measurement technique, the experimental conditions and the water content of the membrane influence the permeability measurement significantly [83]. The permeability of N117-(PEI/Nafion)<sub>10</sub> was  $3.66 \cdot 10^{-12} \text{ mol s}^{-1} \text{ cm}^{-1}$ , i.e. the reduction of  $P$  due to (PEI/Nafion)<sub>10</sub> is approx. 7%.

The reduction in oxygen permeability due to the LbL film can be explained with the solution-diffusion model which is widely used to describe gas transport through polymeric materials [86]. Permeation of gases starts with adsorption of the gas on the surface. Subsequently, the gas is dissolved in the membrane material and then it diffuses through the membrane. Finally, the gas exits the membrane phase by getting dissolved in another phase (e.g. water). Solution and diffusion depend on the interactions of the permeate and the membrane material. In a membrane consisting of only one polymer (such as the unmodified N117), ideally the permeating gas only needs to be dissolved once before it can diffuse through the membrane and leave it by dissolution in another phase. However, in the case of LbL polyelectrolyte film on the membrane the situation

**Table 2**Selected literature values for permeability  $P$  of  $O_2$  through Nafion membranes determined with different measurement techniques and under different conditions.

$P$ [mol s <sup>-1</sup> cm <sup>-1</sup> ]	Membrane	Temperature [°C]	Liquid medium	Method, conditions [reference]
$11.59 \cdot 10^{-12}$	Nafion 117	25	1 N H <sub>2</sub> SO <sub>4</sub>	Electrochemical monitoring technique, gas not humidified, no membrane pretreatment [84]
$1.73 \cdot 10^{-12}$	Nafion 120	20	0.5 M K <sub>2</sub> SO <sub>4</sub>	Electrochemical monitoring technique, gas humidified, boiling pretreatment [47]
$4.2 \cdot 10^{-12}$	Nafion 117	25	–	Electrochemical <i>in situ</i> method in a fuel cell using a microelectrode, 82% relative humidity (RH) [85]
$3.94 \cdot 10^{-12}$	Nafion 117	21	2 M H <sub>2</sub> SO <sub>4</sub>	Electrochemical monitoring technique, membrane pretreated, gas humidified (this study)

is different [35]. The LbL film is not believed to be homogeneous and equally thick but more like an interpenetrating network having a scrambled-egg like structure [35]. This explanation is in good agreement with the increasing roughness of the films with increasing LbL steps. Due to this irregular structure bearing a lot of interfaces between the two polyelectrolytes, gases need to be dissolved, diffuse and get redissolved several times when permeating through the membrane. This slows down the overall mobility of the gas through the membrane and leads to barrier properties of the (PEI/Nafion)<sub>10</sub> [35].

### 3.3. VARFB operation with modified membrane

Fig. 10 shows the charge and the discharge curve of the VARFB operation using a N117 (dashed lines) and using a N117-(PEI/Nafion)<sub>10</sub> membrane (solid lines) at  $j = 20 \text{ mA cm}^{-2}$ . Interestingly, the overpotentials during charging are nearly identical, bearing in mind the reduced proton conductivity of the membrane. This observation reveals that the membrane resistance is only a small part of the total cell resistance and the charge-transfer resistance of the water splitting reaction is the dominant contribution. However, the average discharging potential is lower when using the N117-(PEI/Nafion)<sub>10</sub> membrane compared to the unmodified N117 membrane. This is attributed to a low charge-transfer resistance of the oxygen reduction reaction in comparison to other resistances such as the membrane resistance. The lower discharging potential affects the voltaic efficiency of the VARFB which is 2.5% lower than in the cycle with the unmodified N117 (Table 3). During discharging of the VARFB with the N117-(PEI/Nafion)<sub>10</sub> membrane more capacity can be retrieved from the battery. The coulombic efficiency of the system with N117 in comparison to the N117-(PEI/Nafion)<sub>10</sub> is increased by more than 11% from  $\eta_C = 81.32\%$  to  $\eta_C = 93.18\%$  (Table 3). The reason for the increase of coulombic efficiency is the reduction of both loss mechanisms; i.e. vanadium crossover and oxygen permeability. Overall, the energy

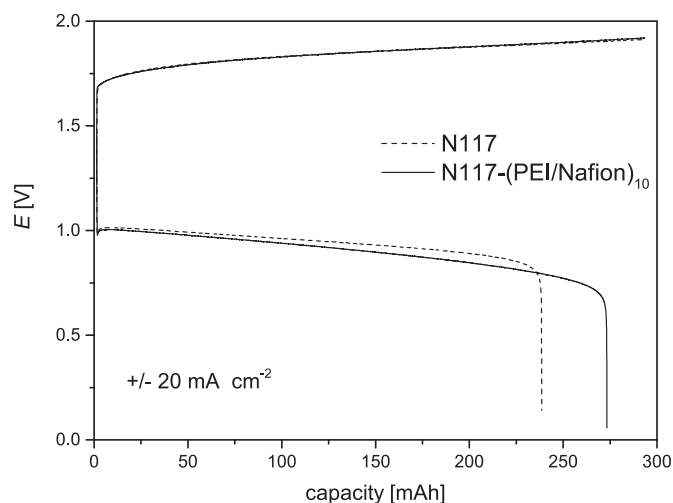


**Fig. 10.** Charge/discharge curves of VARFB operated at  $(21 \pm 1)^\circ\text{C}$  applying an unmodified N117 and N117-(PEI/Nafion)<sub>10</sub>.

**Table 3**Efficiencies and vanadium crossover (determined by ICP-MS of the positive electrolyte) during VARFB operation at  $j = 20 \text{ mA cm}^{-2}$  of N117 and N117-(PEI/Nafion)<sub>10</sub>.

	$\eta_C$ [%]	$\eta_E$ [%]	$\eta_V$ [%]	V crossover [mmol]
N117	81.32	41.54	51.08	0.763
N117-(PEI/Nafion) <sub>10</sub>	93.18	45.2	48.51	0.246

efficiency was increased from  $\eta_E = 41.5\%$  to  $\eta_E = 45\%$ .

ICP-MS measurements were conducted to quantify the irreversible capacity loss due to vanadium crossover during the cycle. The vanadium crossover during VARFB operation is reduced by 0.517 mmol (approx. –70%) if N117 is modified with (PEI/Nafion)<sub>10</sub> (Table 3). In contrast to the determination of permeation coefficients described above, the vanadium crossover during VARFB operation is caused by diffusion, migration and electroosmotic convection (EOC) [87].

Another important influence on the coulombic efficiency and capacity fade during VARFB operation is the water transfer between the electrolytes of the two half-cells. The possible water transfer mechanisms occurring during VARFB operation are the transport of water as hydration shells of diffusing vanadium ions [88], osmosis and EOC/migration (e.g. hydration shell of dragged protons) as depicted in Fig. 11. Table 4 shows the volumes of the negative electrolyte before charging, after charging and after discharging of the VARFB using a N117 membrane and a N117-(PEI/Nafion)<sub>10</sub> membrane, respectively.

Water is transferred from the negative to the positive electrode by the hydration shells of  $V^{2+}$  and  $V^{3+}$  which undergo crossover due to diffusion and in the opposite direction due to osmosis driven by the ion concentration differences between negative and positive electrolyte. Water transfer due to EOC/migration depends on the direction of the electric field and occurs from the positive electrode to the negative electrode during charging and vice versa during discharging. The net water transfer was observed to take place from the positive to the negative electrode during charging whereas it is directed from the negative electrode towards the positive electrode during discharging for both membranes (Table 4). Additionally, it was observed for both membranes that the net water transfer from the positive to the negative electrode

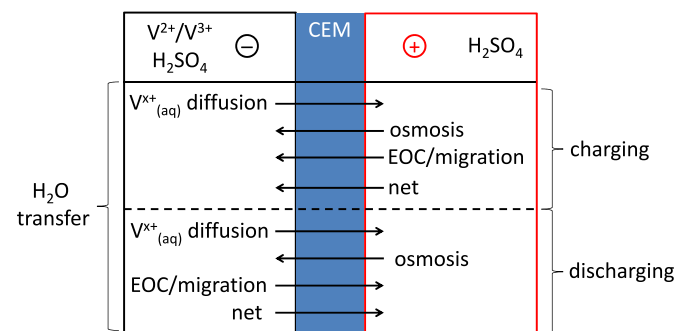


**Fig. 11.** Water transfer during charging and discharging of a VARFB due to hydration shells of diffusing  $V^{x+}$ , osmosis, EOC/migration and the net water transfer.

**Table 4**

Volumes of the negative electrolyte before charging, after charging and after discharging of the VARFB using a N117 or a N117-(PEI/Nafion)<sub>10</sub> membrane.

Volume [mL]	Before charging	After charging	After discharging
N117	12.0	13.9	13.3
N117-(PEI/Nafion) <sub>10</sub>	12.0	13.8	13.6

during charging is higher than the net water transfer from the negative to the positive electrode during discharging (Table 4). As it can be assumed that the water transfer rates due to osmosis and by hydration shells of diffusing vanadium ions are independent of the direction of the electric field, the different net water transfer is caused by the opposite direction of EOC/migration-driven water transfer during charging and discharging.

Comparing the two membranes, the net water transfer is nearly the same for both membranes during charging. However, less water is transferred from the negative electrode to the positive electrode during discharging when a N117-(PEI/Nafion)<sub>10</sub> membrane is used. These observations can be explained under consideration of migration processes accompanied by water transport due to hydration shells. During charging (ideally) only H<sup>+</sup> can migrate in the electric field through the cation exchange membrane from the positive electrode to the negative electrode. During discharging, the electric field is reversed and migration occurs from the negative to the positive electrode. Amongst proton migration, vanadium cation migration can also occur. Each transferred H<sup>+</sup> is accompanied by 2.5 H<sub>2</sub>O molecules [44,89] while 6–7.5 H<sub>2</sub>O molecules as inner hydration shell are carried with each V<sup>2+</sup> ion and 5–6 H<sub>2</sub>O molecules with each V<sup>3+</sup> ion [90]. Thus, the migration of vanadium ions during discharging is connected with a significant water transfer from the negative to the positive electrode. As shown above, the LbL film represents a barrier to multivalent ions such as V<sup>2+</sup> and V<sup>3+</sup>. Hence, it can be assumed that the migration of V<sup>2+</sup> and V<sup>3+</sup> will be reduced when using the N117-(PEI/Nafion)<sub>10</sub> membrane. Consequently, the overall water transfer from the negative electrode to the positive electrode during discharging should be less pronounced when using the N117-(PEI/Nafion)<sub>10</sub> membrane which is in agreement with the observation of the volume changes during discharging (Table 4).

The reduction of oxygen crossover during VARFB operation by using N117-(PEI/Nafion)<sub>10</sub> can be deduced from the increased discharge capacity which is raised by 34.8 mAh (+15%) in comparison to N117 (Fig. 10). Bearing in mind that only V<sup>2+</sup> crossover reduces the coulombic efficiency, the reduced vanadium crossover which corresponds to a charge of 13.9 mAh ( $Q = n \cdot z \cdot F$  with  $z = 1$ ) can account at most for 40% of the discharge capacity increase. Consequently, the additional capacity gain when using the N117-(PEI/Nafion)<sub>10</sub> membrane which cannot be related to reduced vanadium crossover, 20.9 mAh, is an indirect evidence for lower oxygen permeability during VARFB operation.

The stability of the membrane under VARFB cycling conditions was investigated by TGA and IR measurements of the N117-(PEI/Nafion)<sub>10</sub> membrane before and after the VARFB cycle (Figs. 12 and 13). During TGA measurements, the sample after VARFB operation shows a weight loss of 14.7% in the temperature range of 300–400 °C where PEI decomposition occurs (as described above) whereas the sample before VARFB operation lost 9.2% in that temperature region (Fig. 12). This higher weight loss after VARFB operation does not allow any conclusion about the stability of the LbL film but only indicates that after VARFB operation additional substances are present in the membrane which are influencing the thermal degradation. Indeed, a new degradation process beginning at approx. 340 °C can be observed. This process might be caused by vanadium cations incorporated into the membrane during VARFB

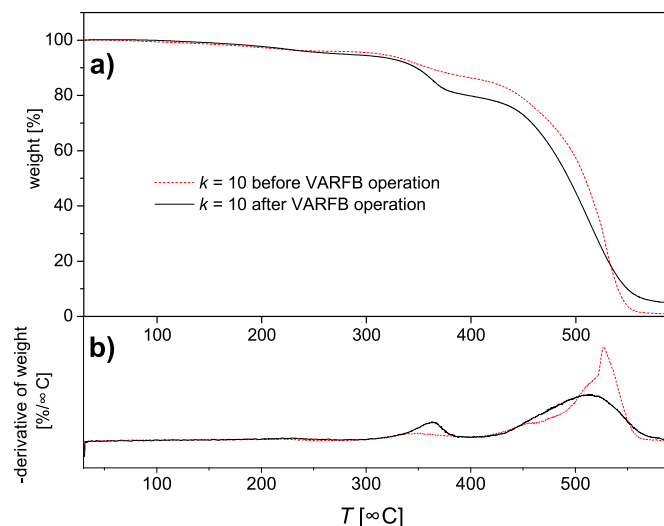


**Fig. 12.** (a) TGA, (b) negative derivative of TGA of the membrane N117-(PEI/Nafion)<sub>10</sub> before and after VARFB operation.

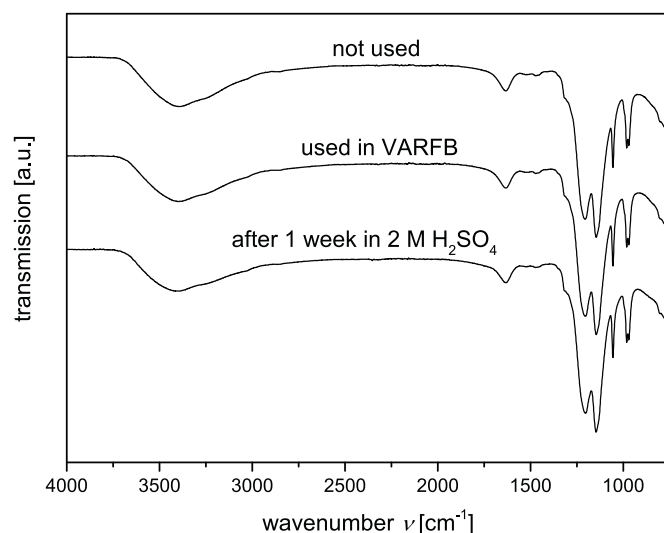


**Fig. 13.** IR spectra of the membrane N117-(PEI/Nafion)<sub>10</sub> before and after VARFB operation and after immersing the membrane in 2 M H<sub>2</sub>SO<sub>4</sub> for one week.

operation. It was shown that cations within a Nafion membrane can reduce the thermal stability since Lewis acids catalyze the breakdown of ether bonds of the side chains [91,92].

In Fig. 13 the IR spectrum of a non-used N117-(PEI/Nafion)<sub>10</sub> membrane is shown in comparison to such a membrane used in a VARFB and another one which was immersed in 2 M H<sub>2</sub>SO<sub>4</sub> for one week. The features related to C–H bonds ( $\nu_a(\text{C-H}) \sim 2930 \text{ cm}^{-1}$ ;  $\nu_s(\text{C-H}) \sim 2815 \text{ cm}^{-1}$ ;  $\delta(\text{C-H}) \sim 1460 \text{ cm}^{-1}$ ); the N–H bond ( $\delta(\text{N-H}) \sim 1585 \text{ cm}^{-1}$ ) can be seen in all three samples. Thus, it can be concluded that the PEI and therefore the LbL film is still present on the membrane even after use in VARFB and after immersion in 2 M H<sub>2</sub>SO<sub>4</sub>. Additionally, the N117-(PEI/Nafion)<sub>10</sub> membrane was slightly opaque (milky color) due to the LBL film modification. This appearance was still present even after VARFB operation.

However, further experimental investigations of the stability of the LbL are necessary. The investigation of the performance of the membrane in a VARFB during several cycles should be conducted to evaluate the stability of the LbL membrane under VARFB cycling conditions as it was done for example by Xi et al. [93] and Lu et al. [20] to prove the stability of LbL modified membranes in VRFB. However, for this purpose the optimization of all VARFB cell

components with regards to longer life-time is necessary which was beyond the scope of this paper.

#### 4. Conclusion

In this contribution we showed the successful modification of N117 membranes with LbL films of PEI and Nafion ionomer and the beneficial effect of the application of a N117-(PEI/Nafion)<sub>10</sub> membrane in VARFB in comparison to a plain N117 membrane. N117-(PEI/Nafion)<sub>10</sub> increased the selectivity  $S = \sigma_{H^+}/P_{V^{2+}}$  by a factor of 21 and decreased oxygen permeation by –13% (oxygen permeability: –7%) compared to bare N117. The N117-(PEI/Nafion)<sub>10</sub> exhibit a better performance in a VARFB in terms of coulombic efficiency, energy efficiency and reduced vanadium crossover which is crucial for the lifetime of the VARFB.

The vanadium crossover reduction is already very efficient with (PEI/Nafion)<sub>10</sub> (–70% in VARFB operation compared to unmodified N117). In this study the focus was the reduction of vanadium crossover which is limiting the lifetime of the battery. However, reduced oxygen permeability is needed for increased coulombic efficiency. The permeability of oxygen is reduced by 7% due to (PEI/Nafion)<sub>10</sub>. Although not the focus in this study, the oxygen permeation might be decreased further using an alternative LbL modification. For example, 70% less oxygen permeability was reported for (polyallylamine hydrochloride/PSS)<sub>20</sub> [94] or reduction by factor 100 by applying 4 quadlayers of PEI, PAA, PEI, and sodium montmorillonite clay [34]. However, these modifications were made in different context (fuel cell and food packaging) and might not be as efficient in VARFB application. Additionally, the modifications might not be efficient in terms of the crucial vanadium crossover reduction.

The modified membranes might also be suitable for application in VRFB for enhanced coulombic efficiency due to reduced crossover. Likewise, they could be beneficial for applications where proton conductivity is needed and at the same time multivalent ion and/or uncharged molecule transport must be reduced. This applies for example to microbial fuel cells (MFC) where the crossmixing of oxygen and fuel (biological material) through the membrane needs to be limited while maintaining proton conductivity of the membrane [95]. The performance of direct methanol fuel cells (DMFC) also suffers from crossover processes such as methanol crossover [96]. Albeit not investigated in this contribution, the presented modified membranes might also reduce methanol crossover due to the layered structure and could increase the performance of DMFC.

For long-term operation the stability of the LbL films needs to be evaluated. There are not many studies in the literature in which the stability of LbL films is the key aspect [26]. The electrostatic forces between the oppositely charged polyelectrolytes are quite strong and the film formation is entropy-driven. Therefore, a high stability against dissolution can be expected [97] but requires experimental verification. Likewise, the performance of the modified membranes at different current densities needs to be evaluated.

#### Acknowledgments

The authors would like to thank Dana Schonvogel for ICP-MS measurements and Pratik Das, Benedikt Berger and Khrysthyna Yezerska for assisting with experimental work. The Reiner-Le-moine-Stiftung is acknowledged for providing a Ph.D. scholarship to Jan grosse Austing.

#### References

- [1] M. Skyllas-Kazacos, M.H. Chakrabarti, S.A. Hajimolana, F.S. Mjalli, M. Saleem, J. Electrochem. Soc. 158 (2011) R55, <http://dx.doi.org/10.1149/1.3599565>, URL <http://jes.ecsd.org/cgi/doi/10.1149/1.3599565>.
- [2] P. Leung, X. Li, C. Ponce de León, L. Berlouis, C.T.J. Low, F.C. Walsh, RSC Adv. 2 (2012) 10125, <http://dx.doi.org/10.1039/c2ra21342g>, URL <http://xlink.rsc.org/?DOI=c2ra21342g>.
- [3] H. Kaneko, A. Negishi, K. Nozaki, K. Sato, M. Nakajima, EU Patent 0517217A1, 1992.
- [4] C. Menictas, M. Skyllas-Kazacos, J. Appl. Electrochem. 41 (2011) 1223–1232, <http://dx.doi.org/10.1007/s10800-011-0342-8>, URL <http://link.springer.com/10.1007/s10800-011-0342-8>.
- [5] J. Noack, C. Cremers, D. Bayer, J. Tübke, K. Pinkwart, J. Power Sources 253 (2014) 397–403, <http://dx.doi.org/10.1016/j.jpowsour.2013.12.070>, URL <http://linkinghub.elsevier.com/retrieve/pii/S0378775313020491>.
- [6] J. Grosse Austing, C. Nunes Kirchner, E.-M. Hammer, L. Komsysiaka, G. Wittstock, J. Power Sour. 273 (2015) 1163–1170, <http://dx.doi.org/10.1016/j.jpowsour.2014.09.177>, URL <http://linkinghub.elsevier.com/retrieve/pii/S0378775314016000>.
- [7] S. Hosseiny, M. Saakes, M. Wessling, Electrochem. Commun. 13 (2011) 751–754, <http://dx.doi.org/10.1016/j.elecom.2010.11.025>, URL <http://linkinghub.elsevier.com/retrieve/pii/S1388248110004996>.
- [8] J. Grosse Austing, C. Nunes Kirchner, L. Komsysiaka, G. Wittstock, J. Power Sour. 306 (2016) 692–701, <http://dx.doi.org/10.1016/j.jpowsour.2015.12.052>.
- [9] H. Prifti, A. Parasuraman, S. Winardi, T.M. Lim, M. Skyllas-Kazacos, Membranes 2 (2012) 275–306, <http://dx.doi.org/10.3390/membranes2020275>, URL <http://www.pubmedcentral.nih.gov/articlerender.fcgi?artid=4021890&tool=pmcentrez&rendertype=abstract>, <http://www.mdpi.com/2077-0375/2/2/275>.
- [10] B. Schwenzler, J. Zhang, S. Kim, L. Li, J. Liu, Z. Yang, ChemSusChem 4 (2011) 1388–1406, <http://dx.doi.org/10.1002/cssc.201100068>, URL <http://doi.wiley.com/10.1002/cssc.201100068>.
- [11] X. Li, H. Zhang, Z. Mai, H. Zhang, I. Vankelecom, Energy Environ. Sci. 4 (2011) 1147, <http://dx.doi.org/10.1039/c0ee00770f>, URL <http://xlink.rsc.org/?DOI=c0ee00770f>.
- [12] Q. Luo, H. Zhang, J. Chen, P. Qian, Y. Zhai, J. Membr. Sci. 311 (2008) 98–103, <http://dx.doi.org/10.1016/j.memsci.2007.11.055>, URL <http://linkinghub.elsevier.com/retrieve/pii/S0378775307008484>.
- [13] D. Chen, S. Kim, V. Sprenkle, M.A. Hickner, J. Power Sour. 231 (2013) 301–306, <http://dx.doi.org/10.1016/j.jpowsour.2013.01.007>.
- [14] S. Liu, L. Wang, D. Li, B. Liu, J. Wang, Y. Song, J. Mater. Chem. A 3 (2015) 17590–17597, <http://dx.doi.org/10.1039/C5TA04351D>, URL <http://xlink.rsc.org/?DOI=C5TA04351D>.
- [15] M.-S.J. Jung, J. Parrondo, C.G. Arges, V. Ramani, J. Mater. Chem. A 1 (2013) 10458–10464, <http://dx.doi.org/10.1039/C3TA11459G>.
- [16] T.N.L. Doan, T.K.A. Hoang, P. Chen, RSC Adv. 5 (2015) 72805–72815, <http://dx.doi.org/10.1039/C5RA05914C>.
- [17] J. Xi, Z. Wu, X. Qiu, L. Chen, J. Power Sour. 166 (2007) 531–536, <http://dx.doi.org/10.1016/j.jpowsour.2007.01.069>, URL <http://linkinghub.elsevier.com/retrieve/pii/S037877530700239X>.
- [18] X. Teng, Y. Zhao, J. Xi, Z. Wu, X. Qiu, L. Chen, J. Power Sour. 189 (2009) 1240–1246, <http://dx.doi.org/10.1016/j.jpowsour.2008.12.040>, URL <http://linkinghub.elsevier.com/retrieve/pii/S0378775308023689>.
- [19] H.H. Zhang, H.H. Zhang, X. Li, Z. Mai, W. Wei, Energy Environ. Sci. 5 (2012) 6299, <http://dx.doi.org/10.1039/c1ee02571f>, URL <http://xlink.rsc.org/?DOI=c1ee02571f>.
- [20] S. Lu, C. Wu, D. Liang, Q. Tan, Y. Xiang, RSC Adv. 4 (2014) 24831, <http://dx.doi.org/10.1039/c4ra01775g>, URL <http://xlink.rsc.org/?DOI=c4ra01775g>.
- [21] X. Teng, Y. Zhao, J. Xi, Z. Wu, X. Qiu, L. Chen, J. Membr. Sci. 341 (2009) 149–154, <http://dx.doi.org/10.1016/j.memsci.2009.05.051>.
- [22] G. Merle, F.C. Ioana, D.E. Demco, M. Saakes, S.S. Hosseiny, Membranes 4 (2013) 1–19, <http://dx.doi.org/10.3390/membranes4010001>.
- [23] J. Zeng, C. Jiang, Y. Wang, J. Chen, S. Zhu, B. Zhao, R. Wang, Electrochem. Commun. 10 (2008) 372–375, <http://dx.doi.org/10.1016/j.elecom.2007.12.025>.
- [24] J. Xi, Z. Wu, X. Teng, Y. Zhao, L. Chen, X. Qiu, J. Mater. Chem. 18 (2008) 1232, <http://dx.doi.org/10.1039/b718526j>, URL <http://xlink.rsc.org/?DOI=b718526j>.
- [25] Y. Li, X. Wang, J. Sun, Chem. Soc. Rev. 41 (2012) 5998, <http://dx.doi.org/10.1039/c2cs35107b>.
- [26] P. Bertrand, A. Jonas, A. Laschewsky, R. Legras, Macromol. Rapid Commun. 21 (2000) 319–348, [http://dx.doi.org/10.1002/\(SICI\)1521-3927\(20000401\)21:73.O.CO;2-7](http://dx.doi.org/10.1002/(SICI)1521-3927(20000401)21:73.O.CO;2-7), URL [http://apps.webofknowledge.com/full\\_record.do?product=UA&search\\_mode=GeneralSearch&qid=1&SID=V1FSIHRC2MX8eV26pd&page=1&doc=1](http://apps.webofknowledge.com/full_record.do?product=UA&search_mode=GeneralSearch&qid=1&SID=V1FSIHRC2MX8eV26pd&page=1&doc=1).
- [27] Y. Xiang, S. Lu, S.P. Jiang, Chem. Soc. Rev. 41 (2012) 7291, <http://dx.doi.org/10.1039/c2cs35048c>.
- [28] L. Xu, D. Pristinski, A. Zhuk, C. Stoddart, J.F. Ankner, S.A. Sukhishvili, Macromolecules 45 (2012) 3892–3901, <http://dx.doi.org/10.1021/ma300157p>, URL <http://pubs.acs.org/doi/abs/10.1021/ma300157p>.
- [29] P. Bieker, M. Schönhoff, Macromolecules 43 (2010) 5052–5059, <http://dx.doi.org/10.1021/ma1007489>, URL <http://pubs.acs.org/doi/abs/10.1021/ma1007489>.
- [30] D.A. Hagen, B. Foster, B. Stevens, J.C. Grunlan, ACS Macro Lett. 3 (2014) 663–666, <http://dx.doi.org/10.1021/mz500276r>.

- [31] W. Xu, X. Li, J. Cao, H. Zhang, H. Zhang, *Sci. Rep.* 4 (2014) 4016, <http://dx.doi.org/10.1038/srep04016>, URL (<http://www.pubmedcentral.nih.gov/articlerender.fcgi?artid=3915323&tool=pmcentrez&rendertype=abstract>).
- [32] Y.H. Yang, M. Haile, Y.T. Park, F.A. Malek, J.C. Grunlan, *Macromolecules* 44 (2011) 1450–1459, <http://dx.doi.org/10.1021/ma1026127>.
- [33] D.A. Hagen, C. Box, S. Greenlee, F. Xiang, O. Regev, J.C. Grunlan, *RSC Adv.* 4 (2014) 18354, <http://dx.doi.org/10.1039/c4ra01621a>, URL (<http://xlink.rsc.org/?DOI=c4ra01621a>).
- [34] B.E. Stevens, P.K. Odenborg, M.A. Priolo, J.C. Grunlan, *J. Polym. Sci. Part B Polym. Phys.* 52 (2014) 1153–1156, <http://dx.doi.org/10.1002/polb.23543>, URL (<http://doi.wiley.com/10.1002/polb.23543>).
- [35] Y.-H. Yang, L. Bolling, M. Haile, J.C. Grunlan, *RSC Adv.* (2012) 12355–12363, <http://dx.doi.org/10.1039/c2ra21845c>.
- [36] S. Abdu, M.C. Martí-Calatayud, J.E. Wong, M. García-Gabaldón, M. Wessling, *ACS Appl. Mater. Interfaces* 6 (2014) 1843–1854, <http://dx.doi.org/10.1021/am4048317>.
- [37] T. Sata, T. Sata, W. Yang, *J. Membr. Sci.* 206 (2002) 31–60, [http://dx.doi.org/10.1016/S0376-7388\(01\)00491-4](http://dx.doi.org/10.1016/S0376-7388(01)00491-4).
- [38] F. Guesmi, C. Hannachi, B. Hamrouni, *Ionics* 18 (2012) 711–717, <http://dx.doi.org/10.1007/s11581-011-0627-2>.
- [39] J. Ping, J. Wu, X. Luo, Y. Ying, *Ionics* 17 (2011) 443–449, <http://dx.doi.org/10.1007/s11581-011-0530-x>.
- [40] D.M. Delongchamp, P.T. Hammond, *Chem. Mater.* 15 (2003) 1165–1173.
- [41] Y. Daiko, K. Katagiri, A. Matsuda, *Chem. Mater.* (2008) 6405–6409, URL (<http://pubs.acs.org/doi/abs/10.1021/cm8007705>).
- [42] Q.H. Liu, G.M. Grim, A.B. Papandrew, A. Turhan, T.A. Zawodzinski, M.M. Mench, *J. Electrochem. Soc.* 159 (2012) A1246–A1252, <http://dx.doi.org/10.1149/2.051208jes>, URL (<http://jes.ecsdl.org/cgi/doi/10.1149/2.051208jes>).
- [43] D.-J. Guo, S.-J. Fu, W. Tan, Z.-D. Dai, *J. Mater. Chem.* 20 (2010) 10159, <http://dx.doi.org/10.1039/c0jm01161d>.
- [44] C. Sun, J. Chen, H. Zhang, X. Han, Q. Luo, *J. Power Sour.* 195 (2010) 890–897, <http://dx.doi.org/10.1016/j.jpowsour.2009.08.041>, URL (<http://linkinghub.elsevier.com/retrieve/pii/S0378775309014153>).
- [45] S. Slade, S. Campbell, T. Ralph, F. Walsh, *J. Electrochem. Soc.* 149 (2002) 1556–1564, <http://dx.doi.org/10.1149/1.1517281>.
- [46] V.A. Sethuraman, S. Khan, J.S. Jur, A.T. Haug, J.W. Weidner, *Electrochim. Acta* 54 (2009) 6850–6860, <http://dx.doi.org/10.1016/j.electacta.2009.06.068>, URL (<http://linkinghub.elsevier.com/retrieve/pii/S0013468609008950>).
- [47] Z. Ogumi, Z. Takehara, S. Yoshizawa, *J. Electrochem. Soc.* 131 (1984) 769–773.
- [48] T. Lehtinen, G. Sundholm, S. Holmberg, F. Sundholm, P. Bjo, *Electrochim. Acta* 43 (1998) 1881–1890.
- [49] J.B. Lindén, M. Larsson, B.R. Coad, W.M. Skinner, M. Nydén, *RSC Adv.* 4 (2014) 25063, <http://dx.doi.org/10.1039/c4ra02223h>, URL (<http://xlink.rsc.org/?DOI=c4ra02223h>).
- [50] T. Yang, A. Hussain, S. Bai, I.A. Khalil, H. Harashima, F. Ahsan, *J. Control. Release* 115 (2006) 289–297, <http://dx.doi.org/10.1016/j.jconrel.2006.08.015>, URL (<http://www.sciencedirect.com/science/article/pii/S0168365906004238>).
- [51] V.D. Noto, R. Gliubizzi, E. Negro, G. Pace, *J. Phys. Chem. B* 110 (2006) 24972–24986.
- [52] Z. Liang, W. Chen, J. Liu, S. Wang, Z. Zhou, W. Li, G. Sun, Q. Xin, *J. Membr. Sci.* 233 (2004) 39–44, <http://dx.doi.org/10.1016/j.memsci.2003.12.008>.
- [53] K. Feng, L. Hou, B. Tang, P. Wu, *Phys. Chem. Chem. Phys.* 17 (2015) 9106–9115, <http://dx.doi.org/10.1039/C5CP00203F>, URL (<http://xlink.rsc.org/?DOI=C5CP00203F>).
- [54] L. Grosmaire, S. Castagnoni, P. Huguet, P. Sistat, M. Boucher, P. Bouchard, P. Bébin, S. Deabate, *Phys. Chem. Chem. Phys.* 10 (2008) 1577–1583, <http://dx.doi.org/10.1039/b714870d>.
- [55] F. Zhang, Z. Zhang, Y. Liu, H. Lu, J. Leng, *Smart Mater. Struct.* 22 (2013) 085020, <http://dx.doi.org/10.1088/0964-1726/22/8/085020>, URL (<http://stacks.iop.org/0964-1726/22/i=8/a=085020?key=crossref.0f9179f29c114794b3e39b1e46fd74c>).
- [56] M. Feng, R. Qu, Z. Wei, L. Wang, P. Sun, Z. Wang, *Sci. Rep.* 5 (2015) 9859, <http://dx.doi.org/10.1038/srep09859>, URL (<http://www.nature.com/doi/finder/10.1038/srep09859>).
- [57] M. Rikukawa, K. Sanui, *Prog. Polym. Sci.* 25 (2000) 1463–1502, [http://dx.doi.org/10.1016/S0079-6700\(00\)00032-0](http://dx.doi.org/10.1016/S0079-6700(00)00032-0).
- [58] S.K. Tiwari, S.K. Nema, Y.K. Agarwal, *Thermochim. Acta* 317 (1998) 175–182.
- [59] L. Zhang, Y. Li, J.C. Yu, Y.Y. Chen, K.M. Chan, *J. Mater. Chem. B* 2 (2014) 7936–7944, <http://dx.doi.org/10.1039/C4TB01577K>, URL (<http://xlink.rsc.org/?DOI=C4TB01577K>).
- [60] G. Lawson, F. Gonzaga, J. Huang, G. de Silveira, M.A. Brook, A. Adronov, *J. Mater. Chem.* 18 (2008) 1694, <http://dx.doi.org/10.1039/b715277a>.
- [61] J. Fu, J. Ji, L. Shen, A. Ku, A. Rosenhahn, J. Shen, M. Grunze, *Langmuir* 25 (2009) 672–675, <http://dx.doi.org/10.1021/la803692v>.
- [62] C. Porcel, P. Lavalle, V. Ball, G. Decher, B. Senger, J.C. Voegel, P. Schaaf, *Langmuir* 22 (2006) 4376–4383, <http://dx.doi.org/10.1021/la053218d>.
- [63] I. Choi, R. Suntivich, F.A. Plamper, C.V. Synatschke, H.E.M. Axel, V.V. Tsukruk, *J. Am. Chem. Soc.* 133 (2011) 9592–9606.
- [64] R.A. Mcaloney, R.A. Mcaloney, M. Sinyor, M. Sinyor, V. Dudnik, V. Dudnik, M. C. Goh, M.C. Goh, *Langmuir* 17 (2001) 6655–6663, <http://dx.doi.org/10.1021/la010136q>.
- [65] K.R. Cooper, *J. Electrochem. Soc.* 157 (2010) B1731, <http://dx.doi.org/10.1149/1.3481561>.
- [66] C. Gardner, A.V. Anantaraman, *J. Electroanal. Chem.* 449 (1998) 209–214, [http://dx.doi.org/10.1016/S0022-0728\(97\)00408-7](http://dx.doi.org/10.1016/S0022-0728(97)00408-7).
- [67] S. Ma, Z. Siroma, H. Tanaka, *J. Electrochem. Soc.* 153 (2006) A2274–A2281, URL (<http://jes.ecsdl.org/content/153/12/A2274.abstract>).
- [68] R.F. Silva, M. De Francesco, A. Pozio, *J. Power Sour.* 134 (2004) 18–26, <http://dx.doi.org/10.1016/j.jpowsour.2004.03.028>.
- [69] M.W. Verbrugge, *J. Electrochem. Soc.* 137 (1990) 3770, <http://dx.doi.org/10.1149/1.2086299>.
- [70] Z. Tang, R. Svoboda, J.S. Lawton, D.S. Aaron, A.B. Papandrew, T.A. Zawodzinski, *J. Electrochem. Soc.* 160 (2013) F1040–F1047, <http://dx.doi.org/10.1149/2.083309jes>, URL (<http://jes.ecsdl.org/content/160/9/F1040.abstract>).
- [71] N. Yoshida, T. Ishisaki, A. Watakabe, M. Yoshitake, *Electrochim. Acta* 43 (1998) 3749–3754, [http://dx.doi.org/10.1016/S0013-4686\(98\)00133-9](http://dx.doi.org/10.1016/S0013-4686(98)00133-9).
- [72] R. Mohr, V. Kudela, J. Schauer, K. Richau, *Desalination* 147 (2002) 191–196, [http://dx.doi.org/10.1016/S0011-9164\(02\)00533-7](http://dx.doi.org/10.1016/S0011-9164(02)00533-7).
- [73] K.D. Kreuer, S.J. Paddison, E. Spohr, M. Schuster, *Chem. Rev.* 104 (2004) 4637–4678, <http://dx.doi.org/10.1021/cr020715f>.
- [74] S. Peighambaridoust, S. Rowshanzamir, M. Amjadi, *Int. J. Hydrog. Energy* 35 (2010) 9349–9384, <http://dx.doi.org/10.1016/j.ijhydene.2010.05.017>, URL (<http://linkinghub.elsevier.com/retrieve/pii/S0360319910009523>).
- [75] T.D. Gierke, G.E. Munn, F.C. Wilson, *J. Polym. Sci. Polym. Phys. Ed.* 19 (1981) 1687–1704, <http://dx.doi.org/10.1002/pol.1981.180191103>.
- [76] Y. Zhai, H. Zhang, Y. Zhang, D. Xing, *J. Power Sour.* 169 (2007) 259–264, <http://dx.doi.org/10.1016/j.jpowsour.2007.03.004>.
- [77] R. Bouchet, *Solid State Ionics* 118 (1999) 287–299, [http://dx.doi.org/10.1016/S0167-2738\(98\)00466-4](http://dx.doi.org/10.1016/S0167-2738(98)00466-4).
- [78] R. Tanaka, H. Yamamoto, A. Shono, K. Kubo, M. Sakurai, *Electrochim. Acta* 45 (2000) 1385–1389, [http://dx.doi.org/10.1016/S0013-4686\(99\)00347-3](http://dx.doi.org/10.1016/S0013-4686(99)00347-3).
- [79] M. Saito, N. Arimura, K. Hayamizu, T. Okada, *J. Phys. Chem. B* 108 (2004) 16064–16070.
- [80] L. Krasemann, B. Tieke, *Langmuir* 16 (2000) 287–290, <http://dx.doi.org/10.1021/la991240z>.
- [81] H. Zhang, *ECS Trans.* 28 (2010) 1–5, <http://dx.doi.org/10.1149/1.3492325>, URL (<http://ecst.ecsdl.org/content/28/22/1.abstract>).
- [82] J. Zhang, H.A. Gasteiger, W. Gu, *J. Electrochem. Soc.* 160 (2013) F616–F622, <http://dx.doi.org/10.1149/2.081306jes>, URL (<http://jes.ecsdl.org/cgi/doi/10.1149/2.081306jes>).
- [83] H. Ito, T. Maeda, A. Nakano, H. Takenaka, *Int. J. Hydrog. Energy* 36 (2011) 10527–10540, <http://dx.doi.org/10.1016/j.ijhydene.2011.05.127>, URL (<http://linkinghub.elsevier.com/retrieve/pii/S0360319911013760>).
- [84] A.T. Haug, R.E. White, *J. Electrochem. Soc.* 147 (2000) 980–983, <http://dx.doi.org/10.1149/1.1393300>.
- [85] P. Gode, G. Lindbergh, G. Sundholm, *J. Electroanal. Chem.* 518 (2002) 115–122, URL (<http://www.sciencedirect.com/science/article/pii/S0022072801006982>).
- [86] J.G. Wijmans, R.W. Baker, *J. Membr. Sci.* 107 (1995) 1–21, [http://dx.doi.org/10.1016/0376-7388\(95\)00102-1](http://dx.doi.org/10.1016/0376-7388(95)00102-1).
- [87] X.-G. Yang, Q. Ye, P. Cheng, T.S. Zhao, *Appl. Energy* 145 (2015) 306–319, <http://dx.doi.org/10.1016/j.apenergy.2015.02.038>, URL (<http://linkinghub.elsevier.com/retrieve/pii/S0306261915002159>).
- [88] T. Mohammadi, *J. Membr. Sci.* 133 (1997) 151–159, URL (<http://www.sciencedirect.com/science/article/pii/S0376738897000926>).
- [89] T.A. Zawodzinski, *J. Electrochem. Soc.* 140 (1993) 1981, <http://dx.doi.org/10.1149/1.220749>.
- [90] S. Cui, S.J. Paddison, *J. Phys. Chem. C* 119 (23) (2015) 12848–12855, URL (<http://pubs.acs.org/doi/abs/10.1021/acs.jpcc.5b02876>), <http://dx.doi.org/10.1021/acs.jpcc.5b02876>.
- [91] D.L. Feldheim, D.R. Lawson, C.R. Martin, *J. Polym. Sci. Part B Polym. Phys.* 31 (1993) 953–957, <http://dx.doi.org/10.1002/polb.1993.090310805>.
- [92] L. Sun, J.S. Thrasher, *Polym. Degrad. Stab.* 89 (2005) 43–49, <http://dx.doi.org/10.1016/j.polydegradstab.2005.01.001>.
- [93] J. Xi, Z. Wu, X. Teng, Y. Zhao, L. Chen, X. Qiu, *J. Mater. Chem.* 18 (2008) 1232, <http://dx.doi.org/10.1039/b718526j>, URL (<http://xlink.rsc.org/?DOI=b718526j>).
- [94] S. Yilmaztürk, N. Ercan, H. Deligöz, *Appl. Surf. Sci.* 258 (2012) 3139–3146, <http://dx.doi.org/10.1016/j.apsusc.2011.11.051>, URL (<http://linkinghub.elsevier.com/retrieve/pii/S0169433211018022>).
- [95] F. Harnisch, U. Schröder, *ChemSusChem* 2 (2009) 921–926, <http://dx.doi.org/10.1002/cssc.200900111>, URL (<http://doi.wiley.com/10.1002/cssc.200900111>).
- [96] A. Yamauchi, T. Ito, T. Yamaguchi, *J. Power Sour.* 174 (2007) 170–175, <http://dx.doi.org/10.1016/j.jpowsour.2007.08.081>, URL (<http://linkinghub.elsevier.com/retrieve/pii/S0378775307017533>).
- [97] K. Ariga, J.P. Hill, Q. Ji, *Phys. Chem. Chem. Phys.* 9 (2007) 2319, <http://dx.doi.org/10.1039/b700410a>, URL (<http://xlink.rsc.org/?DOI=b700410a>).



# Erklärung I

Die Richtigkeit der Darlegung des Eigenanteils an den Publikationen (“Author Contributions”) wird hiermit vom Betreuer der Arbeit bestätigt.

Oldenburg, den \_\_\_\_\_

\_\_\_\_\_  
(Prof. Dr. Gunther Wittstock)



# Erklärung II

Hiermit erkläre ich, Jan Bernhard grosse Austing, geb. 12.06.1983 in Lohne (Oldb.), dass ich die Dissertation selbständig verfasst und die benutzten Hilfsmittel vollständig angegeben habe. Die vorliegende Arbeit wurde in Teilen bereits veröffentlicht. Diese Teile sind die im Kapitel "Publikationen" aufgeführten Veröffentlichungen. Eine Publikationsliste ist der Dissertation beigelegt. Ich erkläre, dass die Dissertation weder in ihrer Gesamtheit noch in Teilen einer anderen wissenschaftlichen Hochschule zur Begutachtung in einem Promotionsverfahren vorliegt bzw. vorlag. Ich erkläre weiterhin, dass die Leitlinien guter wissenschaftlicher Praxis an der Carl von Ossietzky Universität Oldenburg befolgt wurden sind und im Zusammenhang mit dem Promotionsvorhaben keine kommerziellen Vermittlungs- oder Beratungsdienste (Promotionsberatung) in Anspruch genommen wurden.

Oldenburg, den \_\_\_\_\_

\_\_\_\_\_  
(Jan grosse Austing)



# List of Publications

## Printed Publications in Peer-Reviewed Journals

1. Jan grosse Austing, Carolina Nunes Kirchner, Eva-Maria Hammer, Lidiya Komsiyiska, Gunther Wittstock,  
“Study of an unitised bidirectional vanadium/air redox flow battery comprising a two-layered cathode”,  
Journal of Power Sources, Volume 273, Pages 1163–1170,  
DOI: 10.1016/j.jpowsour.2014.09.177.
2. Jan grosse Austing, Carolina Nunes Kirchner, Lidiya Komsiyiska, Gunther Wittstock,  
“Investigation of crossover processes in a unitized bidirectional vanadium/air redox flow battery”,  
Journal of Power Sources, Volume 306, Pages 692-701,  
DOI: 10.1016/j.jpowsour.2015.12.052.
3. Jan grosse Austing, Carolina Nunes Kirchner, Lidiya Komsiyiska, Gunther Wittstock,  
“Layer-by-layer modification of Nafion membranes for increased life-time and efficiency of vanadium/air redox flow batteries”,  
Journal of Membrane Science, Volume 510, Pages 259-269,  
DOI: 10.1016/j.memsci.2016.03.005.

## Conference Proceedings

1. Jan grosse Austing, Carolina Nunes Kirchner, Lidiya Komsiyiska, Gunther Wittstock,  
"Performance of a vanadium/air redox flow battery (VARFB) comprising a two-layered cathode",  
Printed Conference Mini Papers of the International Flow Battery Forum (IFBF) 2014, ISBN: 978-0-9571055-4-6, Pages 10/11.

2. Jan grosse Austing, Carolina Nunes Kirchner, Lidiya Komsiyyska, Oliver Osters, Gunther Wittstock,  
"Investigation of crossover processes in a bidirectional vanadium/air redox flow battery",  
Printed Conference Mini Papers of the International Flow Battery Forum (IFBF) 2015, ISBN: 978-0-9571055-5-3, Pages 18/19.

## Oral Conference Contributions

- Jan grosse Austing, Carolina Nunes Kirchner, Lidiya Komsiyyska, Gunther Wittstock,  
"Performance of a vanadium/air redox flow battery (VARFB) comprising a two-layered cathode",  
International Flow Battery Forum (IFBF) 2014, Hamburg, July 2014.
- Jan grosse Austing, Carolina Nunes Kirchner, Lidiya Komsiyyska, Gunther Wittstock,  
"Performance of a vanadium/air redox flow battery (VARFB) comprising a two-layered cathode",  
Electrochemistry 2014, Mainz, September 2014.
- Jan grosse Austing, Carolina Nunes Kirchner, Lidiya Komsiyyska, Oliver Osters, Gunther Wittstock,  
"Investigation of crossover processes in a bidirectional vanadium/air redox flow battery",  
International Flow Battery Forum (IFBF) 2015, Glasgow, June 2015.
- Jan grosse Austing, Carolina Nunes Kirchner, Lidiya Komsiyyska, Gunther Wittstock,  
"Investigation of crossover processes in a bidirectional vanadium/air redox flow battery",  
ECHEMS - Electrochemistry in renewable energy based on molecular mechanisms, Bad Zwischenahn, June 2015.

## Poster Conference Contributions

- Jan grosse Austing, Udo Martin, Andreas Blömer, Lidiya Komsiyyska, Eva-Maria Hammer,  
"Influence of the membrane electrode assembly preparation procedure on the

discharge performance of Vanadium-Air-Redox-Flow-Batteries (VARFB)”,  
International Flow Battery Forum (IFBF) 2012, Munich, June 2012.

- Jan grosse Austing, Eva-Maria Hammer, Lidiya Komsysiyska, Carolina Nunes-Kirchner, Gunther Wittstock,  
“Preparation and Characterization of Cathodes for Vanadium/Air Redox Flow Batteries (VARFB) by Metal Deposition on Carbon-based 3D Electrodes”,  
International Flow Battery Forum (IFBF) 2013, Dublin, June 2013.
- Jan grosse Austing, Carolina Nunes Kirchner, Lidiya Komsysiyska, Gunther Wittstock,  
"Performance of a vanadium/air redox flow battery (VARFB) comprising a two-layered cathode",  
Kraftwerk Batterie, Münster, March 2014.
- Timo di Nardo, Carolina Nunes Kirchner, Jan grosse Austing, Oliver Osters;  
Lidiya Komsysiyska,  
"Electrochemical deposition of Ir on graphite felt electrode for vanadium air redox flow battery cathodes",  
CIMTEC, Montecatini Terme, June 2014.
- Timo di Nardo, Carolina Nunes Kirchner, Jan grosse Austing, Oliver Osters;  
Lidiya Komsysiyska,  
"Electrochemical deposition of iridium on graphite felt electrode for vanadium air redox flow battery cathodes",  
13th International Fischer Symposium, Lübeck, June 2015.



# Jan Bernhard grosse Austing

## Curriculum Vitae

born on: 12/06/1983  
in: Lohne (Oldb.)



---

## Education & Experiences

- 07/1996 - 06/2003 **Abitur**, Gymnasium Damme, Germany, grade: 1.3.
- 10/2003 - 04/2009 **Mathematics and Chemistry**, 1. Staatsexamen, Philipps University of Marburg, Germany, grade: 1.29.
- 09/2009 - 09/2010 **Voluntary Service „weltwärts“**, Lwandai Secondary School, Mlalo, Tanzania.
- 10/2010 - 06/2012 **Renewable Energies and Energy Efficiency**, M.Sc., University of Kassel, Germany, grade: 1.42.
- 10/2011 - 04/2012 **Master Thesis**, NEXT ENERGY - EWE Research Centre for Energy Technology, Oldenburg, Germany.
- 11/2012 - 09/2015 **PhD Studies**, NEXT ENERGY - EWE Research Centre for Energy Technology, Oldenburg, Germany.
- 08/2013 - 09/2013 **Research Stay**, University of Victoria, British Columbia, Canada.
- since 10/2015 **Project Manager**, *EXIST Forschungstransfer „Resi-Flow“*, NEXT ENERGY - EWE Research Centre for Energy Technology, Oldenburg, Germany.

---

## Awards & Grants

- 10/2012 **Financial Support for PhD Project (5000 €)**, Nord-West-Metall Stiftung.
- 11/2012 **PhD Scholarship (3 years)**, Reiner-Lemoine Stiftung.
- 04/2013 **Award for Environmental Related Master Thesis (1500 €)**, VDI-Gesellschaft für Energie und Umwelt (VDI-GEU).



# Danksagung

Im Folgenden möchte ich mich bei all denjenigen bedanken, die direkt oder indirekt zum Gelingen dieser Dissertation beitrugen. Beginnen möchte ich mit Prof. Dr. Gunther Wittstock, der die wissenschaftliche Betreuung dieser Arbeit und die Begutachtung als Erstgutachter übernommen hat. Er nahm sich immer Zeit für fachliche und organisatorische Fragen, auch kurzfristig. Ebenso danke ich Prof. Dr. Carsten Agert für die Übernahme der Zweitbegutachtung.

Für den intensiven, anregenden fachlichen Austausch bei der täglichen Arbeit gilt mein Dank besonders Dr. Lidiya Komsijska, Dr. Carolina Nunes Kirchner und Dr. Eva-Maria Hammer. Sie haben sich immer Zeit genommen für meine Anliegen und ich habe ihre fachlichen Fähigkeiten aber auch persönlichen Eigenschaften sehr zu schätzen gelernt. Ich danke auch allen anderen Kollegen bei NEXT ENERGY für die hilfsbereite, kollegiale Zusammenarbeit bei vielerlei Fragestellungen. Namentlich nennen möchte ich Hayo Seeba, Frank Bättermann, Dietmar Piehler, Timo di Nardo, Pratik Das, Barbara Satola, Khrystyna Yezerska, Benedikt Berger und Dana Schonvogel.

Ich danke meiner Frau Karina dafür, dass Sie mich immer in meinen Vorhaben immer so aktiv unterstützt. Bei meiner Tochter Thea möchte ich mich dafür bedanken, dass sie insbesondere während der Schreibphase auf meine Anwesenheit als Vater ab und zu verzichten konnte. Meinem Bruder Arne gilt mein Dank für Hinweise und Korrekturvorschläge zur Arbeit. Meinen Eltern danke ich für die gesamte Unterstützung während meines bisherigen Lebens.

Der Reiner-Lemoine Stiftung möchte ich für das Promotionsstipendium danken, durch welches das Arbeiten an diesem Thema im Rahmen einer Doktorarbeit ermöglicht wurde.